Supporting Information

for

Group 10 Metal Dithiolene Bis(isonitrile) Complexes: Synthesis, Structures, Properties and Reactivity

Antony Obanda,[‡] Kendra Valerius,[‡] Joel T. Mague,[‡]
Stephen Sproules,[§] and James P. Donahue[‡,*]

[‡]Dept. of Chemistry, Tulane University, 6400 Freret St., New Orleans, LA 70118-5698, U.S.A.
[§]WestCHEM, School of Chemistry, University of Glasgow, Glasgow, G12 8QQ, United Kingdom

Table of Contents

Procedures for Crystal Growth, Collection and Processing of Diffraction Data, and Solving and Refining of Structures.		S9-S11
Computational Procedures and Details		S12
References		S13
Table S1.	Unit cell and refinement data for $[(Ph_2C_2S_2)Ni(C{\equiv}NCH_2C_6H_5)_2]$, $[(Ph_2C_2S_2)Ni(C{\equiv}NCy)_2]$, $[(Ph_2C_2S_2)Ni(C{\equiv}N^tBu)_2]$, $[(Ph_2C_2S_2)Ni(C{\equiv}N\text{-}1\text{-adamantyl})_2]\cdot\frac{1}{2}Et_2O$, and $[(Ph_2C_2S_2)Ni(C{\equiv}NPh)_2]$.	S14
Table S2.	Unit cell and refinement data for $[(Ph_2C_2S_2)Pd(C{\equiv}NCH_3)_2]$, $[(Ph_2C_2S_2)Pd(C{\equiv}NBn)_2]$, $[(Ph_2C_2S_2)Pd(C{\equiv}NCy)_2]$. $[(Ph_2C_2S_2)Pt(C{\equiv}N\text{-}1\text{-adamantyl})_2]$, and $[(Ph_2C_2S_2)Pd(C{\equiv}NPh)_2]$,	S15
Table S3.	Unit cell and refinement data for $[(Ph_2C_2S_2)Pt(C{\equiv}NCH_3)_2]$, $[(Ph_2C_2S_2)Pt(C{\equiv}NBn)_2]$, $[(Ph_2C_2S_2)Pt(C{\equiv}NCy)_2]$, $[(Ph_2C_2S_2)Pt(C{\equiv}N^tBu)_2]$, $[(Ph_2C_2S_2)Pt(C{\equiv}N\text{-}1\text{-adamantyl})_2]$.	S16
Table S4.	Unit Cell and Refinement Data for $[(adt)Ni(C{\equiv}N^tBu)_2]$, $[(pdt)Pt(C{\equiv}N^tBu)_2][SbCl_6]\cdot CH_2Cl_2$, and $[[(pdt)Ni(C{\equiv}N^tBu)_2]_2(\mu\text{-}Ag_2)][BF_4]_2$.	S17
Table S5.	Unit Cell and Refinement Data for $[(pdt)Ni(CNMe)(PMe_3)]$, $[(pdt)Ni(CNMe)(PPh_3)]$, $[(pdt)Ni(CNMe)]_2(\mu\text{-}1,4\text{-dppb})\cdot ClCH_2CH_2Cl$, $[(pdt)Pd(CNMe)]_2(\mu\text{-}1,4\text{-dppb})\cdot 2ClCH_2CH_2Cl$, and $[(pdt)Pt(CNMe)]_2(\mu\text{-}1,4\text{-dppb})\cdot 2ClCH_2CH_2Cl$.	S18
Table S6.	Unit Cell and Refinement Data for Cyanide and Carbene Compounds.	S19
Figure S1.	Thermal ellipsoid plot (50%) of $[(Ph_2C_2S_2)Ni(CNBn)_2]$.	S20
Figure S2.	Thermal ellipsoid plot (50%) of $[(Ph_2C_2S_2)Ni(CNCy)_2]$, molecule 1 of 3	S20
Figure S3.	Thermal ellipsoid plot (50%) of $[(Ph_2C_2S_2)Ni(CNCy)_2]$, molecule 2 of 3	S21
Figure S4.	Thermal ellipsoid plot (50%) of $[(Ph_2C_2S_2)Ni(CNCy)_2]$, molecule 3 of 3	S21
Figure S5.	Thermal ellipsoid plot (50%) of $[(Ph_2C_2S_2)Ni(CN^tBu)_2]$.	S22
Figure S6.	Thermal ellipsoid plot (50%) of $[(Ph_2C_2S_2)Ni(CN\text{-}1\text{-}Ad)_2]$, molecule 1 of 2.	S22
Figure S7.	Thermal ellipsoid plot (50%) of $[(Ph_2C_2S_2)Ni(CN\text{-}1\text{-}Ad)_2]$, molecule 2 of 2.	S23
Figure S8.	Atom labeling for interstitial Et_2O in $2[(Ph_2C_2S_2)Ni(CN\text{-}1\text{-}Ad)_2]\cdot Et_2O$	S23
Figure S9.	Thermal ellipsoid plot (50%) of $[(Ph_2C_2S_2)Ni(CNPh)_2]$.	S24
Figure S10.	Thermal ellipsoid plot (50%) of $[(Ph_2C_2S_2)Pd(CNMe)_2]$.	S24
Figure S11.	Thermal ellipsoid plot (50%) of $[(Ph_2C_2S_2)Pd(CNBn)_2]$.	S25
Figure S12.	Thermal ellipsoid plot (50%) of $[(Ph_2C_2S_2)Pd(CNCy)_2]$.	S25
Figure S13.	Thermal ellipsoid plot (50%) of $[(Ph_2C_2S_2)Pd(CN\text{-}1\text{-}Adamantyl)_2]$ showing the disordered adamantyl group in one of its two positions.	S26
Figure S14.	Thermal ellipsoid plot (50%) of $[(Ph_2C_2S_2)Pd(CN\text{-}1\text{-}Adamantyl)_2]$ showing the disordered adamantyl group in the second of its two positions.	S26
Figure S15.	Thermal ellipsoid plot (50%) of interstitial solvent in structure of $[(Ph_2C_2S_2)Pd(CN\text{-}1\text{-}Adamantyl)_2]\cdot\frac{1}{2}CH_2Cl_2\cdot\frac{1}{2}Et_2O$.	S27
Figure S16.	Atom labeling with 50% thermal ellipsoids for $[(Ph_2C_2S_2)Pd(CNPh)_2]$.	S27
Figure S17.	Atom labeling with 50% thermal ellipsoids for $[(Ph_2C_2S_2)Pt(CNMe)_2]$, molecule one of two.	S28
Figure S18.	Atom labeling with 50% thermal ellipsoids for $[(Ph_2C_2S_2)Pt(CNMe)_2]$, molecule two of two.	S28

Table of Contents, Continued

Figure S19.	Atom labeling for interstitial $ClCH_2CH_2Cl$ in in $[(Ph_2C_2S_2)Pt(CNMe)_2]\cdot½ClCH_2CH_2Cl$ with 50% ellipsoids.	S29
Figure S20.	Atom labeling with 50% thermal ellipsoids for $[(Ph_2C_2S_2)Pt(CNBn)_2]$.	S29
Figure S21.	Atom labeling with 50% thermal ellipsoids for $[(Ph_2C_2S_2)Pt(CNCy)_2]$.	S30
Figure S22.	Atom labeling with 50% thermal ellipsoids for $[(Ph_2C_2S_2)Pt(CN^tBu)_2]$.	S30
Figure S23.	Thermal ellipsoid plot (50%) of $[(Ph_2C_2S_2)Pt(CN\text{-}1\text{-}Adamantyl)_2]$ showing the disordered adamantyl group in one of its two positions.	S31
Figure S24.	Thermal ellipsoid plot (50%) of $[(Ph_2C_2S_2)Pt(CN\text{-}1\text{-}Adamantyl)_2]$ showing the disordered adamantyl group in the second of its two positions.	S31
Figure S25.	Isotropic thermal ellipsoid plot (30%) of disordered Et_2O molecule in $[(Ph_2C_2S_2)Pt(CN\text{-}1\text{-}Adamantyl)_2]\cdot Et_2O$. Hydrogen atoms omitted for clarity.	S32
Figure S26.	Thermal ellipsoid plot (50%) with complete atom labeling for $[[(Ph_2C_2S_2)Ni(CN^tBu)_2]_2(\mu\text{-}Ag)_2]^{2+}$. Hydrogen atoms are omitted for clarity.	S32
Figure S27.	Thermal ellipsoid plot (50%) for $[[(Ph_2C_2S_2)Ni(CN^tBu)_2]_2(\mu\text{-}Ag)_2][BF_4]$ with atom labeling for anion. Hydrogen atoms are omitted for clarity.	S33
Figure S28.	Thermal ellipsoid plot (50%) for $[(Ph_2C_2S_2)Pt(CN^tBu)_2]_2^{2+}$, dication #1. Hydrogen atoms are omitted for clarity.	S33
Figure S29.	Thermal ellipsoid plot (50%) for $[(Ph_2C_2S_2)Pt(CN^tBu)_2]_2^{2+}$, dication #2. Hydrogen atoms are omitted for clarity.	S34
Figure S30.	Thermal ellipsoid plot (50%) for $[SbCl_6]^{1-}$ and for interstitial CH_2Cl_2 in $[(Ph_2C_2S_2)Pt(CN^tBu)_2]_2[SbCl_6]_2\cdot 2CH_2Cl_2$. H atoms are omitted for clarity.	S34
Figure S31.	Thermal ellipsoid plot (50%) of $[Et_4N][(Ph_2C_2S_2)Pd(CN)(CNMe)]$. Hydrogen atoms are omitted for clarity.	S35
Figure S32.	Thermal ellipsoid plot (50%) of $[Et_4N][(Ph_2C_2S_2)Pt(CN)(CNMe)]$. Hydrogen atoms are omitted for clarity.	S35
Figure S33.	Thermal ellipsoid plot (50%) of $[(Ph_2C_2S_2)Pd(CNMe)(IPr)]$. Hydrogen atoms are omitted for clarity.	S36
Figure S34.	Thermal ellipsoid plot (50%) of $[(Ph_2C_2S_2)Pd(CNMe)(IPr)]\cdot ½ClCH_2CH_2Cl$ with atom labeling for interstitial $ClCH_2CH_2Cl$. Hydrogen atoms are omitted for clarity.	S36
Figure S35.	Thermal ellipsoid plot (50%) of $[(Ph_2C_2S_2)Pt(CNMe)(C(NMe)(IPr))]$, molecule one of two. Hydrogen atoms are omitted for clarity.	S37
Figure S36.	Thermal ellipsoid plot (50%) of $[(Ph_2C_2S_2)Pt(CNMe)(C(NMe)(IPr))]$, molecule two of two. Hydrogen atoms are omitted for clarity.	S37
Figure S37.	Thermal ellipsoid plot (50%) of $[(Ph_2C_2S_2)Ni(CNMe)(C(NHMe)(NMe_2))]$ Hydrogen atoms are omitted for clarity.	S38
Figure S38.	Thermal ellipsoid plot (50%) of $[(Ph_2C_2S_2)Ni(CNMe)](C(NHMe)(NMe_2))]\cdot$ ^{t}BuOMe with atom labeling for interstitial solvent. Hydrogen atoms are omitted for clarity.	S38
Figure S39.	Thermal ellipsoid plot (50%) of $[(2,6\text{-}Me_2py)Ni]_2(\mu\text{-}S',S'\text{-}pdt)_2$. All H atoms are omitted for clarity.	S39
Figure S40.	Side perspective of $[(2,6\text{-}Me_2py)Ni]_2(\mu\text{-}S',S'\text{-}pdt)_2$ represented as a 50% thermal ellipsoid plot. All H atoms are omitted for clarity.	S39
Figure S41.	Thermal ellipsoid plot (50%) of $[(Ph_2C_2S_2)Ni(CNMe)(PPh_3)]$ with H atoms omitted for clarity.	S40

Table of Contents, Continued

Figure S42. Thermal ellipsoid plot (50%) of [($Ph_2C_2S_2$)Ni(CNMe)(PMe_3)] with H atoms omitted for clarity. S40

Figure S43. Thermal ellipsoid plot (50%) of [($Ph_2C_2S_2$)Ni(CNMe)]$_2$(μ-1,4-(Ph_2P)$_2C_6H_4$)]. All hydrogen atoms are omitted for clarity. S41

Figure S44. Thermal ellipsoid plot (50%) of $ClCH_2CH_2Cl$ in the structure of [($Ph_2C_2S_2$)Ni(CNMe)]$_2$(μ-1,4-(Ph_2P)$_2C_6H_4$)]·$ClCH_2CH_2Cl$. All hydrogen atoms are omitted for clarity. S41

Figure S45. Thermal ellipsoid plot (50%) of [($Ph_2C_2S_2$)Pd(CNMe)]$_2$(μ-1,4-(Ph_2P)$_2C_6H_4$)]. All hydrogen atoms are omitted for clarity. S42

Figure S46. Thermal ellipsoid plot (50%) of [($Ph_2C_2S_2$)Pd(CNMe)]$_2$(μ-1,4-(Ph_2P)$_2C_6H_4$)]· $ClCH_2CH_2Cl$ with atom labeling for interstitial $ClCH_2CH_2Cl$ molecule. All hydrogen atoms are omitted for clarity. S42

Figure S47. Thermal ellipsoid plot (50%) of [($Ph_2C_2S_2$)Pt(CNMe)]$_2$(μ-1,4-(Ph_2P)$_2C_6H_4$)]. All hydrogen atoms are omitted for clarity. S43

Figure S48. Thermal ellipsoid plot (50%) of [($Ph_2C_2S_2$)Pt(CNMe)]$_2$(μ-1,4-(Ph_2P)$_2C_6H_4$)]· $ClCH_2CH_2Cl$ with atom labeling for interstitial $ClCH_2CH_2Cl$ molecule. All hydrogen atoms are omitted for clarity. S43

Figure S49. ^{1}H NMR spectrum (CD_2Cl_2) of [($Ph_2C_2S_2$)Ni(C≡N$CH_2C_6H_5$)$_2$]. S44

Figure S50. ^{13}C NMR spectrum (CD_2Cl_2) of [($Ph_2C_2S_2$)Ni(C≡N$CH_2C_6H_5$)$_2$]. S44

Figure S51. Solution IR spectrum (CH_2Cl_2) of [($Ph_2C_2S_2$)Ni(C≡N$CH_2C_6H_5$)$_2$]. S45

Figure S52. UV-vis spectrum (CH_2Cl_2) of [($Ph_2C_2S_2$)Ni(C≡N$CH_2C_6H_5$)$_2$]. S45

Figure S53. Cyclic voltammogram (CH_2Cl_2) of [($Ph_2C_2S_2$)Ni(C≡N$CH_2C_6H_5$)$_2$] at 50 mV/sec with [^{n}Bu$_4$N][PF_6] supporting electrolyte. S46

Figure S54. Elemental analysis for [($Ph_2C_2S_2$)Ni(C≡N$CH_2C_6H_5$)$_2$], Galbraith Laboratories. S47

Figure S55. ^{1}H NMR spectrum (CD_2Cl_2) of [($Ph_2C_2S_2$)Ni(C≡NCy)$_2$]. S48

Figure S56. ^{13}C NMR spectrum (CD_2Cl_2) of [($Ph_2C_2S_2$)Ni(C≡NCy)$_2$]. S48

Figure S57. Solution IR spectrum (CH_2Cl_2) of [($Ph_2C_2S_2$)Ni(C≡NCy)$_2$]. S49

Figure S58. UV-vis spectrum (CH_2Cl_2) of [($Ph_2C_2S_2$)Ni(C≡NCy)$_2$]. S49

Figure S59. Cyclic voltammogram (CH_2Cl_2) of [($Ph_2C_2S_2$)Ni(C≡NCy)$_2$] at 50 mV/sec with [^{n}Bu$_4$N][PF_6] supporting electrolyte. S50

Figure S60. Elemental analysis for [($Ph_2C_2S_2$)Ni(C≡N$CH_2C_6H_5$)$_2$], Midwest Microlabs. S51

Figure S61. ^{1}H NMR spectrum (CD_2Cl_2) of [($Ph_2C_2S_2$)Ni(C≡N^{t}Bu)$_2$]. S52

Figure S62. ^{13}C NMR spectrum ($CDCl_3$) of [($Ph_2C_2S_2$)Ni(C≡N^{t}Bu)$_2$]. S52

Figure S63. Solution IR spectrum (CH_2Cl_2) of [($Ph_2C_2S_2$)Ni(C≡N^{t}Bu)$_2$]. S53

Figure S64. UV-vis spectrum (CH_2Cl_2) of [($Ph_2C_2S_2$)Ni(C≡N^{t}Bu)$_2$]. S53

Figure S65. Cyclic voltammogram (CH_2Cl_2) of [($Ph_2C_2S_2$)Ni(C≡N^{t}Bu)$_2$] with [^{n}Bu$_4$N][PF_6] supporting electrolyte. S54

Figure S66. Elemental analysis for [($Ph_2C_2S_2$)Ni(C≡N^{t}Bu)$_2$], Midwest Microlabs. S55

Figure S67. ^{1}H NMR spectrum (CD_2Cl_2) of [($Ph_2C_2S_2$)Ni(C≡N-1-Adamantyl)$_2$]. S56

Figure S68. ^{13}C NMR spectrum (CD_2Cl_2) of [($Ph_2C_2S_2$)Ni(C≡N-1-Adamantyl)$_2$]. S56

Figure S69. Solution IR spectrum (CH_2Cl_2) of [($Ph_2C_2S_2$)Ni(C≡N-1-Adamantyl)$_2$]. S57

Figure S70. UV-vis spectrum (CH_2Cl_2) of [($Ph_2C_2S_2$)Ni(C≡N-1-Adamantyl)$_2$]. S57

Figure S71. Cyclic voltammogram (CH_2Cl_2) of [($Ph_2C_2S_2$)Ni(C≡N-1-Adamantyl)$_2$] with [^{n}Bu$_4$N][PF_6] supporting electrolyte. S58

Table of Contents, Continued

Figure S72.	Elemental analysis for [($Ph_2C_2S_2$)Ni(C≡N-1-Adamantyl)$_2$],. Midwest Microlabs	S59
Figure S73.	^{1}H NMR spectrum (CD_2Cl_2) of [($Ph_2C_2S_2$)Ni(C≡NPh)$_2$].	S60
Figure S74.	^{13}C NMR spectrum (CD_2Cl_2) of [($Ph_2C_2S_2$)Ni(C≡NPh)$_2$].	S60
Figure S75.	Solution IR spectrum (CH_2Cl_2) of [($Ph_2C_2S_2$)Ni(C≡NPh)$_2$].	S61
Figure S76.	UV-vis spectrum (CH_2Cl_2) of [($Ph_2C_2S_2$)Ni(C≡NPh)$_2$].	S61
Figure S77.	Cyclic voltammogram (CH_2Cl_2) of [($Ph_2C_2S_2$)Ni(C≡NPh)$_2$] with [^{n}Bu$_4$N][PF_6] supporting electrolyte.	S62
Figure S78.	Elemental analysis for [($Ph_2C_2S_2$)Ni(C≡NPh)$_2$], Midwest Microlabs.	S63
Figure S79.	^{1}H NMR spectrum (CD_2Cl_2) of [((CH_3O-*p*-C_6H_4)$_2C_2S_2$)Ni(C≡N^{t}Bu)$_2$].	S64
Figure S80.	^{13}C NMR spectrum ($CDCl_3$) of [((CH_3O-*p*-C_6H_4)$_2C_2S_2$)Ni(C≡N^{t}Bu)$_2$].	S64
Figure S81.	Solution IR spectrum (CH_2Cl_2) of [((CH_3O-*p*-C_6H_4)$_2C_2S_2$)Ni(C≡N^{t}Bu)$_2$].	S65
Figure S82.	UV-vis spectrum (CH_2Cl_2) of [((CH_3O-*p*-C_6H_4)$_2C_2S_2$)Ni(C≡N^{t}Bu)$_2$].	S65
Figure S83.	Cyclic voltammogram (CH_2Cl_2) of [((CH_3O-*p*-C_6H_4)$_2C_2S_2$)Ni(C≡N^{t}Bu)$_2$] with [^{n}Bu$_4$N][PF_6] supporting electrolyte.	S66
Figure S84.	Elemental analysis for [((CH_3O-*p*-C_6H_4)$_2C_2S_2$)Ni(C≡N^{t}Bu)$_2$], Galbraith Laboratories.	S67
Figure S85.	^{1}H NMR spectrum (CD_2Cl_2) of [($Ph_2C_2S_2$)Pd(C≡Me$_2$].	S68
Figure S86.	^{13}C NMR spectrum (CD_2Cl_2) of [($Ph_2C_2S_2$)Pd(C≡NMe)$_2$].	S68
Figure S87.	Solution IR spectrum (CH_2Cl_2) of [($Ph_2C_2S_2$)Pd(C≡NMe)$_2$].	S69
Figure S88.	UV-vis spectrum (CH_2Cl_2) of [($Ph_2C_2S_2$)Pd(C≡NMe)$_2$].	S69
Figure S89.	Cyclic voltammogram (CH_2Cl_2) of [($Ph_2C_2S_2$)Pd(C≡NMe)$_2$] at 50 mV/sec with [^{n}Bu$_4$N][PF_6] supporting electrolyte.	S70
Figure S90.	^{1}H NMR spectrum (CD_2Cl_2) of [($Ph_2C_2S_2$)Pd(C≡N$CH_2C_6H_5$)$_2$].	S71
Figure S91.	^{13}C NMR spectrum (CD_2Cl_2) of [($Ph_2C_2S_2$)Pd(C≡N$CH_2C_6H_5$)$_2$].	S71
Figure S92.	Solution IR spectrum (CH_2Cl_2) of [($Ph_2C_2S_2$)Pd(C≡N$CH_2C_6H_5$)$_2$].	S72
Figure S93.	UV-vis spectrum (CH_2Cl_2) of [($Ph_2C_2S_2$)Pd(C≡N$CH_2C_6H_5$)$_2$].	S72
Figure S94.	Cyclic voltammogram (CH_2Cl_2) of [($Ph_2C_2S_2$)Pd(C≡N$CH_2C_6H_5$)$_2$] at 50 mV/sec with [^{n}Bu$_4$N][PF_6] supporting electrolyte.	S73
Figure S95.	Elemental analysis for [($Ph_2C_2S_2$)Pd(C≡N$CH_2C_6H_5$)$_2$], Kolbe Microanalytical Laboratory.	S73
Figure S96.	^{1}H NMR spectrum (CD_2Cl_2) of [($Ph_2C_2S_2$)Pd(C≡NCy)$_2$].	S74
Figure S97.	^{13}C NMR spectrum (CD_2Cl_2) of [($Ph_2C_2S_2$)Pd(C≡NCy)$_2$].	S74
Figure S98.	Solution IR spectrum (CH_2Cl_2) of [($Ph_2C_2S_2$)Pd(C≡NCy)$_2$].	S75
Figure S99.	UV-vis spectrum (CH_2Cl_2) of [($Ph_2C_2S_2$)Pd(C≡NCy)$_2$].	S75
Figure S100.	Cyclic voltammogram (CH_2Cl_2) of [($Ph_2C_2S_2$)Pd(C≡NCy)$_2$] at 50 mV/sec with [^{n}Bu$_4$N][PF_6] supporting electrolyte.	S76
Figure S101.	Elemental analysis for [($Ph_2C_2S_2$)Pd(C≡NCy)$_2$], Kolbe Microanalytical Laboratory.	S77
Figure S102.	^{1}H NMR spectrum (CD_2Cl_2) of [($Ph_2C_2S_2$)Pd(C≡N-1-Ad)$_2$].	S78
Figure S103.	^{13}C NMR spectrum (CD_2Cl_2) of [($Ph_2C_2S_2$)Pd(C≡N-1-Ad)$_2$].	S78
Figure S104.	Solution IR spectrum (CH_2Cl_2) of [($Ph_2C_2S_2$)Pd(C≡N-1-Ad)$_2$].	S79
Figure S105.	UV-vis spectrum (CH_2Cl_2) of [($Ph_2C_2S_2$)Pd(C≡N-1-Ad)$_2$].	S79
Figure S106.	Cyclic voltammogram (CH_2Cl_2) of [($Ph_2C_2S_2$)Pd(C≡N-1-Ad)$_2$] at 50 mV/sec with [^{n}Bu$_4$N][PF_6] supporting electrolyte.	S80

Table of Contents, Continued

Figure S107. ^{1}H NMR spectrum (CD_2Cl_2) of [$(Ph_2C_2S_2)Pd(C{\equiv}NPh)_2$]. S80
Figure S108. Solution IR spectrum (CH_2Cl_2) of [$(Ph_2C_2S_2)Pd(C{\equiv}NPh)_2$]. S81
Figure S109. UV-vis spectrum (CH_2Cl_2) of [$(Ph_2C_2S_2)Pd(C{\equiv}NPh)_2$]. S81
Figure S110. Cyclic voltammogram (CH_2Cl_2) of [$(Ph_2C_2S_2)Pd(C{\equiv}NPh)_2$] at 50 mV/sec with [$^{n}Bu_4N$][$PF_6$] supporting electrolyte. S82
Figure S111. ^{1}H NMR spectrum (CD_2Cl_2) of [$(Ph_2C_2S_2)Pt(C{\equiv}NMe)_2$]. S82
Figure S112. ^{13}C NMR spectrum (CD_2Cl_2) of [$(Ph_2C_2S_2)Pt(C{\equiv}NMe)_2$]. S83
Figure S113. Solution IR spectrum (CH_2Cl_2) of [$(Ph_2C_2S_2)Pt(C{\equiv}NMe)_2$]. S83
Figure S114. UV-vis spectrum (CH_2Cl_2) of [$(Ph_2C_2S_2)Pt(C{\equiv}NMe)_2$]. S84
Figure S115. Cyclic voltammogram (CH_2Cl_2) of [$(Ph_2C_2S_2)Pt(C{\equiv}NMe)_2$] at 50 mV/sec with [$^{n}Bu_4N$][$PF_6$] supporting electrolyte. S84
Figure S116. Elemental analysis for [$(Ph_2C_2S_2)Pt(C{\equiv}NMe)_2$], Galbraith Labs. S85
Figure S117. ^{1}H NMR spectrum (CD_2Cl_2) of [$(Ph_2C_2S_2)Pt(C{\equiv}NCH_2C_6H_5)_2$]. S86
Figure S118. ^{13}C NMR spectrum (CD_2Cl_2) of [$(Ph_2C_2S_2)Pt(C{\equiv}NCH_2C_6H_5)_2$]. S86
Figure S119. Solution IR spectrum (CH_2Cl_2) of [$(Ph_2C_2S_2)Pt(C{\equiv}NCH_2C_6H_5)_2$]. S87
Figure S120. UV-vis spectrum (CH_2Cl_2) of [$(Ph_2C_2S_2)Pt(C{\equiv}NCH_2C_6H_5)_2$]. S87
Figure S121. Cyclic voltammogram (CH_2Cl_2) of [$(Ph_2C_2S_2)Pt(C{\equiv}NCH_2C_6H_5)_2$] at 50 mV/sec with [$^{n}Bu_4N$][$PF_6$] supporting electrolyte. S88
Figure S122. Elemental analysis for [$(Ph_2C_2S_2)Pt(C{\equiv}NCH_2C_6H_5)_2$], Kolbe Microanal. Lab. S88
Figure S123. ^{1}H NMR spectrum (CD_2Cl_2) of [$(Ph_2C_2S_2)Pt(C{\equiv}NCy)_2$]. S89
Figure S124. ^{13}C NMR spectrum (CD_2Cl_2) of [$(Ph_2C_2S_2)Pt(C{\equiv}NCy)_2$]. S89
Figure S125. Solution IR spectrum (CH_2Cl_2) of [$(Ph_2C_2S_2)Pt(C{\equiv}NCy)_2$]. S90
Figure S126. UV-vis spectrum (CH_2Cl_2) of [$(Ph_2C_2S_2)Pt(C{\equiv}NCy)_2$]. S90
Figure S127. Cyclic voltammogram (CH_2Cl_2) of [$(Ph_2C_2S_2)Pt(C{\equiv}NCy)_2$] at 50 mV/sec with [$^{n}Bu_4N$][$PF_6$] supporting electrolyte. S91
Figure S128. ^{1}H NMR spectrum (CD_2Cl_2) of [$(Ph_2C_2S_2)Pt(C{\equiv}N^{t}Bu)_2$]. S92
Figure S129. Solution IR spectrum (CH_2Cl_2) of [$(Ph_2C_2S_2)Pt(C{\equiv}N^{t}Bu)_2$]. S92
Figure S130. UV-vis spectrum (CH_2Cl_2) of [$(Ph_2C_2S_2)Pt(C{\equiv}N^{t}Bu)_2$]. S93
Figure S131. Cyclic voltammogram (CH_2Cl_2) of [$(Ph_2C_2S_2)Pt(C{\equiv}N^{t}Bu)_2$] at 50 mV/sec with [$^{n}Bu_4N$][$PF_6$] supporting electrolyte. S93
Figure S132. Elemental analysis for [$(Ph_2C_2S_2)Pt(C{\equiv}NCH_2C_6H_5)_2$], Kolbe Microanal. Lab S94
Figure S133. ^{1}H NMR spectrum (CD_2Cl_2) of [$(Ph_2C_2S_2)Pt(C{\equiv}N\text{-}1\text{-}Ad)_2$]. S95
Figure S134. Solution IR spectrum (CH_2Cl_2) of [$(Ph_2C_2S_2)Pt(C{\equiv}N\text{-}1\text{-}Ad)_2$]. S95
Figure S135. UV-vis spectrum (CH_2Cl_2) of [$(Ph_2C_2S_2)Pt(C{\equiv}N\text{-}1\text{-}Ad)_2$]. S96
Figure S136. Cyclic voltammogram (CH_2Cl_2) of [$(Ph_2C_2S_2)Pt(C{\equiv}N\text{-}1Ad)_2$] S96
Figure S137. ^{1}H NMR spectrum in CD_2Cl_2 of [$[(Ph_2C_2S_2)Ni(C{\equiv}N^{t}Bu)_2]_2(\mu\text{-}Ag)_2$][$BF_4$]$_2$. S97
Figure S138. IR spectrum in CH_2Cl_2 of [$[(Ph_2C_2S_2)Ni(C{\equiv}N^{t}Bu)_2]_2(\mu\text{-}Ag)_2$][$BF_4$]$_2$. S97
Figure S139. UV-vis spectrum in CH_2Cl_2 of [$[(Ph_2C_2S_2)Ni(C{\equiv}N^{t}Bu)_2]_2(\mu\text{-}Ag)_2$][$BF_4$]$_2$. S98
Figure S140. ^{1}H NMR spectrum in CD_2Cl_2 of [$[(Ph_2C_2S_2)Pt(C{\equiv}N^{t}Bu)_2]_2$][$SbCl_6$]$_2$. S98
Figure S141. IR spectrum in CH_2Cl_2 of [$[(Ph_2C_2S_2)Pt(C{\equiv}N^{t}Bu)_2]_2$][$SbCl_6$]$_2$. S99
Figure S142. UV-vis spectrum in CH_2Cl_2 of [$[(Ph_2C_2S_2)Pt(C{\equiv}N^{t}Bu)_2]_2$][$SbCl_6$]$_2$. S99
Figure S143. ^{1}H NMR spectrum in CD_2Cl_2 of [(2,6-Me_2py)Ni(μ_2-η^1,η^1-S′,η^1-S″-C_2Ph_2)]$_2$. S100
Figure S144. Calculated and experimental UV-vis spectrum in CH_2Cl_2 of [(2,6-Me_2py)Ni(μ_2-η^1,η^1-S′,η^1-S″-C_2Ph_2)]$_2$. S100
Figure S145. CV in CH_2Cl_2 of [(2,6-Me_2py)Ni(μ_2-η^1,η^1-S′,η^1-S″-C_2Ph_2)]$_2$ with S101

Table of Contents, Continued

[Bu_4N][PF_6] supporting electrolyte.

Figure S146. Differential pulse voltammogram in CH_2Cl_2 of [(2,6-Me_2py)Ni(μ_2-η^1,η^1-S′,η^1-S″-C_2Ph_2)]$_2$ with [Bu_4N][PF_6] supporting electrolyte. S101

Figure S147. ^{1}H NMR spectrum in CD_2Cl_2 of [($Ph_2C_2S_2$)Ni(C≡NMe)(PPh_3)]. S102

Figure S148. ^{1}H NMR spectrum in CD_2Cl_2 of [[($Ph_2C_2S_2$)Ni(C≡NMe)(PPh_3)]. S102

Figure S149. IR spectrum in CH_2Cl_2 of [($Ph_2C_2S_2$)Ni(C≡NMe)(PPh_3)]. S103

Figure S150. UV-vis spectrum in CH_2Cl_2 of [($Ph_2C_2S_2$)Ni(C≡NMe)(PPh_3)]. S103

Figure S151. ^{1}H NMR spectrum in CD_2Cl_2 of [($Ph_2C_2S_2$)Ni(C≡NMe)(PMe_3)]. S104

Figure S152. ^{13}C NMR spectrum in CD_2Cl_2 of [($Ph_2C_2S_2$)Ni(C≡NMe)(PMe_3)]. S104

Figure S153. ^{31}P NMR spectrum in CD_2Cl_2 of [($Ph_2C_2S_2$)Ni(C≡NMe)(PMe_3)]. S105

Figure S154. IR spectrum in CH_2Cl_2 of [($Ph_2C_2S_2$)Ni(C≡NMe)(PMe_3)]. S105

Figure S155. UV-vis spectrum in CH_2Cl_2 of [($Ph_2C_2S_2$)Ni(C≡NMe)(PMe_3)]. S106

Figure S156. ^{1}H NMR spectrum in CD_2Cl_2 of [($Ph_2C_2S_2$)Ni(C≡NMe)]$_2$(μ-1,4-dppb). S107

Figure S157. ^{31}P NMR spectrum in CD_2Cl_2 of [($Ph_2C_2S_2$)Ni(C≡NMe)]$_2$(μ-1,4-dppb). S107

Figure S158. IR spectrum in CH_2Cl_2 of [($Ph_2C_2S_2$)Ni(C≡NMe)]$_2$(μ-1,4-dppb). S108

Figure S159. UV-vis spectrum in CH_2Cl_2 of [($Ph_2C_2S_2$)Ni(C≡NMe)]$_2$(μ-1,4-dppb). S108

Figure S160. Cyclic voltammogram in CH_2Cl_2 of [($Ph_2C_2S_2$)Ni(C≡NMe)]$_2$(μ-1,4-dppb) with [Bu_4N][PF_6] supporting electrolyte. S109

Figure S161. DPV in CH_2Cl_2 of [($Ph_2C_2S_2$)Ni(C≡NMe)]$_2$(μ-1,4-dppb) with [Bu_4N][PF_6]. S109

Figure S162. ^{1}H NMR spectrum in CD_2Cl_2 of [($Ph_2C_2S_2$)Pd(C≡NMe)]$_2$(μ-1,4-dppb). S110

Figure S163. ^{31}P NMR spectrum in CD_2Cl_2 of [($Ph_2C_2S_2$)Pd(C≡NMe)]$_2$(μ-1,4-dppb). S110

Figure S164. IR spectrum in CH_2Cl_2 of [($Ph_2C_2S_2$)Pd(C≡NMe)]$_2$(μ-1,4-dppb). S111

Figure S165. UV-vis spectrum in CH_2Cl_2 of [($Ph_2C_2S_2$)Pd(C≡NMe)]$_2$(μ-1,4-dppb). S111

Figure S166. Cyclic voltammogram in CH_2Cl_2 of [($Ph_2C_2S_2$)Pd(C≡NMe)]$_2$(μ-1,4-dppb) with [Bu_4N][PF_6] supporting electrolyte. S112

Figure S167. DPV in CH_2Cl_2 of [($Ph_2C_2S_2$)Pd(C≡NMe)]$_2$(μ-1,4-dppb) with [Bu_4N][PF_6] supporting electrolyte. S112

Figure S168. ^{1}H NMR spectrum in CD_2Cl_2 of [($Ph_2C_2S_2$)Pt(C≡NMe)]$_2$(μ-1,4-dppb). S113

Figure S169. ^{31}P NMR spectrum in CD_2Cl_2 of [($Ph_2C_2S_2$)Pt(C≡NMe)]$_2$(μ-1,4-dppb). S113

Figure S170. IR spectrum in CH_2Cl_2 of [($Ph_2C_2S_2$)Pt(C≡NMe)]$_2$(μ-1,4-dppb). S114

Figure S171. UV-vis spectrum in CH_2Cl_2 of [($Ph_2C_2S_2$)Pt(C≡NMe)]$_2$(μ-1,4-dppb). S114

Figure S172. Cyclic voltammogram in CH_2Cl_2 of [($Ph_2C_2S_2$)Pt(C≡NMe)]$_2$(μ-1,4-dppb) with [Bu_4N][PF_6] supporting electrolyte. S115

Figure S173. DPV in CH_2Cl_2 of [($Ph_2C_2S_2$)Pt(C≡NMe)]$_2$(μ-1,4-dppb) with [Bu_4N][PF_6] supporting electrolyte. S115

Figure S174. ^{1}H NMR spectrum in CD_2Cl_2 of [Et_4N][($Ph_2C_2S_2$)Pd(C≡NMe)(CN)]. S116

Figure S175. IR spectrum in CH_2Cl_2 of [Et_4N][($Ph_2C_2S_2$)Pd(C≡NMe)(CN)]. S116

Figure S176. UV-vis spectrum in CH_2Cl_2 of [Et_4N][($Ph_2C_2S_2$)Pd(C≡NMe)(CN)]. S117

Figure S177. CV in CH_2Cl_2 of [Et_4N][($Ph_2C_2S_2$)Pd(C≡NMe)(CN)] with [Bu_4N][PF_6]. S117

Figure S178. ^{1}H NMR spectrum in CD_2Cl_2 of [Et_4N][($Ph_2C_2S_2$)Pt(C≡NMe)(CN)]. S118

Figure S179. ^{13}C NMR spectrum in CD_2Cl_2 of [Et_4N][($Ph_2C_2S_2$)Pt(C≡NMe)(CN)]. S118

Figure S180. IR spectrum in CH_2Cl_2 of [Et_4N][($Ph_2C_2S_2$)Pt(C≡NMe)(CN)]. S119

Figure S181. UV-vis spectrum in CH_2Cl_2 of [Et_4N][($Ph_2C_2S_2$)Pt(C≡NMe)(CN)]. S119

Figure S182. CV in CH_2Cl_2 of [Et_4N][($Ph_2C_2S_2$)Pt(C≡NMe)(CN)] with [Bu_4N][PF_6]. S120

Figure S183. ^{1}H NMR spectrum in CD_2Cl_2 of [($Ph_2C_2S_2$)Pd(C≡NMe)(IPr)]. S121

Table of Contents, Continued

Figure S184. ^{13}C NMR spectrum in CD_2Cl_2 of [($Ph_2C_2S_2$)Pd(C≡NMe)(IPr)]. S121
Figure S185. IR spectrum in CH_2Cl_2 of [($Ph_2C_2S_2$)Pd(C≡NMe)(IPr)]. S122
Figure S186. UV-vis spectrum in CH_2Cl_2 of [($Ph_2C_2S_2$)Pd(C≡NMe)(IPr)]. S122
Figure S187. CV in CH_2Cl_2 of [($Ph_2C_2S_2$)Pd(C≡NMe)(IPr)] with [Bu_4N][PF_6]. S123
Figure S188. ^{1}H NMR spectrum in CD_2Cl_2 of [($Ph_2C_2S_2$)Pt(C≡NMe)((C(NMe)(IPr))]. S124
Figure S189. IR spectrum in CH_2Cl_2 of [($Ph_2C_2S_2$)Pt(C≡NMe)((C(NMe)(IPr))]. S124
Figure S190. UV-vis spectrum in CH_2Cl_2 of [($Ph_2C_2S_2$)Pt(C≡NMe)((C(NMe)(IPr))]. S125
Figure S191. Cyclic voltammogram in CH_2Cl_2 of [($Ph_2C_2S_2$)Pt(C≡NMe)((C(NMe)(IPr))] with [Bu_4N][PF_6] supporting electrolyte. S125
Figure S192. ^{1}H NMR spectrum (CD_2Cl_2) of [($Ph_2C_2S_2$)Ni(C≡NMe)((C(NHMe)(NMe_2))]. S126
Figure S193. ^{13}C NMR spectrum in CD_2Cl_2 for [($Ph_2C_2S_2$)Ni(C≡NMe)((C(NHMe)(NMe_2))]. S126
Figure S194. IR spectrum in CH_2Cl_2 of [($Ph_2C_2S_2$)Ni(C≡NMe)((C(NHMe)(NMe_2))]. S127
Figure S195. UV-vis spectrum in CH_2Cl_2 of [($Ph_2C_2S_2$)Ni(C≡NMe)((C(NHMe)(NMe_2))]. S127
Figure S196. Cyclic voltammogram in CH_2Cl_2 of [($Ph_2C_2S_2$)Ni(C≡NMe)((C(NHMe)(NMe_2))] with [Bu_4N][PF_6] S128

Procedures for Crystal Growth, Collection and Processing of Diffraction Data, and Solving and Refining of Structures.

All crystals used in X-ray diffraction data collections were obtained by the vial-in-a-vial vapor diffusion technique. The following solvent pairs provide specific combinations successfully employed as solvent/diffusing vapor for crystal growth: $[(Ph_2C_2S_2)Ni(C{\equiv}NCH_2C_6H_5)_2]$ ($ClCH_2CH_2Cl$/hexanes), $[(Ph_2C_2S_2)Ni(C{\equiv}NCy)_2]$ (CH_2Cl_2/Et_2O), $[(Ph_2C_2S_2)Ni(C{\equiv}N^tBu)_2]$ (CH_2Cl_2/*n*-pentane), $[(Ph_2C_2S_2)Ni(C{\equiv}N\text{-}1\text{-adamantyl})_2]\cdot\frac{1}{2}Et_2O$ (CH_2Cl_2/Et_2O), $[(Ph_2C_2S_2)Ni(C{\equiv}NPh)_2]$ (CH_2Cl_2/Et_2O), $[(Ph_2C_2S_2)Pd(C{\equiv}NCH_3)_2]$ (CH_2Cl_2/Et_2O), $[(Ph_2C_2S_2)Pd(C{\equiv}NCH_2C_6H_5)_2]$ (CH_2Cl_2/*n*-pentane), $[(Ph_2C_2S_2)Pd(C{\equiv}NCy)_2]$ (CH_2Cl_2/*n*-pentane), $[(Ph_2C_2S_2)Pd(C{\equiv}N\text{-}1\text{-adamantyl})_2]\cdot\frac{1}{2}CH_2Cl_2\cdot\frac{1}{2}Et_2O$ (CH_2Cl_2/Et_2O), $[(Ph_2C_2S_2)Pd(C{\equiv}NPh)_2]$ (CH_2Cl_2/Et_2O), $[(Ph_2C_2S_2)Pt(C{\equiv}NCH_3)_2]\cdot\frac{1}{2}ClCH_2CH_2Cl$ ($ClCH_2CH_2Cl$/hexanes), $[(Ph_2C_2S_2)Pt(C{\equiv}NCH_2C_6H_5)_2]$ ($ClCH_2CH_2Cl$/hexanes), $[(Ph_2C_2S_2)Pt(C{\equiv}NCy)_2]$ (CH_2Cl_2/Et_2O), $[(Ph_2C_2S_2)Pt(C{\equiv}N^tBu)_2]$ ($ClCH_2CH_2Cl$/hexanes), $[(Ph_2C_2S_2)Pt(C{\equiv}N\text{-}1\text{-adamantyl})_2]\cdot Et_2O$ (CH_2Cl_2/Et_2O), $[((CH_3O\text{-}p\text{-}C_6H_4)_2C_2S_2)Ni(C{\equiv}N^tBu)_2]$ (CH_2Cl_2/Et_2O), $[(Ph_2C_2S_2)Pt(C{\equiv}N^tBu)_2]_2[SbCl_6]_2\cdot 2CH_2Cl_2$ (CH_2Cl_2/Et_2O), $[((Ph_2C_2S_2)Ni(C{\equiv}N^tBu)_2)_2(\mu\text{-}Ag)_2][BF_4]_2$ (CH_2Cl_2/Et_2O), $[(2,6\text{-}Me_2py)Ni(\mu_2\text{-}\eta^1,\eta^1\text{-}S',\eta^1\text{-}S''\text{-}C_2Ph_2)]_2$ ($ClCH_2CH_2Cl$/hexanes), $[(Ph_2C_2S_2)Ni(CNMe)(PMe_3)]$ ($ClCH_2CH_2Cl$/hexanes), $[(Ph_2C_2S_2)Ni(CNMe)(PPh_3)]$ ($ClCH_2CH_2Cl$/hexanes), $[(Ph_2C_2S_2)Ni(CNMe)]_2(\mu\text{-}1,4\text{-}(Ph_2P)_2C_6H_4)]\cdot ClCH_2CH_2Cl$ ($ClCH_2CH_2Cl$/hexanes), $[(Ph_2C_2S_2)Pd(CNMe)]_2(\mu\text{-}1,4\text{-}(Ph_2P)_2C_6H_4)]\cdot 2ClCH_2CH_2Cl$ ($ClCH_2CH_2Cl$/hexanes), $[(Ph_2C_2S_2)Pt(CNMe)]_2(\mu\text{-}1,4\text{-}(Ph_2P)_2C_6H_4)]\cdot 2ClCH_2CH_2Cl$ ($ClCH_2CH_2Cl/^tBuOMe$), $[Et_4N][(Ph_2C_2S_2)Pd(CN)(CNMe)]$ ($MeCN/Et_2O$), $[Et_4N][(Ph_2C_2S_2)Pt(CN)(CNMe)]$ ($MeCN/^tBuOMe$), $[(Ph_2C_2S_2)Pd(IPr)(CNMe)]\cdot ClCH_2CH_2Cl$ ($ClCH_2CH_2Cl$/hexanes), $[(Ph_2C_2S_2)Pt(CNMe)(C(IPr)NMe)]$ (EtOAc/^{t}BuOMe), $[(Ph_2C_2S_2)Ni(CNMe)(C(NHMe)(NMe_2))]$ ($ClCH_2CH_2Cl/^tBuOMe$). The color and morphology of each crystal are presented in **Tables S1-S6**.

All crystals were coated with paratone oil and mounted on the end of a nylon loop attached to the end of the goniometer. Data were obtained at a temperature of 100, 150 or 158 K that was maintained by a cold nitrogen stream supplied under the control of an Oxford Cryostream system. The data collection instrument was either a Bruker D8 Venture Photon 100 instrument, the radiation source for which was a Cu Incoatec I microfocus source generating X-rays with λ =

1.54178 nm, or a Bruker Smart APEX CCD diffractometer equipped with a Mo fine-focus sealed tube providing radiation at λ = 0.71073 nm. The data sets obtained with the D8 Venture were hemispheres of data comprised from the following assemblies of ω-scan frames and frame times: $[(Ph_2C_2S_2)Ni(C{\equiv}NCH_2C_6H_5)_2]$: 6 sets of 326 or 330 frames at 10 or 20 sec/frame; $[(Ph_2C_2S_2)Ni(C{\equiv}N^tBu)_2]$: 6 sets of 326 or 330 frames at 30 or 60 sec/frame; $[(Ph_2C_2S_2)Pd(C{\equiv}NCH_2C_6H_5)_2]$: 6 sets of 326 or 330 frames at 15 or 20 sec/frame; $[(Ph_2C_2S_2)Pt(C{\equiv}N^tBu)_2]$: 12 sets of 332 frames at 10 sec/frame; $[((CH_3O\text{-}p\text{-}C_6H_4)_2C_2S_2)Ni(C{\equiv}N^tBu)_2]$: 15 sets of 326 or 330 frames at 20 sec/frame; $[(Ph_2C_2S_2)Ni(CNMe)(PPh_3)]$: 3 sets of 363 frames at 10 or 20 sec/frame; $[(Ph_2C_2S_2)Ni(CNMe)]_2(\mu\text{-}1,4\text{-}(Ph_2P)_2C_6H_4)]\cdot ClCH_2CH_2Cl$: 7 sets of 367-371 frames at 10 or 20 sec/frame. The data sets were collected with the APEX II diffractometer implemented one of the following programmed routines: (1) Three sets of 363 frames in ω (0.5°/scan) with φ held constant at 0, 120, and then 240°; (2) Three sets of 606 frames in ω (0.3°/scan) with φ held constant at 0, 120, and then 240°; (3) Three sets of 400 frames in ω (0.5°/scan), collected at φ = 0.00, 90.00 and 180.00° and two sets of 800 frames in φ (0.45°/scan) collected with ω constant at -30.00 and 210.00°. The data collection program and frame time used for these data sets were as follows: $[(Ph_2C_2S_2)Ni(C{\equiv}NCy)_2]$: Routine 1, 60 sec; $[(Ph_2C_2S_2)Ni(C{\equiv}N\text{-}1\text{-adamantyl})]\cdot ½Et_2O$: Routine 3, 20 sec; $[(Ph_2C_2S_2)Ni(C{\equiv}NPh)_2]$: Routine 3, 30 sec; $[(Ph_2C_2S_2)Pd(C{\equiv}NMe)_2]$: Routine 3, 10 sec; $[(Ph_2C_2S_2)Pd(C{\equiv}NCy)_2]$: Routine 3, 10 sec; $[(Ph_2C_2S_2)Pd(C{\equiv}N\text{-}1\text{-adamantyl})_2]\cdot ½CH_2Cl_2\cdot ½Et_2O$: Routine 3, 10 sec; $[(Ph_2C_2S_2)Pd(C{\equiv}NPh)_2]$: Routine 3, 10 sec; $[(Ph_2C_2S_2)Pt(C{\equiv}NMe)_2]\cdot ½ClCH_2CH_2Cl$: Routine 3, 20 sec; $[(Ph_2C_2S_2)Pt(C{\equiv}NCH_2C_6H_5)_2]$: Routine 3, 10 sec; $[(Ph_2C_2S_2)Pt(C{\equiv}NCy)_2]$: Routine 3, 20 sec; $[(Ph_2C_2S_2)Pt(C{\equiv}N\text{-}1\text{-adamantyl})_2]\cdot Et_2O$: Routine 3, 10 sec; $[(Ph_2C_2S_2)Pt(C{\equiv}N^tBu)_2]_2[SbCl_6]_2\cdot 2CH_2Cl_2$: Routine 1, 120 sec; $[[(Ph_2C_2S_2)Ni(C{\equiv}N^tBu)_2]_2(\mu\text{-}Ag_2)][BF_4]_2$: Routine 3, 10 sec; $[(2,6\text{-}Me_2py)Ni(\mu_2\text{-}\eta^1,\eta^1\text{-}S',\eta^1\text{-}S''\text{-}C_2Ph_2)]_2$: Routine 3, 20 sec; $[(Ph_2C_2S_2)Ni(CNMe)(PMe_3)]$: Routine 3, 60 sec; $[(Ph_2C_2S_2)Pd(CNMe)]_2(\mu\text{-}1,4\text{-}(Ph_2P)_2C_6H_4)]\cdot 2ClCH_2CH_2Cl$: Routine 3, 20 sec; $[(Ph_2C_2S_2)Pt(CNMe)]_2(\mu\text{-}1,4\text{-}(Ph_2P)_2C_6H_4)]\cdot 2ClCH_2CH_2Cl$: Routine 3, 10 sec; $[Et_4N][(Ph_2C_2S_2)Pd(CN)(CNMe)]$: Routine 3, 20 sec; $[Et_4N][(Ph_2C_2S_2)Pt(CN)(CNMe)]$: Routine 3, 20 sec; $[(Ph_2C_2S_2)Pd(IPr)(CNMe)]\cdot ClCH_2CH_2Cl$: Routine 3, 10 sec; $[(Ph_2C_2S_2)Pt(CNMe)(C(IPr)NMe)]$: Routine 3, 20 sec; $[(Ph_2C_2S_2)Ni(CNMe)(C(NHMe)(NMe_2))]$: Routine 1, 40 sec.

All data were collected under control of *APEX2*[1a-1b] or *APEX3*[1c] software packages. Raw data were reduced to F^2 values using the *SAINT*[2] software, and a global refinement of unit cell parameters was performed using ~4,000–9,900 selected reflections from the full data set. For [(pdt)Ni($CNCH_2C_6H_5$)$_2$] and [(pdt)Pd($CNCH_2C_6H_5$)$_2$], the data were corrected for absorption using a face-indexing (numerical) method. All other data sets were corrected for absorption on the basis of multiple measurements of symmetry equivalent reflections with the use of *SADABS*,[3] as described by Krause *et al*.[4] All structure solutions were obtained by direct methods using *SHELXT*,[5] while refinements were accomplished by full-matrix least-squares procedures using *SHELXL*.[6] Both the *SHELXS* and *SHELXL* programs are incorporated into the *SHELXTL*[7] and *APEX2*/*APEX3*[1] software suites.

All structure refinements were routine except as noted: (**1**) For [($Ph_2C_2S_2$)Ni(C≡NCy)$_2$], The asymmetric unit consists of one full molecule and two half molecules, each of which has crystallographically-imposed C_2 symmetry. In the full molecule, one of the cyclohexyl groups is disordered over two alternate chair conformations in an 82/18 ratio. The two components of the disorder have been refined with restraints such that their geometries are comparable. (**2**) For [($Ph_2C_2S_2$)Ni(C≡N-1-adamantyl)$_2$]·½Et_2O, one ethyl group of the lattice diethyl ether is disordered over two resolved sites. The components of the disorder were refined subject to restraints such that their geometries are approximately equal. Additional small areas of density which could not be satisfactorily modeled as lattice solvent have been removed with the *SQUEEZE* option that is available in *PLATON*.[8] The adamantyl group C63-C72 appeared to be slightly rotationally disordered, but attempts to model the disorder with two rigid body components were unsuccessful. (**3**) In [($Ph_2C_2S_2$)Pd($CNMe_2$)$_2$], both phenyl rings and one isocyanide ligand are disordered over two resolved sites in approximately equal amounts. The phenyl rings were refined as rigid hexagons, while the isocyanide is restrained to be approximately linear. (**4**) For [($Ph_2C_2S_2$)Pd(C≡N-1-adamantyl)$_2$]·½CH_2Cl_2·½Et_2O, one of the adamantyl groups of one isonitrile ligand is disordered over two positions related by rotation. A satisfactory split atom model is found with a 59:41 distribution. An interstitial space is occupied by solvent molecule(s). The electron density map appears consistent with the presence of both CH_2Cl_2 and Et_2O, each at half occupancy. The Et_2O molecule occurs near an inversion center, which does not permit placement of H atoms using HFIX. Hydrogen atoms are therefore placed at calculated positions and held in place using DFIX restraints. (**5**) In the case of [($Ph_2C_2S_2$)Pt(C≡N-1-adamantyl)$_2$]·Et_2O,

one of the two adamantyl substituents on the dithiolene ligand was disordered between two orientations related to one another by a ~60 degree rotation about the carbon-carbon single bond joining the adamantyl group to the dithiolene backbone. A single molecule of diethyl ether was evident in the asymmetric unit. It was disordered over two positions and refined as a best fit distribution by the refinement software. One of the carbon-carbon bonds of the diethyl ether molecule was restrained to a chemically reasonable value. (**6**) For $[[(Ph_2C_2S_2)Ni(C{\equiv}N^tBu)_2]_2(\mu\text{-}Ag_2)][BF_4]_2$, density associated with a severely disordered molecule of THF in the lattice was removed with the SQUEEZE option in PLATON.[8]

In all the structures, hydrogen atoms were added in calculated positions and included as riding contributions with isotropic displacement parameters 1.2-1.5 times those of the carbon atoms to which they were attached. For $[(Ph_2C_2S_2)Ni(CNMe)(C(NHMe)(NMe_2))]$, the hydrogen atom attached to nitrogen was placed in a location derived from a difference map, and its coordinates were adjusted to give N–H = 0.91 Å. Thermal ellipsoid images have been created with the use of *XP*, which also is part of the *SHELXTL* package. All structures were checked for overlooked symmetry and other errors by the checkCIF service provided by the International Union of Crystallography.[9] Final unit cell data and refinement statistics are collected in **Tables S1**-**S4**.

Computational Procedures

The density functional theory (DFT) calculations were carried out at the Becke, 3-Parameter, Lee-Yang-Parr (B3LYP) level of theory.[10] Frequency calculations were done to confirm the validity of all structures. For the transition metals (nickel, palladium and platinum), a double-ζ (DZ) basis set with an effective electron core potential (LANL2DZ ECP) was implemented.[11] The 6-31G(d,p) basis set was chosen for the light main group elements, whereas the triple-ζ (TZVP) was used for the heavier elements (S and P), and a Gaussian split valence (SV) basis set[13] was used for the hydrogen atoms. The Mulliken population and atomic orbital composition analyses were calculated via a fragmentation approach using QMForge,[14] and all molecular orbital images were rendered using jmol[15] at the 0.03 or 0.04 contour level.

References

(**1**) (**a**) *APEX2*, Bruker-AXS, Inc., Madison, Wisconsin, USA, 2014. (**b**) *APEX2*, Bruker-AXS, Inc., Madison, Wisconsin, USA, 2015. (**c**) *APEX3*, Bruker-AXS, Inc., Madison, Wisconsin, USA, 2016.

(**2**) (**a**) *SAINT*, Bruker AXS, Inc., Madison, Wisconsin, 2014. (**b**) *SAINT*, Bruker AXS, Inc., Madison, Wisconsin, 2015. (**c**) *SAINT*, Bruker AXS, Inc., Madison, Wisconsin, 2016.

(**4**) Krause, L.; Herbst-Irmer, R.; Sheldrick, G.M.; Stalke; D. *J. Appl. Cryst.* **2015**, *48*, 3-10.

(**3**) (**a**) Sheldrick, G. M. *SADABS*, Universität Göttingen, Göttingen, Germany, 2014. (**b**) Sheldrick, G. M. *SADABS*, Universität Göttingen, Göttingen, Germany, 2015. (**c**) Sheldrick, G. M. *SADABS*, Universität Göttingen, Göttingen, Germany, 2016.

(**5**) Sheldrick, G. M. *"SHELXT – Integrated Space-Group and Crystal-Structure Determination." Acta Crystallogr., Sect A* **2015**, *71*, 3-8.

(**6**) (**a**) Sheldrick, G. M. *SHELXL-2014/7*. University of Göttingen, Göttingen, Germany, 2014. (**b**) Sheldrick, G. M. *SHELXL*. University of Göttingen, Göttingen, Germany, 2015. (**c**) Sheldrick, G. M. *SHELXL-2016/6* University of Göttingen, Göttingen, Germany, 2016. (**d**) Sheldrick, G. M. *SHELXL-2018/1* University of Göttingen, Göttingen, Germany, 2018.

(**7**) (**a**) *SHELXTL*, Bruker-AXS, Madison, WI, 2014. (**b**) *SHELXTL*, Bruker-AXS, Madison, WI, 2015. (**c**) *SHELXTL*, Bruker-AXS, Madison, WI, 2016.

(**8**) Spek, A. L. *PLATON, A Multipurpose Crystallographic Tool*, Utrecht University, Utrecht, The Netherlands, 2007, 2009.

(**9**) See http://checkcif.iucr.org/

(**10**) (**a**) Becke, A. D. Density-Functional Thermochemistry. III. The Role of Exact Exchange. *J. Chem. Phys.* **1993**, *98*, 5648-5652. (**b**) Lee, C. T.; Yang, W. T.; Parr, R. G. Development of the Colle-Salvetti Correlation-Energy Formula into a Functional of the Electron Density *Phys. Rev. B* **1988**, *37*, 785-789.

(**11**) https://bse.pnl.gov/bse/portal (Accessed 12 October 2019).

(**12**) Schäfer, A.; Horn, H.; Ahlrichs, R. Fully Optimized Contracted Gaussian Basis Sets for Atoms Li to Kr. *J. Chem. Phys.* **1992**, *97*, 2571-2577.

(**13**) Tenderholt, A. L. QMForge: A Tool for Analyzing the Output of QM Calculations, Version 2.4; *Http://Qmforge.Sourceforge.Net* (Accessed March 10, 2020).

(**14**) Jmol: An Open-Source Java Viewer for Chemical Structures in 3D. *Http://Www.Jmol.Org/* (Accessed March 10, 2020).

Table S1. Unit Cell and Refinement Data for [(pdt)Ni(C≡NR)$_2$] Compounds.

compound	[(pdt)Ni(C≡NBn)$_2$]	[(pdt)Ni(C≡NCy)$_2$]	[(pdt)Ni(C≡N^{t}Bu)$_2$]	[(pdt)Ni(C≡N-1-Ad)$_2$]	[(pdt)Ni(C≡NPh)$_2$]
compound #	**1b**	**1c**	**1d**	**1e**	**1f**
structure code	JPD932_0m_a	JPD700_0m_a	JPD656_0m_a	JPD707_0m_sq	JPD682_0m_a
solvent	none	none	none	0.5Et$_2$O	none
formula	$C_{30}H_{24}N_2NiS_2$	$C_{28}H_{32}N_2NiS_2$	$C_{24}H_{28}N_2NiS_2$	$C_{38}H_{45}N_2NiO_{0.5}S_2$	$C_{28}H_{30}N_2NiS_2$
fw	535.34	519.38	467.31	660.59	507.29
temperature, K	150	150	150	150	150
wavelength, Å	1.54178	0.71073	1.54178	0.71073	0.71073
2θ range, deg.	7.940 -144.332	2.552 - 56.548	7.098 - 144.764	3.400 - 58.422	2.900 – 58.394
crystal system	triclinic	monoclinic	monoclinic	triclinic	triclinic
space group	$P\bar{1}$	$P2/c$	$C2/c$	$P\bar{1}$	$P\bar{1}$
a, Å	10.5799(3)	14.3336(12)	20.3824(4)	10.164(3)	9.2344(19)
b, Å	11.4092(4)	15.9644(14)	15.9160(3)	16.458(5)	9.4710(19)
c, Å	11.6103(4)	22.8241(19)	7.5564(1)	21.738(6)	14.668(3)
α, deg.	96.749(1)	90	90	99.118(4)	73.27(3)
β, deg.	101.545(1)	99.157(1)	101.106(1)	96.435(4)	88.52(3)
γ, deg.	110.493(1)	90	90	92.857(4)	82.31(3)
volume, Å^3	1259.05(7)	5156.2(8)	2405.44(7)	3559.2(18)	1217.4(5)
Z	2	8	4	4	2
density, g/cm^3	1.412	1.338	1.290	1.233	1.384
μ, mm^{-1}	2.821	0.933	2.864	0.692	0.987
crystal size	0.239 x 0.099 x 0.051	0.040 x 0.140 x 0.150	0.050 x 0.104 x 0.170	0.070 x 0.200 x 0.230	0.150 x 0.220 x 0.370
color, habit	light green column	yellow plate	yellow column	blue plate	dark green block
limiting indices, h	$-13 \le h \le 12$	$-18 \le h \le 18$	$-25 \le h \le 21$	$-13 \le h \le 13$	$-12 \le h \le 12$
limiting indices, k	$-14 \le k \le 12$	$-21 \le k \le 21$	$-18 \le k \le 18$	$-22 \le k \le 22$	$-12 \le k \le 12$
limiting indices, l	$-13 \le l \le 14$	$-30 \le l \le 30$	$-9 \le l \le 9$	$-29 \le l \le 29$	$-19 \le l \le 20$
reflections collected	9684	48314	9090	18943	23325
independent data	4673	12677	2346	18943	6420
restraints	0	1	0	16	0
parameters refined	316	617	135	787	298
GooF[a]	1.052	1.030	1.088	1.124	1.082
R1,[b,c] wR2[d,c]	0.0326, 0.0797	0.0561, 0.1165	0.0301, 0.0713	0.0628, 0.1730	0.0408, 0.1129
R1,[b,e] wR2[d,e]	0.0355, 0.0818	0.1122, 0.1371	0.0358, 0.0747	0.0995, 0.1929	0.0471, 0.1169
largest diff. peak, e·Å^{-3}	0.218	1.028	0.412	1.705	1.422
largest diff. hole, e·Å^{-3}	–0.498	–0.399	–0.168	–0.564	–0.394
abs structure parameter	-		-	-	-

[a]GooF = $\{\Sigma[w(F_o^2 - F_c^2)^2]/(n-p)\}^{½}$, where n= number of reflections and p is the total number of parameters refined; [b]R1 = $\Sigma||F_o| - |F_c||/\Sigma|F_o|$; [c]R indices for data cut off at I > 2σ(I); [d]wR2 = $\{[\Sigma w(F_o^2 - F_c^2)^2/\Sigma w(F_o^2)^2\}^{1/2}$; $w = 1/[\sigma^2(F_o^2) + (xP)^2 + yP]$, where $P = (F_o^2 + 2F_c^2)/3$; [e]R indices for all data.

Table S2. Unit Cell and Refinement Data for [(pdt)Pd(C≡NR)$_2$] Compounds.

compound	[(pdt)Pd(C≡NMe)$_2$]	[(pdt)Pd(C≡NBn)$_2$]	[(pdt)Pd(C≡NCy)$_2$]	[(pdt)Pd(C≡N-1-Ad)$_2$]	[(pdt)Pd(C≡NPh)$_2$]
compound #	**2a**	**2b**	**2c**	**2e**	**2f**
structure code	JPD759_0m	JPD953_0m_a	JPD727_0m_a	JPD721_0m_a	JPD747_0m_a
solvent	none	none	none	0.5CH_2Cl_2·0.5Et_2O	none
formula	$C_{18}H_{16}N_2PdS_2$	$C_{30}H_{24}N_2PdS_2$	$C_{28}H_{32}N_2PdS_2$	$C_{38.50}H_{46}ClN_2O_{0.5}PdS_2$	$C_{28}H_{20}N_2PdS_2$
fw	430.85	583.03	567.07	750.74	554.98
temperature, K	100	150	100	100	100
wavelength, Å	0.71073	1.54178	0.71073	0.71073	0.71073
2θ range, deg.	4.072 - 58.754	6.724 - 149.156	3.130 - 60.432	3.264 - 58.840	3.314 - 60.274
crystal system	triclinic	triclinic	monoclinic	monoclinic	triclinic
space group	$P\bar{1}$	$P\bar{1}$	$P2_1/n$	$P2_1/c$	$P\bar{1}$
a, Å	8.8402(11)	10.3218(2)	7.9416(10)	10.6254(10)	9.9390(12)
b, Å	10.5718(13)	10.4872(2)	18.186(2)	22.433(2)	10.0502(12)
c, Å	11.4329(14)	13.3850(3)	18.800(2)	15.1307(14)	12.2946(14)
α, deg.	111.838(2)	82.789(1)	90	90	89.485(2)
β, deg.	99.332(2)	79.733(1)	97.636(2)	97.076(1)	88.690(2)
γ, deg.	110.298(2)	66.693(1)	90	90	82.968(2)
volume, Å^3	876.64(19)	1306.93(5)	2691.1(6)	3579.0(6)	1218.5(2)
Z	2	2	4	4	2
density, g/cm^3	1.632	1.482	1.400	1.393	1.513
μ, mm^{-1}	1.296	7.376	0.863	0.741	0.952
crystal size	0.060 x 0.190 x 0.300	0.086 x 0.144 x 0.193	0.146 x 0.197 x 0.434	0.070 x 0.180 x 0.310	0.238 x 0.339 x 0.538
color, habit	pink plate	red plate	orange prism	red plate	red-orange block
limiting indices, *h*	$-12 \le h \le 12$	$-12 \le h \le 12$	$-11 \le h \le 11$	$-14 \le h \le 14$	$-13 \le h \le 13$
limiting indices, *k*	$-14 \le k \le 14$	$-12 \le k \le 13$	$-25 \le k \le 25$	$-30 \le k \le 30$	$-14 \le k \le 13$
limiting indices, *l*	$-15 \le l \le 15$	$-15 \le l \le 16$	$-26 \le l \le 26$	$-20 \le l \le 20$	$-17 \le l \le 16$
reflections collected	17062	10161	52088	69671	23590
independent data	4688	4948	7636	9779	6659
restraints	20	0	0	8	0
parameters refined	210	316	298	485	298
GooF[a]	1.095	1.030	1.097	1.097	1.063
R1,[b,c] wR2[d,c]	0.0303, 0.0777	0.0284, 0.0713	0.0245, 0.0670	0.0464, 0.1295	0.0321, 0.0904
R1,[b,e] wR2[d,e]	0.0348, 0.0788	0.0296, 0.0724	0.0283, 0.0682	0.0654, 0.1382	0.0335, 0.0916
largest diff. peak, e·Å^{-3}	1.324	0.489	1.327	1.805	2.069
largest diff. hole, e·Å^{-3}	–0.647	–0.960	–0.239	–0.585	–1.576
abs struct parameter	-	-	-	-	-

[a]GooF = $\{\Sigma[w(F_o^2 - F_c^2)^2]/(n-p)\}^{½}$, where *n*= number of reflections and *p* is the total number of parameters refined; [b]R1 = $\Sigma||F_o| - |F_c||/\Sigma|F_o|$; [c]R indices for data cut off at I > 2σ(I); [d]wR2 = $\{[\Sigma w(F_o^2 - F_c^2)^2/\Sigma w(F_o^2)^2\}^{1/2}$; $w = 1/[\sigma^2(F_o^2) + (xP)^2 + yP]$, where $P = (F_o^2 + 2F_c^2)/3$; [e]R indices for all data.

Table S3. Unit Cell and Refinement Data for [(pdt)Pt(C≡NR)$_2$] Compounds.

compound	[(pdt)Pt(C≡NMe)$_2$]	[(pdt)Pt(C≡NBn)$_2$]	[(pdt)Pt(C≡NCy)$_2$]	[(pdt)Pt(C≡N^{t}Bu)$_2$]	[(pdt)Pt(C≡N-1-Ad)$_2$]
compound #	**3a**	**3b**	**3c**	**3d**	**3e**
structure code	JPD748_0m_a	JPD957_0m_a	JPD705_0m	JPD717_0m	JPD733_0m_a
solvent	0.5ClCH$_2$CH$_2$Cl	none	none	none	Et$_2$O
formula	$C_{19}H_{18}ClN_2PtS_2$	$C_{30}H_{24}N_2PtS_2$	$C_{28}H_{32}N_2PtS_2$	$C_{24}H_{28}N_2PtS_2$	$C_{40}H_{50}N_2OPtS_2$
fw	569.01	671.72	655.76	603.69	834.03
temperature, K	100	150	150	150	100
wavelength, Å	0.71073	0.71073	0.71073	1.54178	0.71073
2θ range, deg.	3.124 - 60.520	4.222 - 58.940	3.124 - 58.452	8.602 – 139.758	3.258 - 60.462
crystal system	triclinic	triclinic	monoclinic	monoclinic	monoclinic
space group	$P\bar{1}$	$P\bar{1}$	$P2_1/n$	$P2_1/n$	$P2_1/c$
a, Å	9.6182(9)	10.306(3)	7.9823(6)	10.9849	10.6520(8)
b, Å	13.6682(12)	10.524(3)	18.1725(13)	17.8057	22.3770(16)
c, Å	16.4171(15)	13.397(4)	18.9185(14)	13.0946	15.2159(11)
α, deg.	105.200(1)	82.934(4)	90	90	90
β, deg.	105.133(1)	79.976(4)	98.689(1)	106.003(1)	97.736(1)
γ, deg.	94.243(1)	66.669(3)	90	90	90
volume, Å^3	1986.9(3)	1311.6(6)	2712.8(3)	2461.97(9)	3593.9(5)
Z	4	2	4	4	4
density, g/cm^3	1.632	1.701	1.606	1.629	1.591
μ, mm^{-1}	1.902	5.530	5.344	12.325	4.054
crystal size	0.047 x 0.243 x 0.375	0.172 x 0.195 x 0.384	0.030 x 0.120 x 0.170	0.080 x 0.080 x 0.150	0.208 x 0.256 x 0.280
color, habit	yellow plate	yellow column	colorless plate	yellow block	pale yellow block
limiting indices, *h*	$-13 \le h \le 13$	$-14 \le h \le 14$	$-10 \le h \le 10$	$-13 \le h \le 13$	$-14 \le h \le 14$
limiting indices, *k*	$-19 \le k \le 19$	$-14 \le k \le 14$	$-24 \le k \le 24$	$-21 \le k \le 21$	$-30 \le k \le 31$
limiting indices, *l*	$-22 \le l \le 22$	$-18 \le l \le 18$	$-25 \le l \le 25$	$-15 \le l \le 15$	$-21 \le l \le 21$
reflections collected	35637	25558	52497	40566	69841
independent data	10889	7087	7314	4630	10154
restraints	0	0	0	0	1
parameters refined	455	316	298	269	430
GooF[a]	1.042	1.039	1.022	1.083	1.076
R1,[b,c] wR2[d,c]	0.0336, 0.0836	0.0256, 0.0572	0.0328, 0.0705	0.0214, 0.0514	0.0313, 0.0864
R1,[b,e] wR2[d,e]	0.0435, 0.0888	0.0315, 0.0582	0.0524, 0.0753	0.0235, 0.0524	0.0366, 0.0885
largest diff. peak, e·Å^{-3}	4.413	1.565	1.923	0.548	3.508
largest diff. hole, e·Å^{-3}	–2.246	–0.967	–1.054	–0.707	–1.114
abs struct parameter	-	-	-	-	-

[a]GooF = $\{\Sigma[w(F_o^2 - F_c^2)^2]/(n-p)\}^{½}$, where *n*= number of reflections and *p* is the total number of parameters refined; [b]R1 = $\Sigma||F_o| - |F_c||/\Sigma|F_o|$; [c]R indices for data cut off at I > 2σ(I); [d]wR2 = $\{[\Sigma w(F_o^2 - F_c^2)^2/\Sigma w(F_o^2)^2\}^{1/2}$; $w = 1/[\sigma^2(F_o^2) + (xP)^2 + yP]$, where $P = (F_o^2 + 2F_c^2)/3$; [e]R indices for all data.

Table S4. Unit Cell and Refinement Data for [(adt)Ni(C≡N^{t}Bu)$_2$], [(pdt)Pt(C≡N^{t}Bu)$_2$][SbCl$_6$]· CH_2Cl_2, and [[(pdt)Ni(C≡N^{t}Bu)$_2$]$_2$(μ-Ag$_2$)][BF$_4$]$_2$.

compound	[(adt)Ni(C≡N^{t}Bu)$_2$]	[(pdt)Pt(C≡N^{t}Bu)$_2$]$_2$[SbCl$_6$]$_2$	[[(pdt)Ni(C≡N^{t}Bu)$_2$]$_2$(μ-Ag$_2$)][BF$_4$]$_2$	[(2,6-Me$_2$py)Ni(μ_2-pdt)]$_2$
compound #	**4bd**	[**6d**]$_2$[SbCl$_6$]$_2$	[**7**][BF$_4$]$_2$	**8**
structure code	JPD687_0m_a	JPD1004	JPD833a_0m_a_sq	JPD999_0m_a
solvent	none	2CH_2Cl_2	none	none
formula	$C_{26}H_{32}N_2NiO_2S_2$	$C_{50}H_{60}Cl_{16}N_4Pt_2S_4Sb_2$	$C_{48}H_{56}Ag_2B_2F_8N_4Ni_2S_4$	$C_{42}H_{38}N_2Ni_2S_4$
fw	527.36	2046.14	1323.98	816.36
temperature, K	150	150	150	158
wavelength, Å	1.54178	0.71073	0.71073	0.71073
2θ range, deg.	148.918	1.374 to 23.936	3.170 - 58.446	2.016 – 23.681
crystal system	monoclinic	triclinic	monoclinic	monoclinic
space group	$P2_1/c$	$P\bar{1}$	$P2_1/c$	$P2_1/n$
a, Å	10.9908(2)	14.6760(19)	13.4447(7)	17.549(3)
b, Å	13.3676(2)	15.883(2)	13.8422(7)	12.451(2)
c, Å	18.5858(3)	16.932(2)	17.2438(9)	18.712(3)
α, deg.	90	97.816(2)	90	90
β, deg.	100.118(1)	90.973(2)	107.165(1)	112.549(2)
γ, deg.	90	109.270(2)	90	90
volume, Å^3	2688.17(8)	3682.9(8)	3066.2(3)	3775.9(12)
Z	4	2	2	4
density, g/cm^3	1.303	1.845	1.434	1.436
μ, mm^{-1}	2.680	5.241	1.427	1.252
crystal size	0.032 x 0.078 x 0.180	0.135 x 0.236 x 0.241	0.120 x 0.250 x 0.288	0.080 x 0.429 x 0.487
color, habit	blue plate	brown-black irregular	red-orange thick plate	thick brown-black plate
limiting indices, *h*	$-13 \le h \le 13$	$-16 \le h \le 16$	$-18 \le h \le 18$	$-19 \le h \le 19$
limiting indices, *k*	$-16 \le k \le 16$	$-18 \le k \le 18$	$-18 \le k \le 18$	$-14 \le k \le 14$
limiting indices, *l*	$-23 \le l \le 21$	$-19 \le l \le 19$	$-23 \le l \le 23$	$-21 \le l \le 21$
reflections collected	51625	24997	58589	48400
independent data	5497	11390	8255	5677
restraints	0	0	0	0
parameters refined	306	725	322	455
GooF[a]	1.037	1.024	1.024	1.064
R1,[b,c] wR2[d,c]	0.0288, 0.0691	0.0512, 0.1358	0.0306, 0.0800	0.0534, 0.1342
R1,[b,e] wR2[d,e]	0.0354, 0.0726	0.0758, 0.1526	0.0381, 0.0820	0.0619, 0.1379
largest diff. peak, e·Å^{-3}	0.238	3.840	1.787	2.578
largest diff. hole, e·Å^{-3}	–0.256	–1.356	–0.477	–1.161
abs struct parameter	-	-	-	-

Table S5. Unit Cell and Refinement Data for Phosphine Compounds.

compound	[(pdt)Ni(CNMe)(PPh$_3$)]	[(pdt)Ni(CNMe)(PMe$_3$)]	[(pdt)Ni(CNMe)]$_2$(dppb)	[(pdt)Pd(CNMe)]$_2$(dppb)	[(pdt)Pt(CNMe)]$_2$(dppb)
compound #	**12**	**13**	**9**	**10**	**11**
structure code	JPD1000_0m_a	JPD993_0m_a	JPD931_0m_a	JPD923_0m_a_sq	JPD910_0m_a
solvent	none	none	$ClCH_2CH_2Cl$	$2ClCH_2CH_2Cl$	$2ClCH_2CH_2Cl$
formula	$C_{34}H_{28}NNiPS_2$	$C_{19}H_{22}NNiPS_2$	$C_{64}H_{54}Cl_2N_2Ni_2P_2S_4$	$C_{66}H_{58}Cl_4N_2P_2Pd_2S_4$	$C_{66}H_{58}Cl_4N_2P_2Pt_2S_4$
fw	604.37	418.17	1229.59	1423.92	1601.30
temperature, K	150	150	150	120	150
wavelength, Å	1.54178	0.71073	1.54178	0.71073	0.71073
2θ range, deg.	7.306 – 145.026	60.480	144.068	58.302	60.434
crystal system	monoclinic	monoclinic	monoclinic	triclinic	triclinic
space group	$P2_1/n$	$C2/c$	$P2_1/c$	$P\bar{1}$	$P\bar{1}$
a, Å	9.8216(3)	11.5465(9)	9.6474(2)	9.1864(10)	9.1319(14)
b, Å	16.6885(5)	17.2201(13)	31.3752(6)	11.6084(12)	11.3306(17)
c, Å	17.6120(5)	19.4910(15)	19.4512(4)	15.5424(17)	15.881(2)
α, deg.	90	90	90	81.089(2)	81.089(2)
β, deg.	94.007(1)	98.365(1)	93.481(1)	78.819(2)	82.245(2)
γ, deg.	90	90	90	75.478(1)	78.958(2)
volume, Å^3	2879.69(15)	3834.2(5)	5876.8(2)	1564.1(3)	1583.9(4)
Z	4	8	4	1	1
density, g/cm^3	1.394	1.449	1.390	1.512	1.679
μ, mm^{-1}	3.032	1.314	3.796	0.973	4.804
crystal size	0.098 x 0.147 x 0.311	0.197 x 0.239 x 0.474	0.044 x 0.087 x 0.269	0.136 x 0.146 x 0.158	0.085 x 0.141 x 0.462
color, habit	dark yellow column	orange-brown column	light green plate	orange block	yellow parallelpiped
limiting ind., *h*	$-11 \le h \le 11$	$-16 \le h \le 16$	$-11 \le h \le 11$	$-12 \le h \le 12$	$-12 \le h \le 12$
limiting ind., *k*	$-19 \le k \le 20$	$-23 \le k \le 24$	$-37 \le k \le 38$	$-15 \le k \le 15$	$-15 \le k \le 15$
limiting ind., *l*	$-21 \le l \le 21$	$-27 \le l \le 26$	$-23 \le l \le 23$	$-21 \le l \le 21$	$-21 \le l \le 22$
refl. collected	21704	37321	50614	30340	30746
indep. data	5634	5484	11433	8294	8750
restraints	0	0	1	0	0
parameters ref'd	353	221	691	362	363
GooF[a]	1.064	1.014	1.035	1.045	1.102
R1,[b,c] wR2[d,c]	0.0337, 0.0821	0.0351, 0.0931	0.0444, 0.0995	0.0448, 0.1283	0.0333, 0.0922
R1,[b,e] wR2[d,e]	0.0376, 0.0846	0.0422, 0.0944	0.0607, 0.1079	0.0607, 0.1350	0.0380, 0.0941
diff. peak, e·Å^{-3}	0.487	1.290	0.676	1.408	3.081
diff. hole, e·Å^{-3}	–0.426	–0.487	–0.684	–1.023	–2.217
abs struct par.	-	-	-	-	-

[a]GooF = $\{\Sigma[w(F_o^2 - F_c^2)^2]/(n-p)\}^{½}$, where *n*= number of reflections and *p* is the total number of parameters refined; [b]R1 = $\Sigma||F_o| - |F_c||/\Sigma|F_o|$; [c]R indices for data cut off at I > 2σ(I); [d]wR2 = $\{[\Sigma w(F_o^2 - F_c^2)^2/\Sigma w(F_o^2)^2\}^{1/2}$; $w = 1/[\sigma^2(F_o^2) + (xP)^2 + yP]$, where $P = (F_o^2 + 2F_c^2)/3$; [e]R indices for all data.

Table S6. Unit Cell and Refinement Data for Cyanide and Carbene Compounds.

compound	[Et_4N][(pdt)Pd($CNCH_3$)(CN)]	[Et_4N][(pdt)Pt($CNCH_3$)(CN)]	[(pdt)Pd(IPr)(CNMe)]	[(pdt)Pt(IPr)(CNMe)(C(NMe)(IPr)]	[(pdt)Ni(CNMe)(C(NMe_2)(NHMe))]
compound #	[Et_4N][**16**]	[Et_4N][**17**]	**19**	**20**	**21**
structure code	JPD874_0m_a	JPD884_0m_a	JPD991_01m_a	JPD892_5_sq	JPD971_0ma_a
solvent	none	none	$ClCH_2CH_2Cl$	none	^{t}BuOMe
formula	$C_{25}H_{33}N_3PdS_2$	$C_{25}H_{33}N_3PtS_2$	$C_{45}H_{53}Cl_2N_3PdS_2$	$C_{45}H_{52}N_4PtS_2$	$C_{25}H_{35}N_3NiOS_2$
fw	546.06	634.75	877.32	908.11	516.39
temperature, K	100	100	150	100	150
wavelength, Å	0.71073	0.71073	0.71073	0.71073	0.71073
2θ range, deg.	3.044 - 59.294	3.054 - 59.508	3.716 - 49.540	3.384 - 56.880	2.572 – 56.028
crystal system	monoclinic	monoclinic	orthorhombic	triclinic	monoclinic
space group	$P2_1/n$	$P2_1/n$	$P2_12_12_1$	$P\bar{1}$	$P2_1/c$
a, Å	9.269(2)	9.2836(14)	12.696(2)	14.2859(18)	15.829(3)
b, Å	26.754(6)	26.670(4)	16.595(3)	18.345(2)	13.461(2)
c, Å	10.257(2)	10.2477(16)	21.726(4)	19.440(2)	12.3174(19)
α, deg.	90	90	90	77.177(2)	90
β, deg.	95.663(3)	95.857(2)	90	79.234(2)	90.395(2)
γ, deg.	90	90	90	78.738(2)	90
volume, $Å^3$	2531(1)	2524.1(7)	4577.4(15)	4817.0(10)	2624.3(7)
Z	4	4	4	4	4
density, g/cm^3	1.433	1.670	1.273	1.252	1.307
μ, mm^{-1}	0.915	5.742	0.646	3.030	0.920
crystal size	0.078 x 0.166 x 0.229	0.062 x 0.062 x 0.375	0.289 x 0.333 x 0.381	0.120 x 0.134 x 0.208	0.100 x 0.262 x 0.306
color, habit	light orange tablet	colorless column	orange block	yellow block	orange plate
limiting ind., *h*	$-12 \le h \le 12$	$-12 \le h \le 12$	$-14 \le h \le 14$	$-19 \le h \le 19$	$-20 \le h \le 20$
limiting ind., *k*	$-36 \le k \le 36$	$-36 \le k \le 37$	$-19 \le k \le 19$	$-24 \le k \le 14$	$-17 \le k \le 17$
limiting ind., *l*	$-13 \le l \le 14$	$-14 \le l \le 14$	$-25 \le l \le 25$	$-26 \le l \le 26$	$-16 \le l \le 16$
refl. collected	49187	49202	66353	131565	24103
indep. data	7014	7080	7859	131565	6317
restraints	125	0	0	540	36
parameters ref'd	314	286	487	958	290
GooF[a]	1.078	1.039	0.993	1.044	1.056
R1,[b,c] wR2[d,c]	0.0313, 0.0829	0.0214, 0.0513	0.0365, 0.0895	0.0615, 0.1473	0.0568, 0.1550
R1,[b,e] wR2[d,e]	0.0419, 0.0853	0.0277, 0.0524	0.0407, 0.0908	0.1010, 0.1670	0.0810, 0.1689
diff. peak, $e·Å^{-3}$	1.297	1.789	1.436	6.288	1.335
diff. hole, $e·Å^{-3}$	–0.355	–0.623	–0.549	–2.468	–0.554
abs struct par.	-	-	-0.067(9)	-	

[a]GooF = $\{\Sigma[w(F_o^2 - F_c^2)^2]/(n-p)\}^{½}$, where *n*= number of reflections and *p* is the total number of parameters refined; [b]R1 = $\Sigma||F_o| - |F_c||/\Sigma|F_o|$; [c]R indices for data cut off at I > 2σ(I); [d]wR2 = $\{[\Sigma w(F_o^2 - F_c^2)^2/\Sigma w(F_o^2)^2\}^{1/2}$; $w = 1/[\sigma^2(F_o^2) + (xP)^2 + yP]$, where $P = (F_o^2 + 2F_c^2)/3$; [e]R indices for all data.

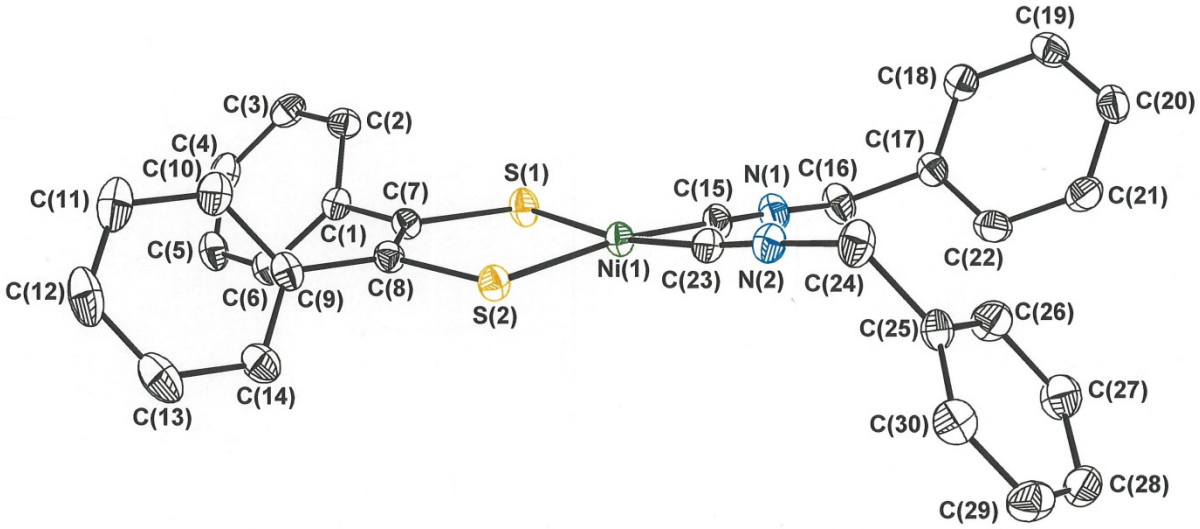

Figure S1. Thermal ellipsoid plot at the 50% probability level for $[(Ph_2C_2S_2)Ni(C{\equiv}NCH_2C_6H_5)_2]$. All hydrogen atoms have been omitted for clarity.

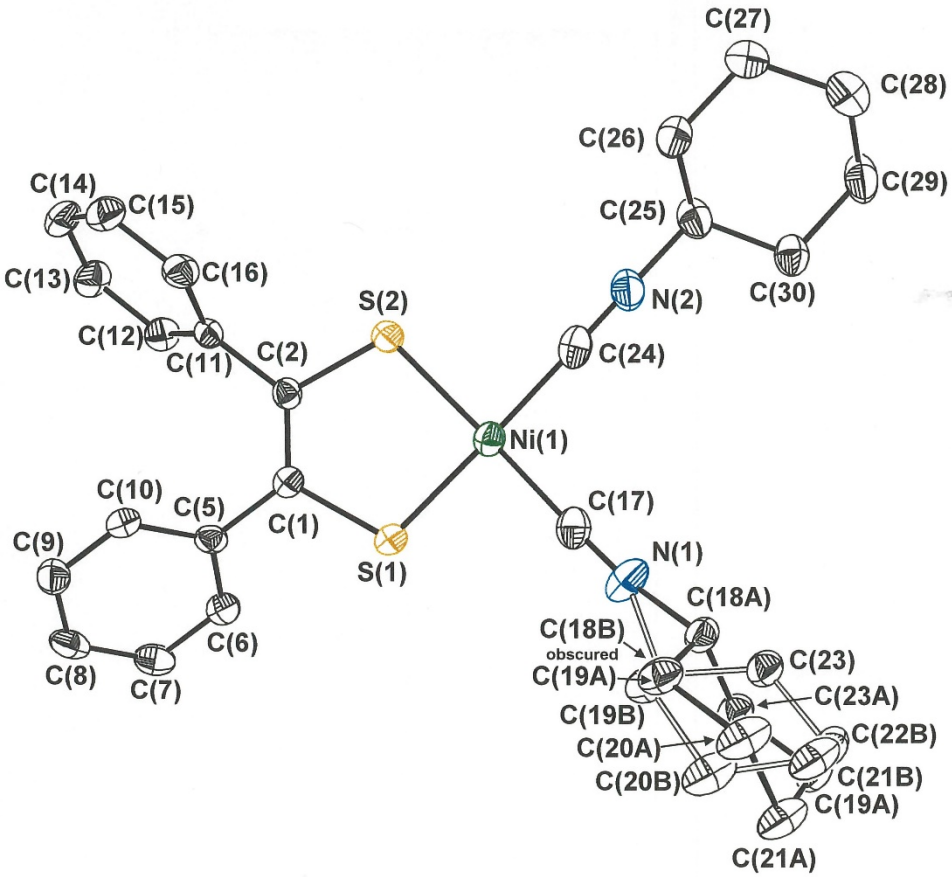

Figure S2. Thermal ellipsoid plot at the 50% probability level for $[(Ph_2C_2S_2)Ni(C{\equiv}NCy)_2]$, molecule one of three. Hydrogen atoms have been omitted for clarity. One cyclohexyl group is disordered over two positions, the distribution between which has been fit by the refinement software.

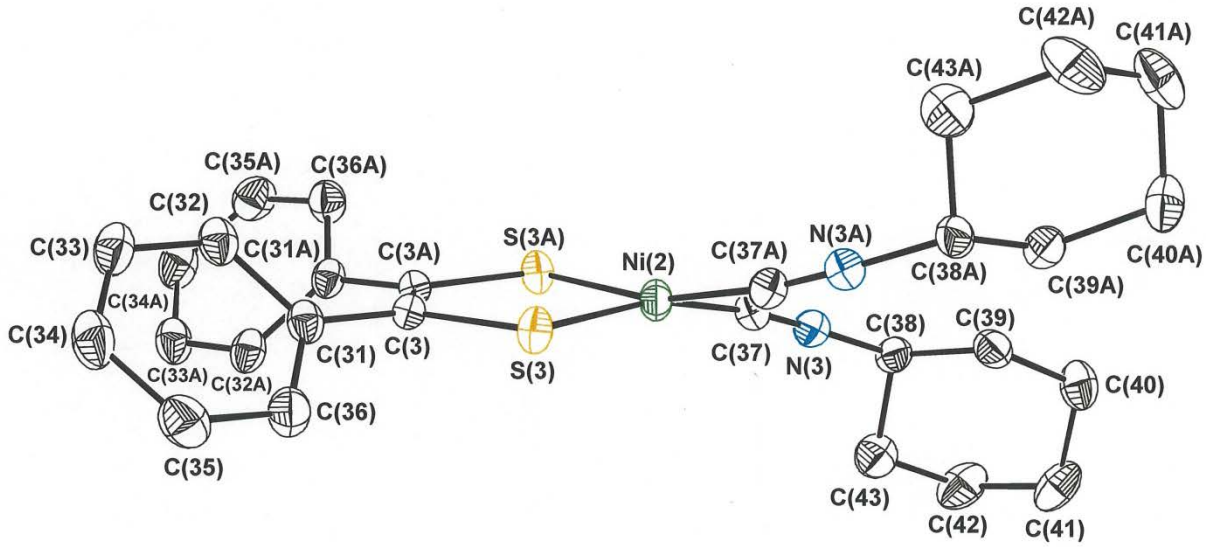

Figure S3. Thermal ellipsoid plot at the 50% probability level for [($Ph_2C_2S_2$)Ni(C≡NCy)$_2$], molecule two of three. Hydrogen atoms have been omitted for clarity. A crystallographic twofold axis bisects the S(3)–Ni(2)–S(3A) angle.

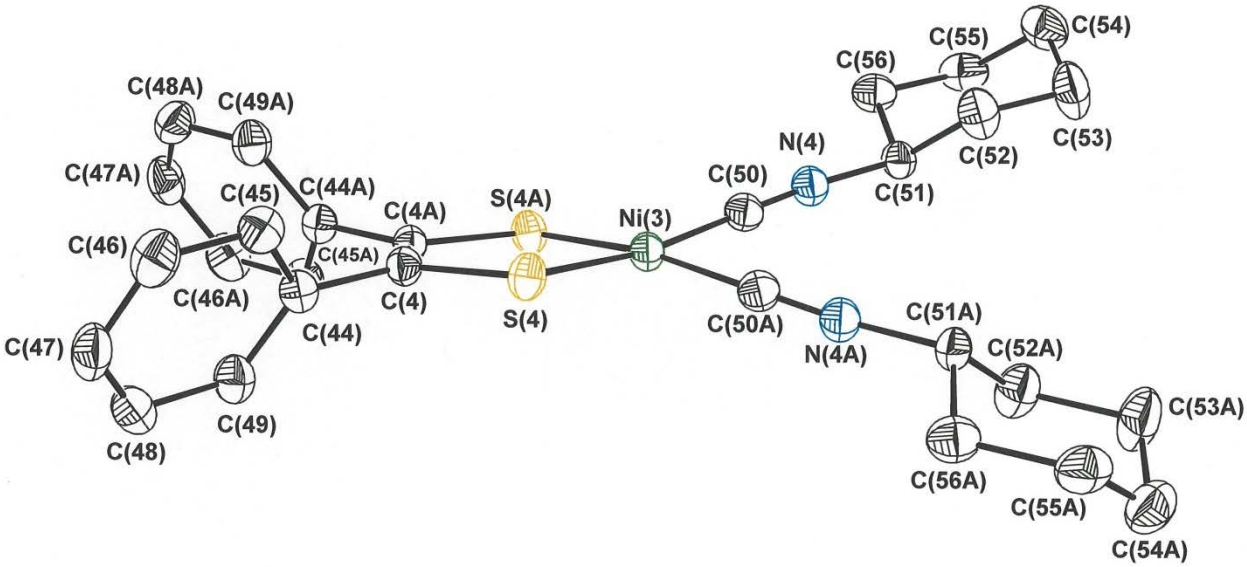

Figure S4. Thermal ellipsoid plot at the 50% probability level for [($Ph_2C_2S_2$)Ni(C≡NCy)$_2$], molecule three of three. Hydrogen atoms have been omitted for clarity. A crystallographic twofold axis bisects the S(4)–Ni(3)–S(4A) angle.

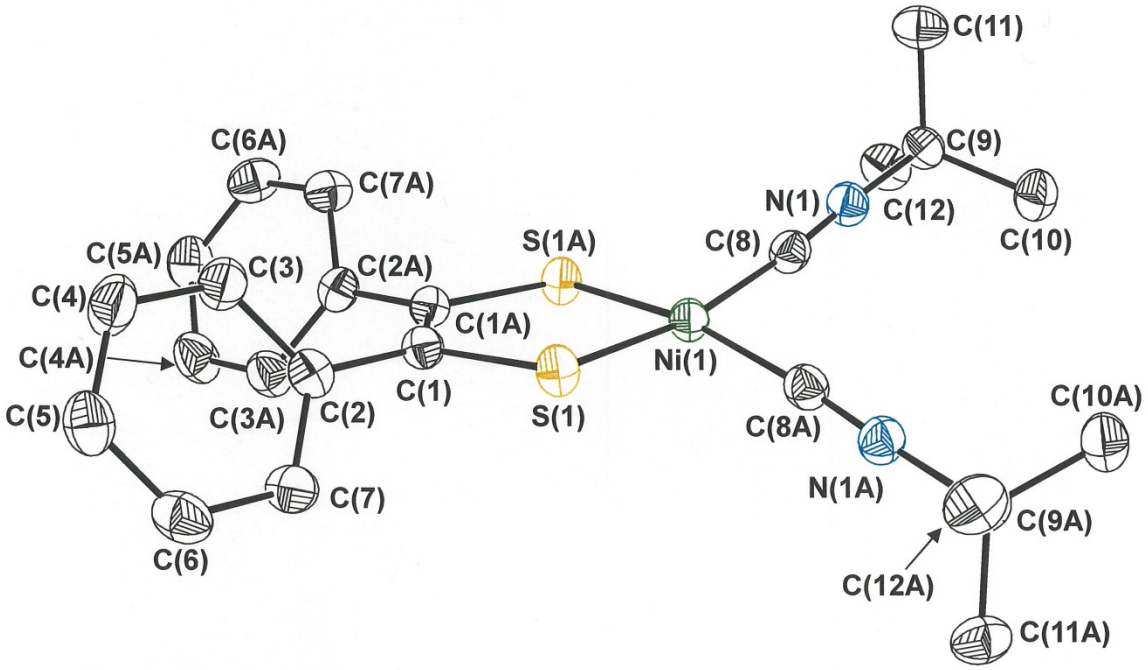

Figure S5. Thermal ellipsoid plot at the 50% probability level for $[(Ph_2C_2S_2)Ni(C{\equiv}N^tBu)_2]$. Hydrogen atoms have been omitted for clarity. A crystallographic twofold axis bisects the S(1)–Ni(1)–S(1A) angle.

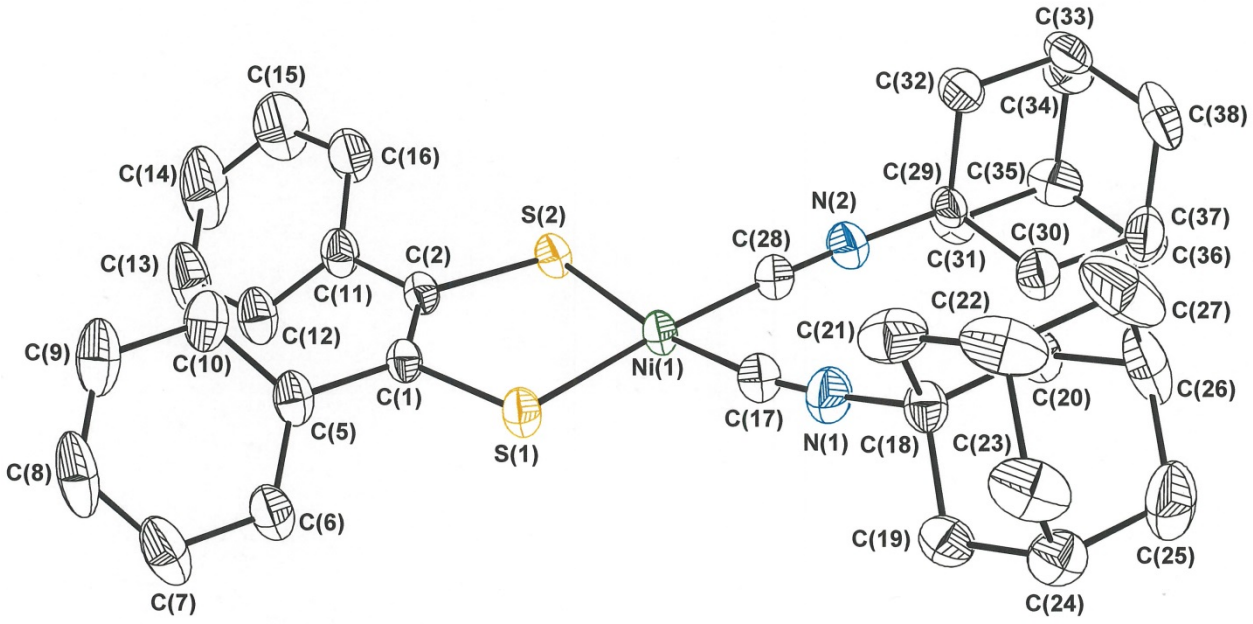

Figure S6. Thermal ellipsoid plot at the 50% probability level for $[(Ph_2C_2S_2)Ni(C{\equiv}N\text{-}1\text{-adamantyl})_2]$, molecule one of two. Hydrogen atoms have been omitted for clarity.

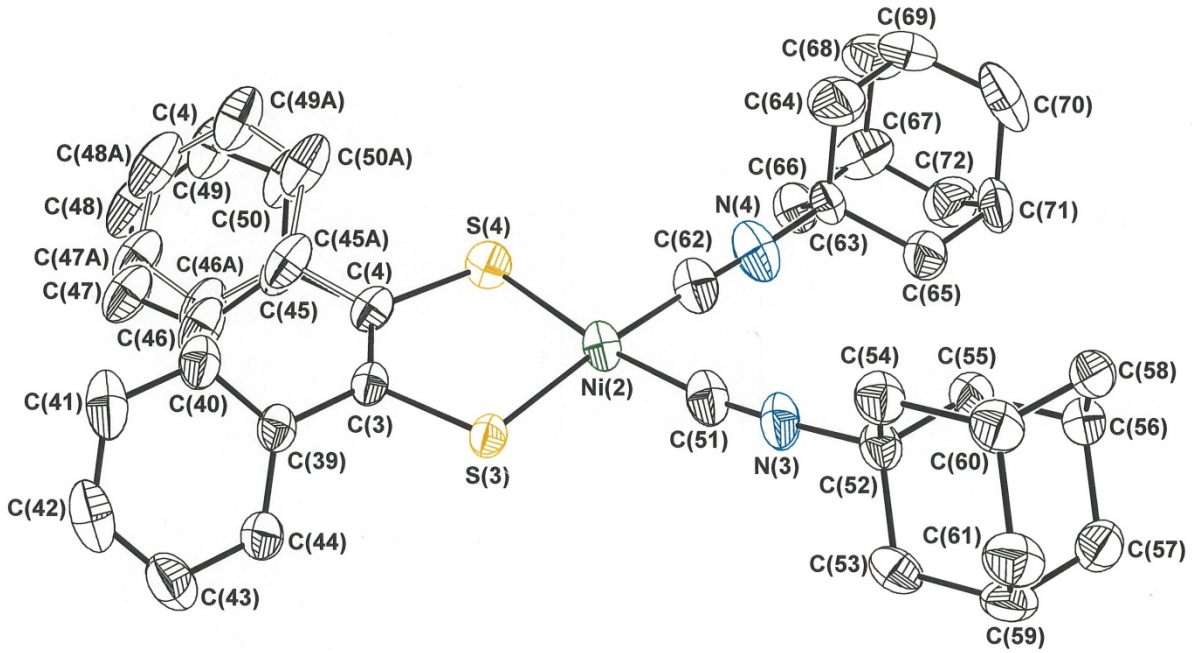

Figure S7. Thermal ellipsoid plot at the 50% probability level for [($Ph_2C_2S_2$)Ni(C≡N-1-adamantyl)$_2$], molecule two of two. Hydrogen atoms have been omitted for clarity. One phenyl ring of the dithiolene ligand is disordered and refined as a best fit distribution over two positions.

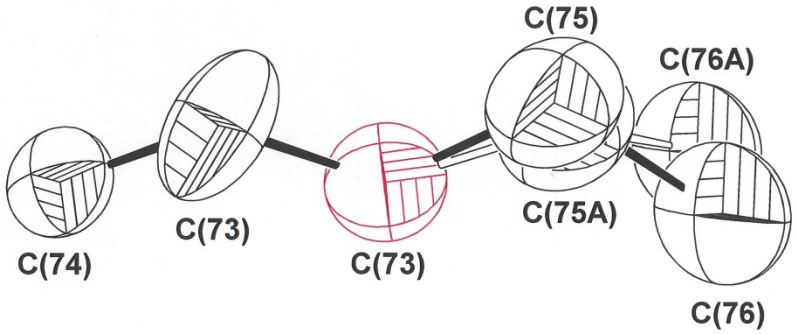

Figure S8. Thermal ellipsoid plot of interstitial Et_2O molecule in structure of [($Ph_2C_2S_2$)Ni(C≡N-1-adamantyl)$_2$]·½Et_2O. Hydrogen atoms have been omitted for clarity.

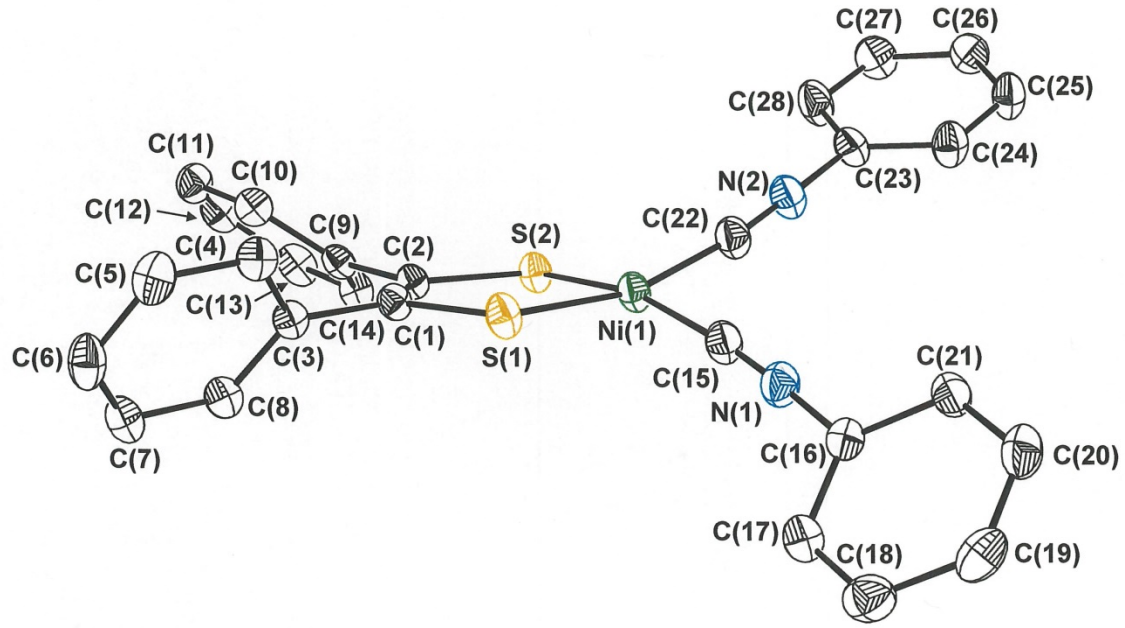

Figure S9. Thermal ellipsoid plot at the 50% probability level for $[(Ph_2C_2S_2)Ni(C{\equiv}NPh)_2]$. Hydrogen atoms have been omitted for clarity.

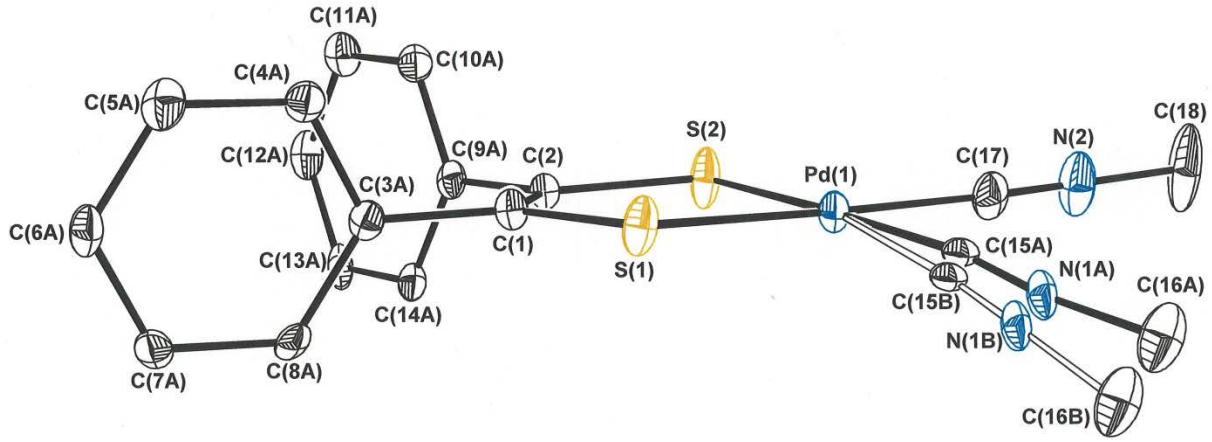

Figure S10. Thermal ellipsoid plot at the 50% probability level for $[(Ph_2C_2S_2)Pd(C{\equiv}NMe)_2]$. Hydrogen atoms have been omitted for clarity. One C≡NMe ligand is disordered over two positions and refined as a best fit distribution between the two.

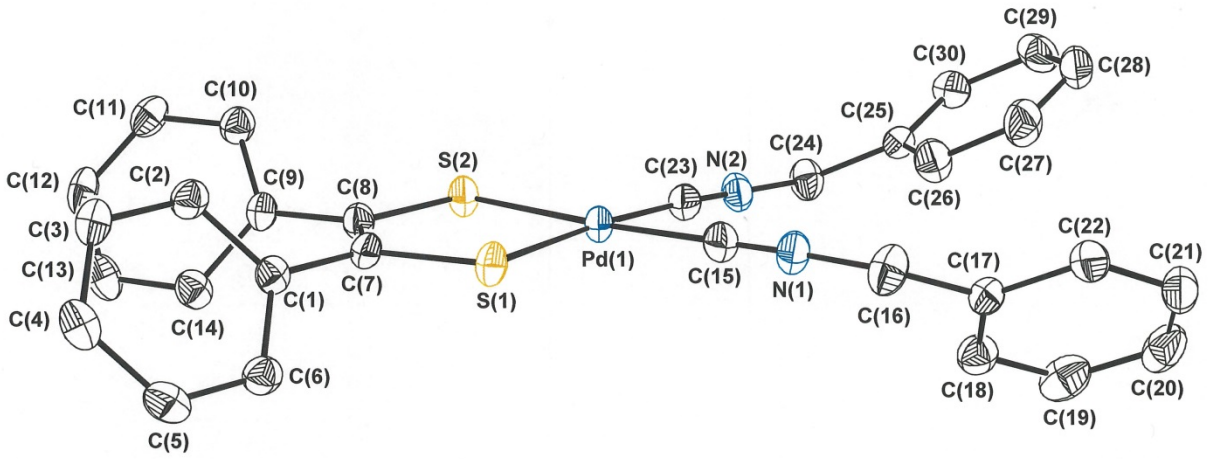

Figure S11. Thermal ellipsoid plot at the 50% probability level for $[(Ph_2C_2S_2)Pd(C{\equiv}NCH_2C_6H_5)_2]$. All hydrogen atoms have been omitted for clarity.

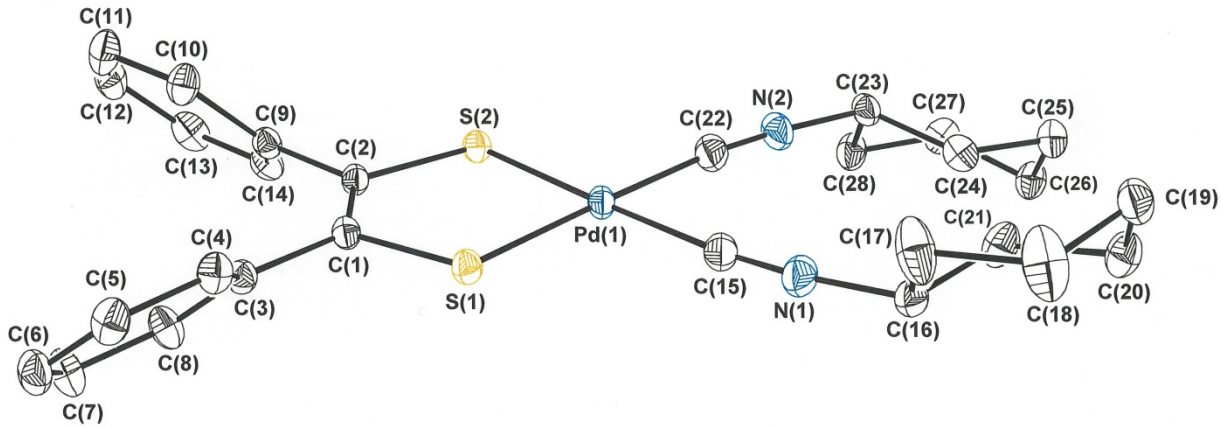

Figure S12. Thermal ellipsoid plot at the 50% probability level for $[(Ph_2C_2S_2)Pd(C{\equiv}NCy)_2]$. All hydrogen atoms have been omitted for clarity.

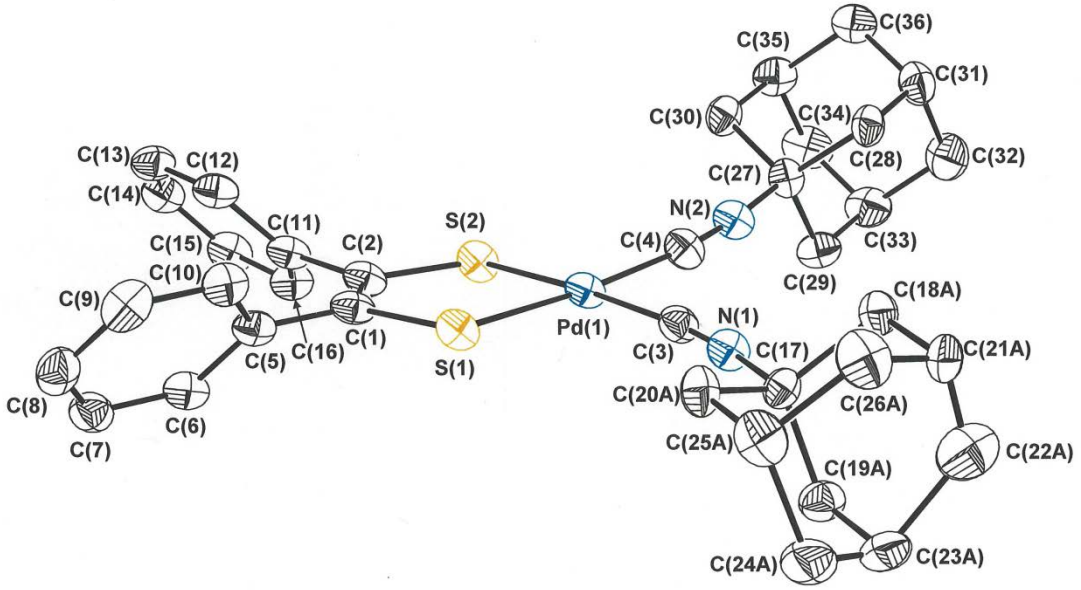

Figure S13. Thermal ellipsoid plot at the 50% probability level for [($Ph_2C_2S_2$)Pd(C≡N-1-adamantyl)$_2$]. Hydrogen atoms have been omitted for clarity. The adamantly group extending from N(1) is disordered over two positions, one of which is shown.

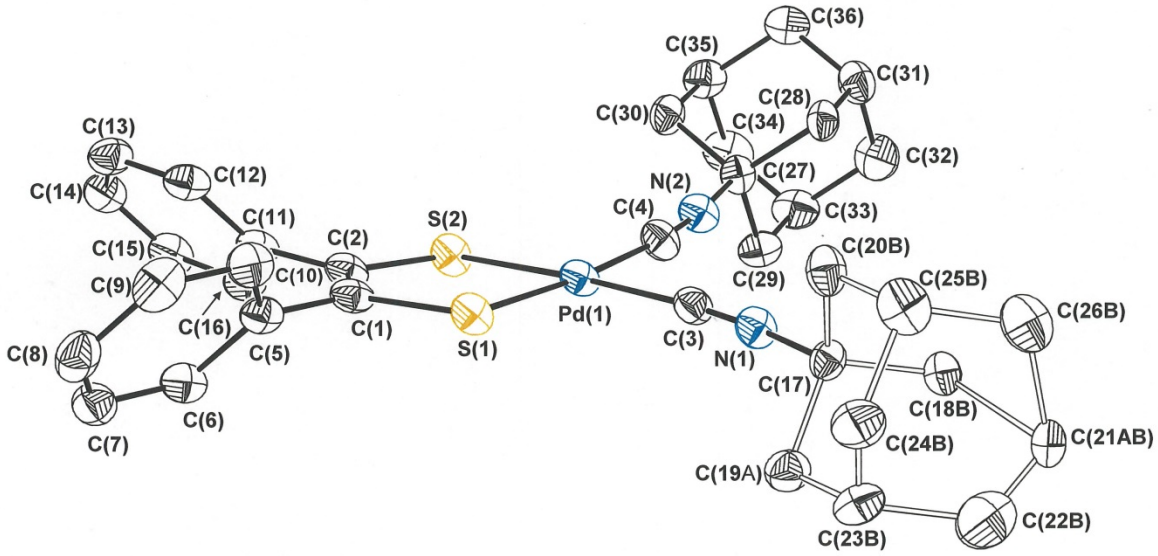

Figure S14. Thermal ellipsoid plot at the 50% probability level for [($Ph_2C_2S_2$)Pd(C≡N-1-adamantyl)$_2$]. Hydrogen atoms have been omitted for clarity. The adamantly group extending from N(1) is disordered over two positions, the second of which is shown.

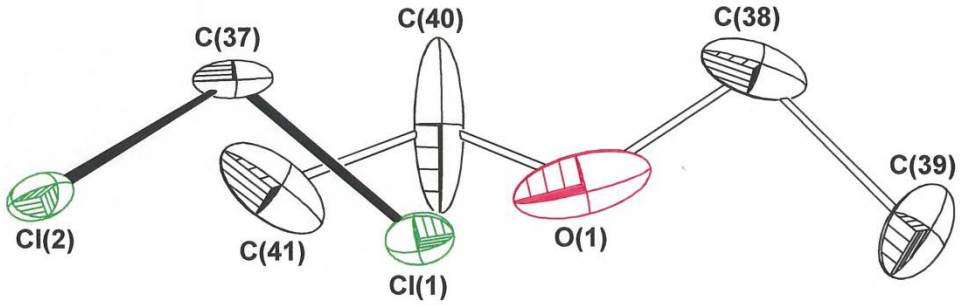

Figure S15. Thermal ellipsoid plot at the 50% probability level of interstitial Et_2O and CH_2Cl_2 molecules in structure of $[(Ph_2C_2S_2)Ni(C{\equiv}N\text{-}1\text{-}adamantyl)_2]\cdot\frac{1}{2}Et_2O\cdot\frac{1}{2}CH_2Cl_2$. Hydrogen atoms have been omitted for clarity.

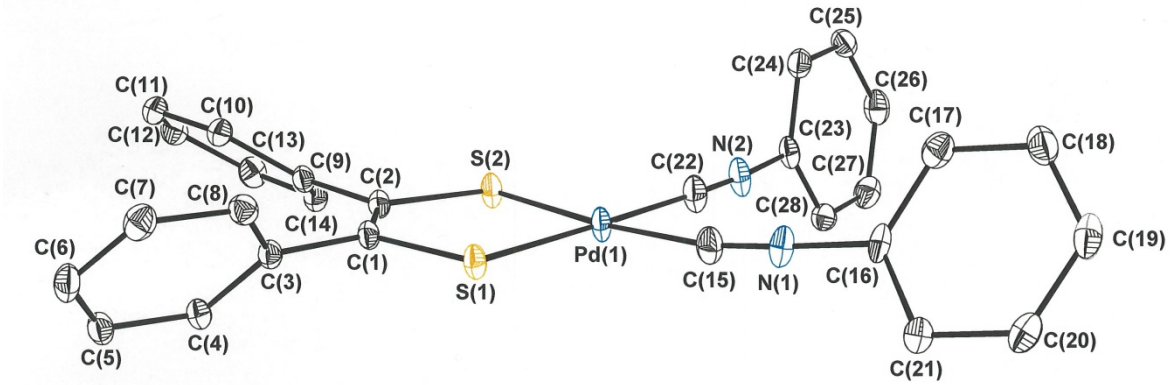

Figure S16. Thermal ellipsoid plot at the 50% probability level for $[(Ph_2C_2S_2)Pd(C{\equiv}NPh)_2]$. Hydrogen atoms have been omitted for clarity.

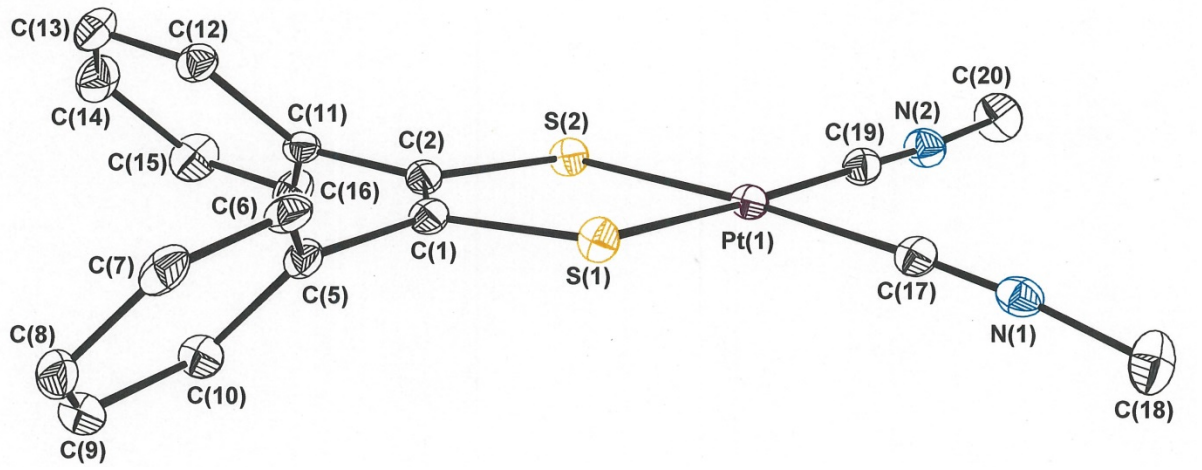

Figure S17. Thermal ellipsoid plot at the 50% probability level of $[(Ph_2C_2S_2)Pt(CNMe)_2]$, molecule one of two. Hydrogen atoms are omitted for clarity.

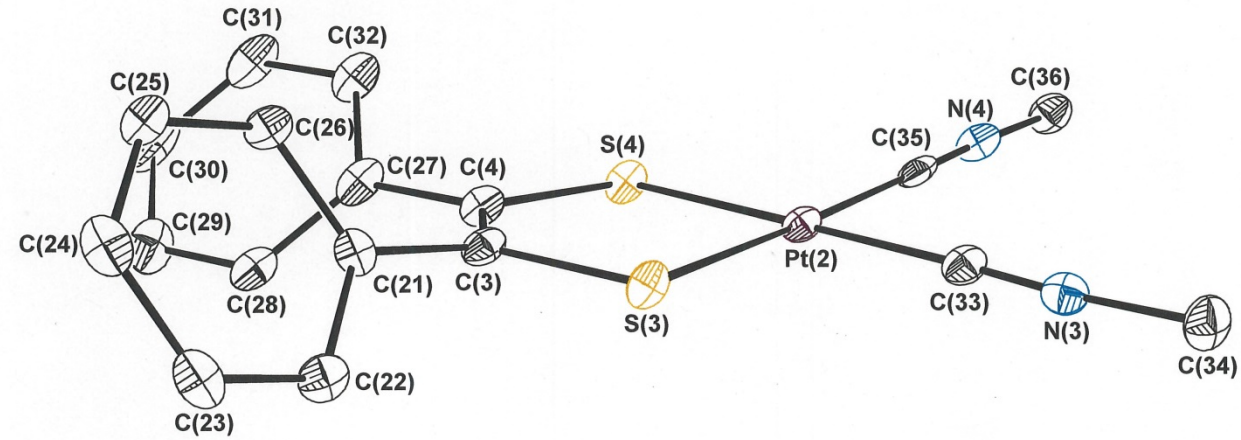

Figure S18. Thermal ellipsoid plot at the 50% probability level of $[(Ph_2C_2S_2)Pt(CNMe)_2]$, molecule two of two. Hydrogen atoms are omitted for clarity.

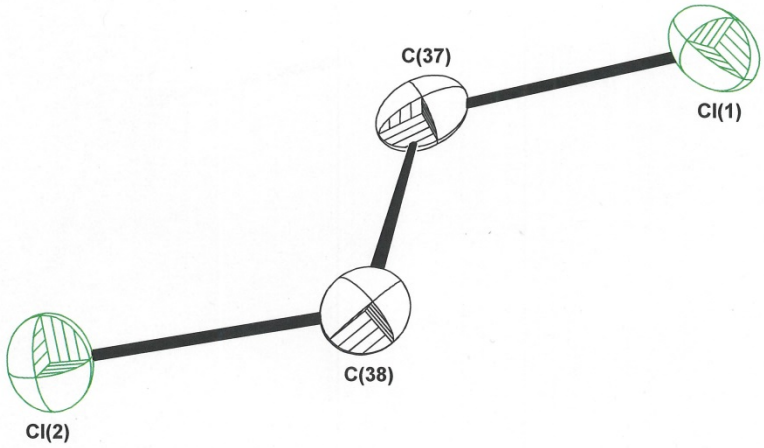

Figure S19. Thermal ellipsoid plot (50%) of interstitial $ClCH_2CH_2Cl$ in structure of $[(Ph_2C_2S_2)Pt(CNMe)_2]$. Hydrogen atoms are omitted for clarity.

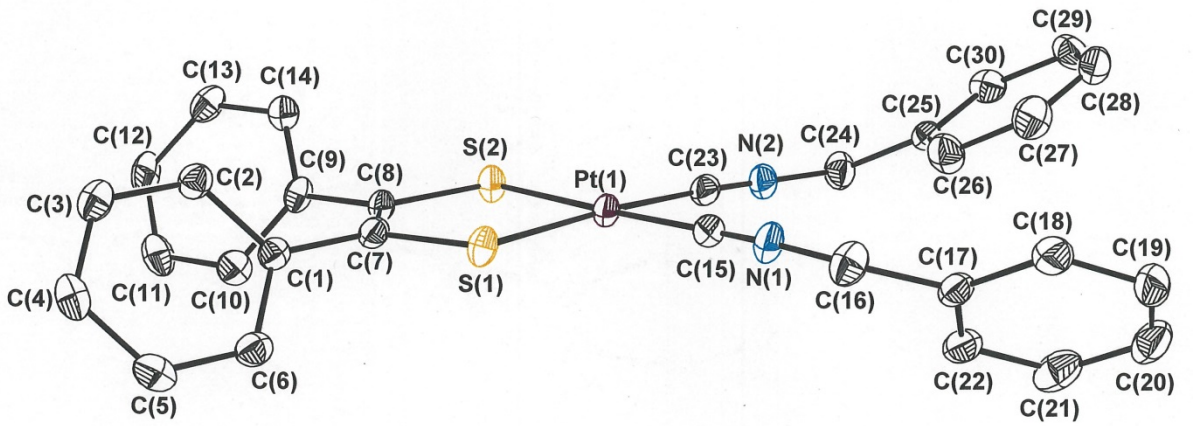

Figure S20. Thermal ellipsoid plot at the 50% probability level of $[(Ph_2C_2S_2)Pt(CNBn)_2]$. Hydrogen atoms are omitted for clarity.

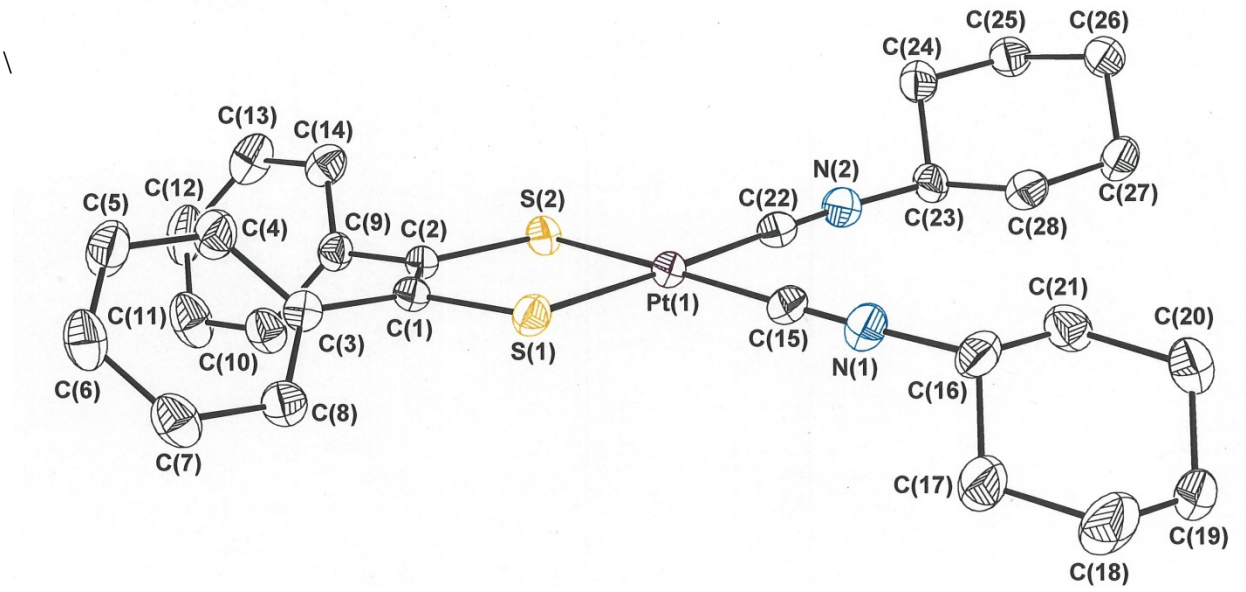

Figure S21. Thermal ellipsoid plot at the 50% probability level of $[(Ph_2C_2S_2)Pt(CNCy)_2]$. Hydrogen atoms are omitted for clarity.

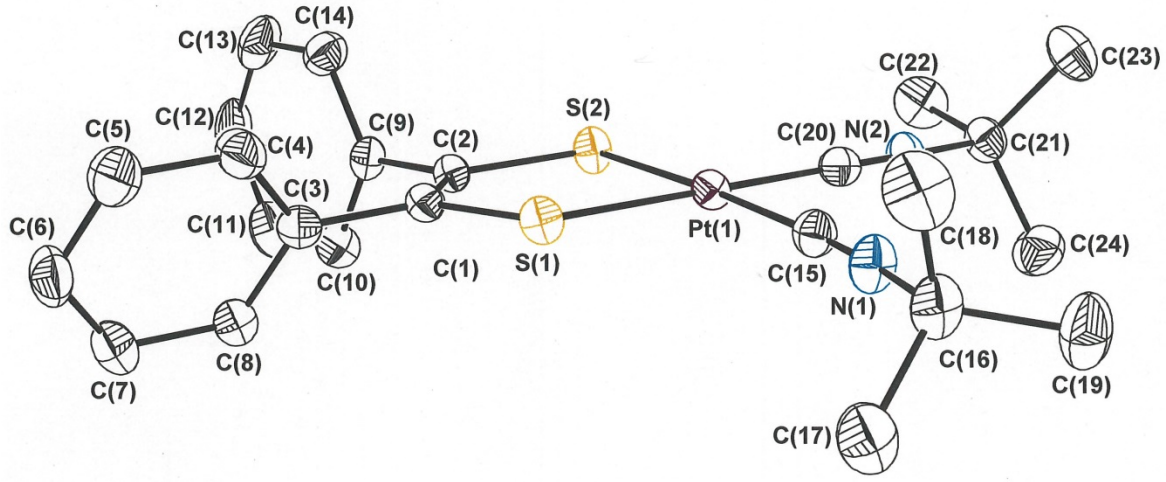

Figure S22. Thermal ellipsoid plot at the 50% probability level of $[(Ph_2C_2S_2)Pt(CN^tBu)_2]$. Hydrogen atoms are omitted for clarity.

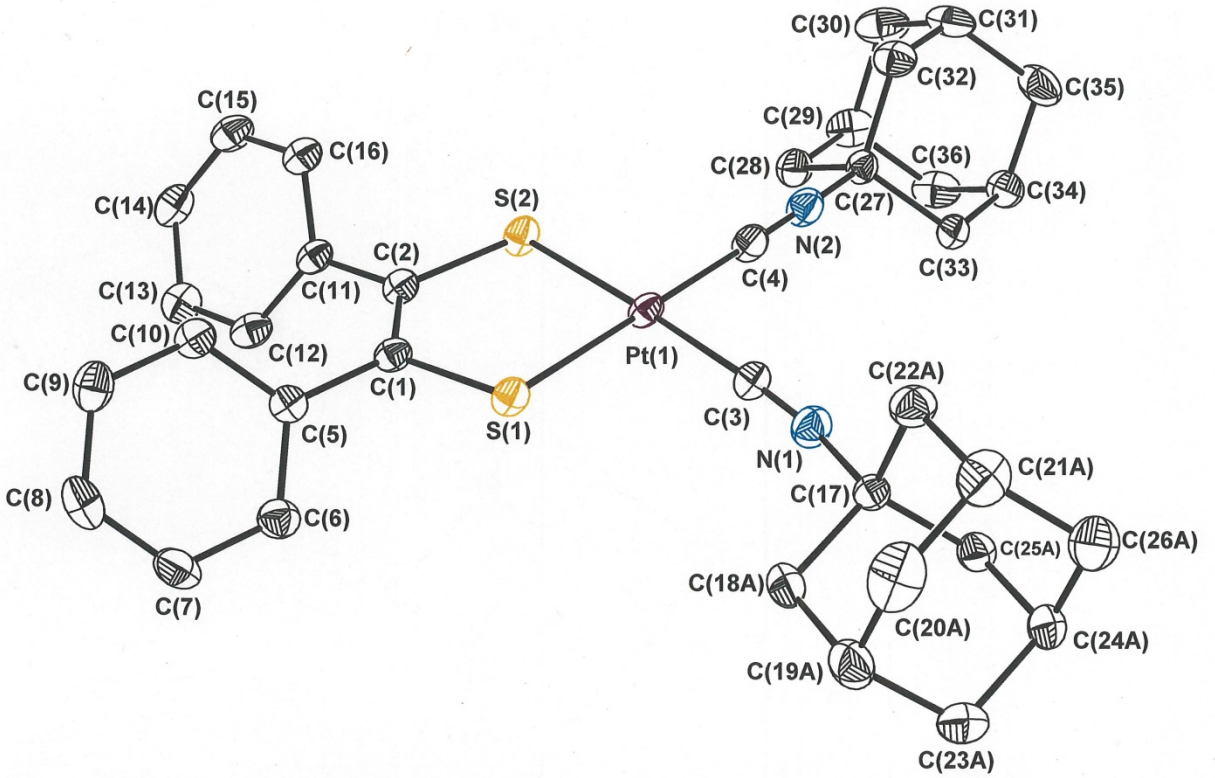

Figure S23. Thermal ellipsoid plot at the 50% probability level of $[(Ph_2C_2S_2)Pt(CN\text{-}1\text{-}Adamantyl)_2]$. Hydrogen atoms are omitted for clarity. The adamantyl group attached to N(1) is disordered over two positions, one of which is shown.

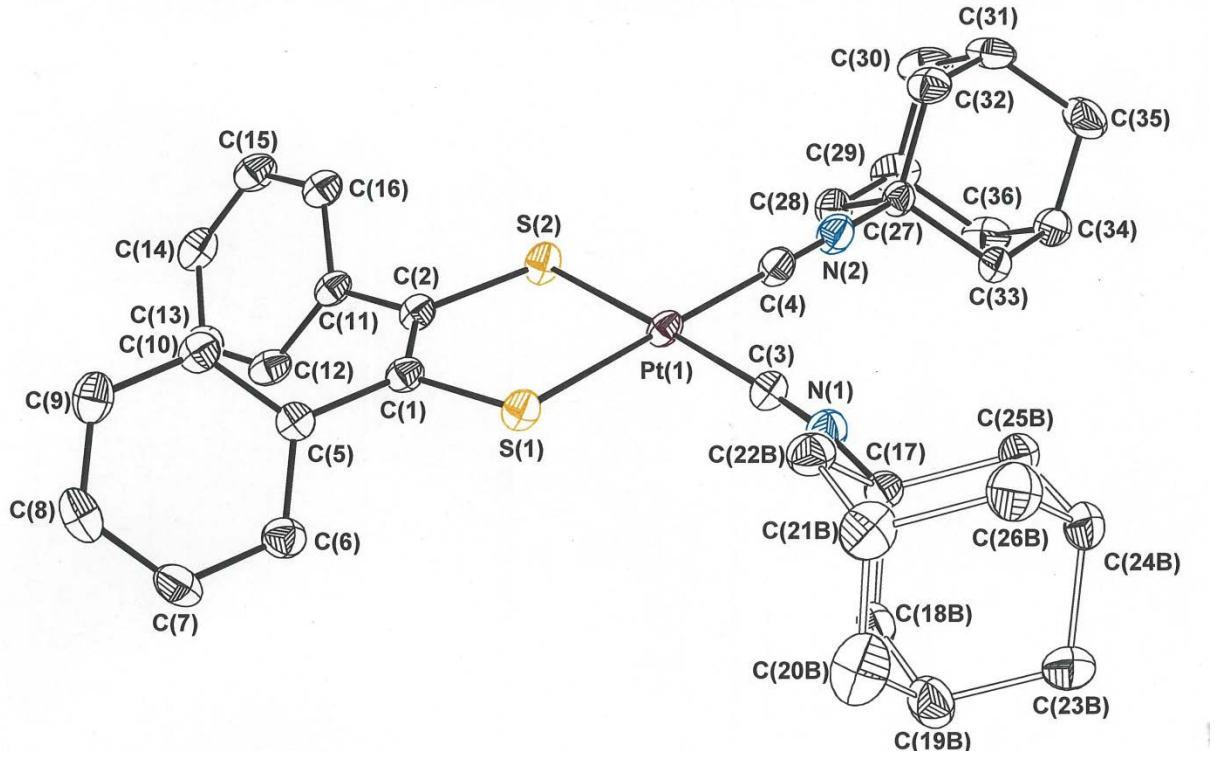

Figure S24. Thermal ellipsoid plot at the 50% probability level of $[(Ph_2C_2S_2)Pt(CN\text{-}1\text{-}Adamantyl)_2]$. Hydrogen atoms are omitted for clarity. The second position of the disordered adamantyl group attached to N(1) is shown (*cf*. **Figure S23** above.).

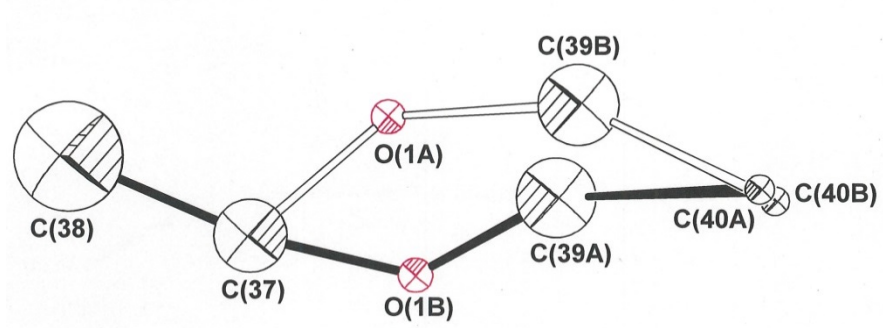

Figure S25. Isotropic thermal ellipsoid plot at the 30% probability level of disordered interstitial Et_2O molecule in the structure of $[(Ph_2C_2S_2)Pt(CN\text{-}1\text{-}Adamantyl)_2]\cdot Et_2O$. Hydrogen atoms are omitted for clarity.

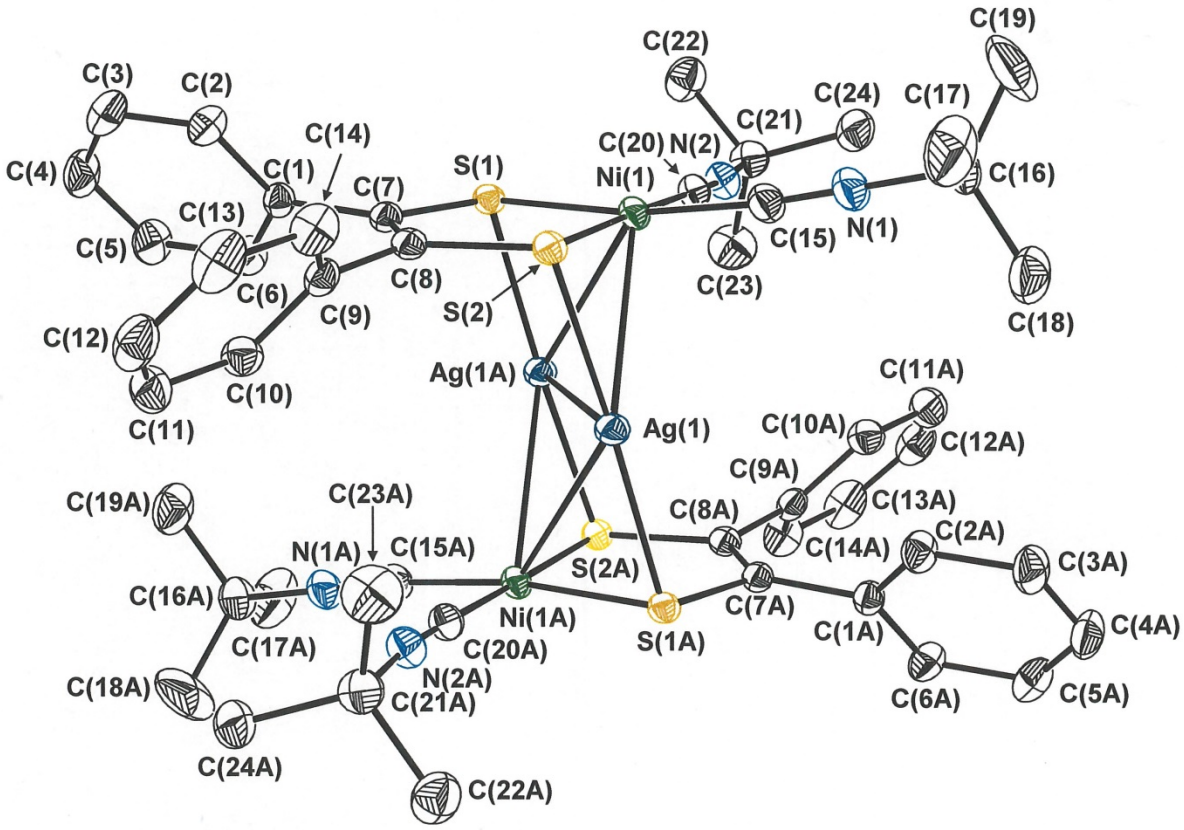

Figure S26. Thermal ellipsoid plot at the 50% probability level of $[[(Ph_2C_2S_2)Ni(CN^tBu)_2]_2(\mu\text{-}Ag)_2]^{2+}$. Hydrogen atoms are omitted for clarity.

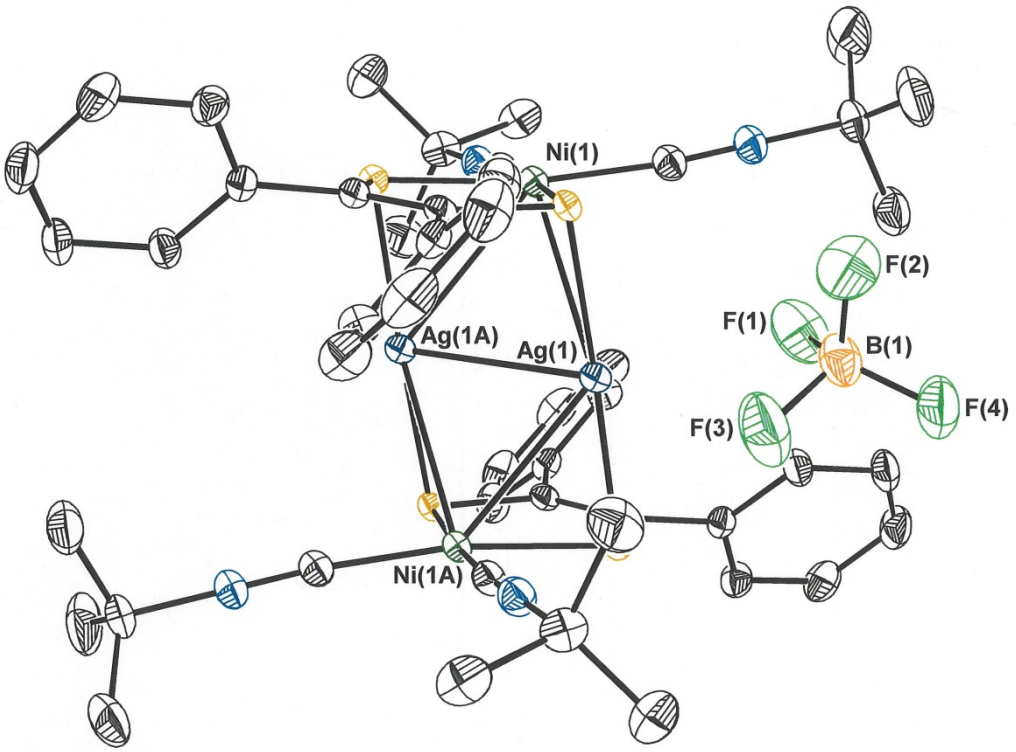

Figure S27. Thermal ellipsoid plot at the 50% probability level of $[[(Ph_2C_2S_2)Ni(CN^tBu)_2]_2(\mu\text{-}Ag)_2][BF_4]_2$ with atom labeling shown for the $[BF_4]^{1-}$ anion. A second anion occurs with this compound and is related to that which is shown by an inversion center. Hydrogen atoms are omitted for clarity.

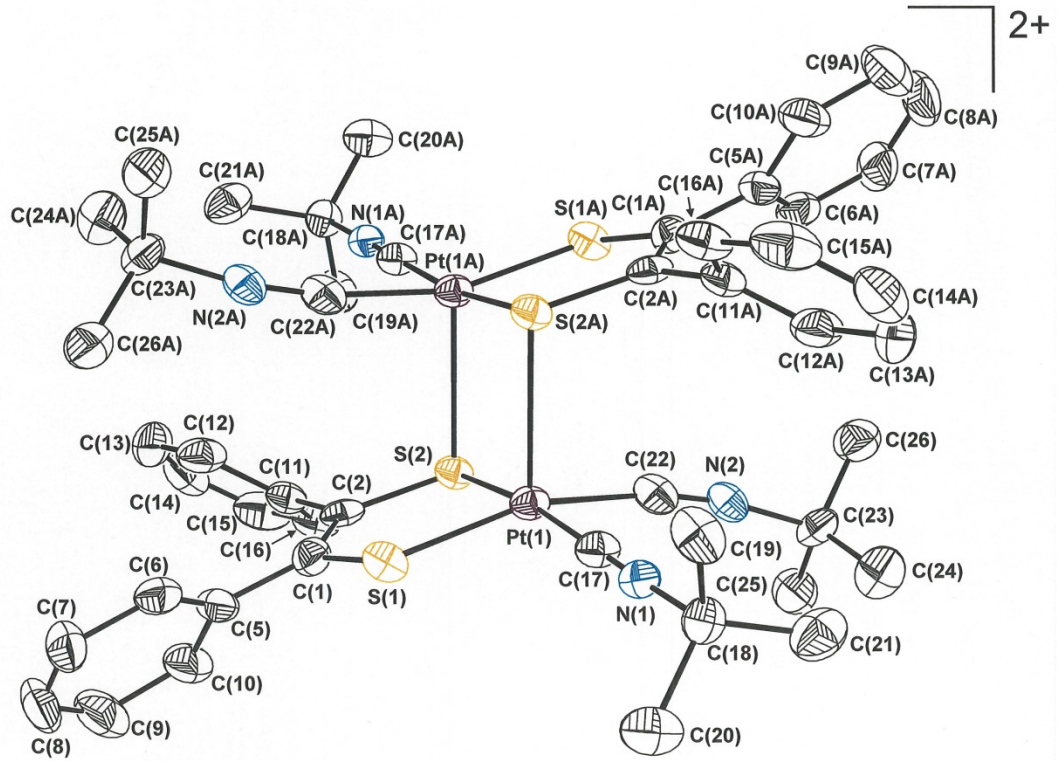

Figure S28. Thermal ellipsoid plot at the 50% probability level for dication one of $[[(Ph_2C_2S_2)Pt(CN^tBu)_2]_2[SbCl_6]_2$. Hydrogen atoms are omitted for clarity. The cation resides on an inversion center at the middle of the Pt_2S_2 rhomb.

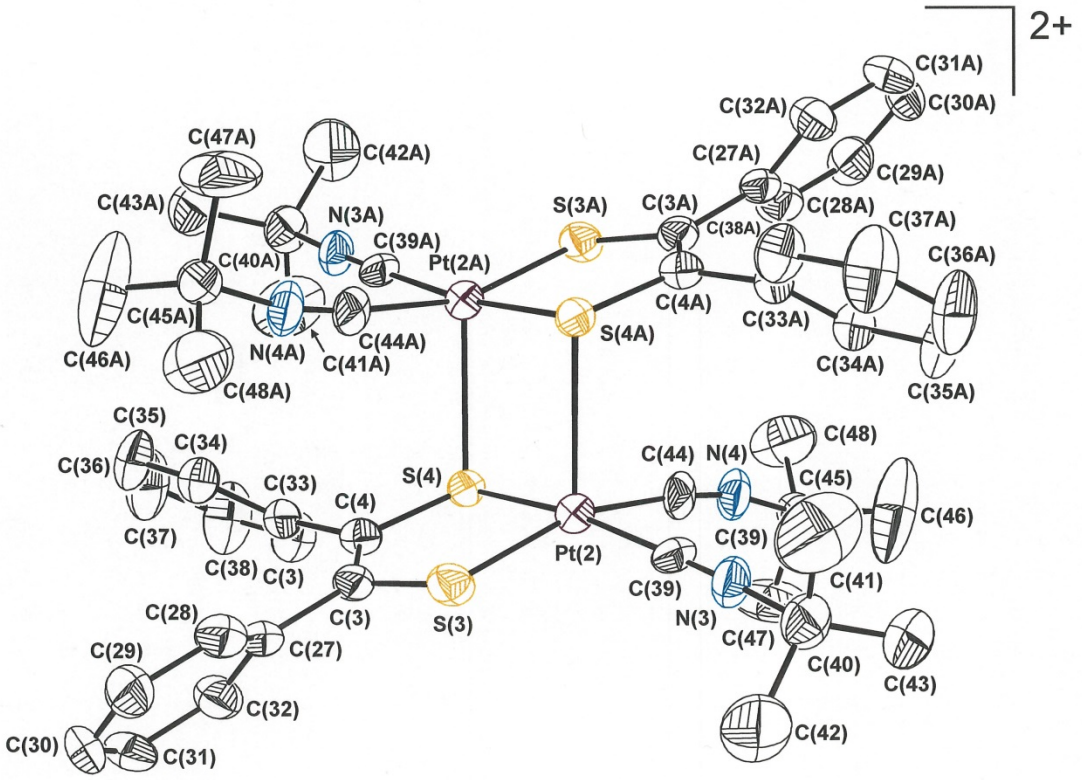

Figure S29. Thermal ellipsoid plot at the 50% probability level for dication two of $[[(Ph_2C_2S_2)Pt(CN^tBu)_2]_2[SbCl_6]_2$. Hydrogen atoms are omitted for clarity. The cation resides on an inversion center at the middle of the Pt_2S_2 rhomb.

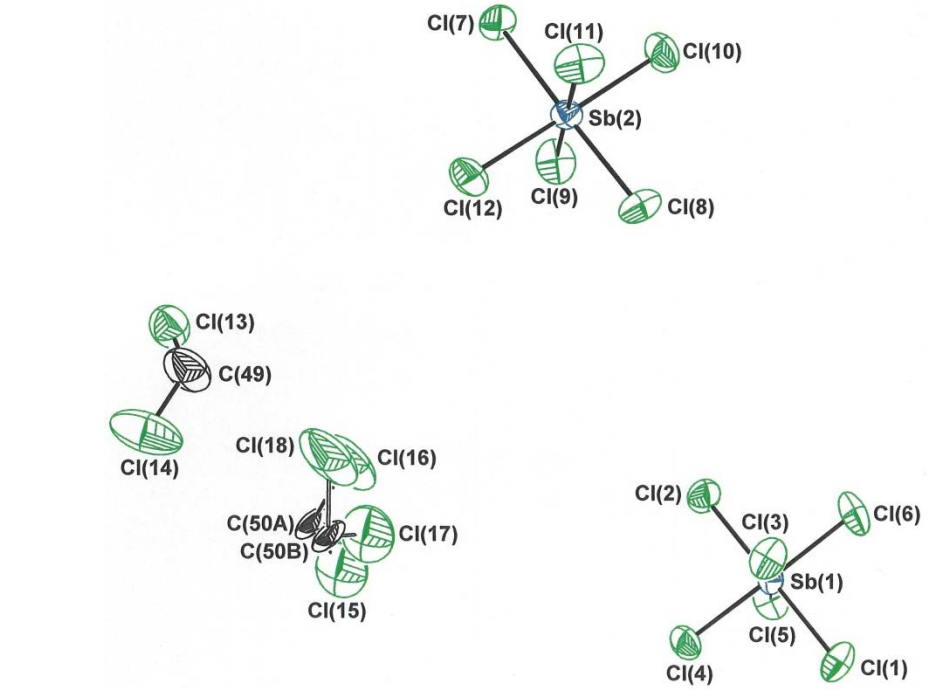

Figure S30. Thermal ellipsoid plot at the 50% probability level for the $[SbCl_6]^{1-}$ counteranions and for the interstitial CH_2Cl_2 in $[(Ph_2C_2S_2)Pt(CN^tBu)_2]_2[SbCl_6]_2 \cdot 2CH_2Cl_2$. Hydrogen atoms are omitted for clarity.

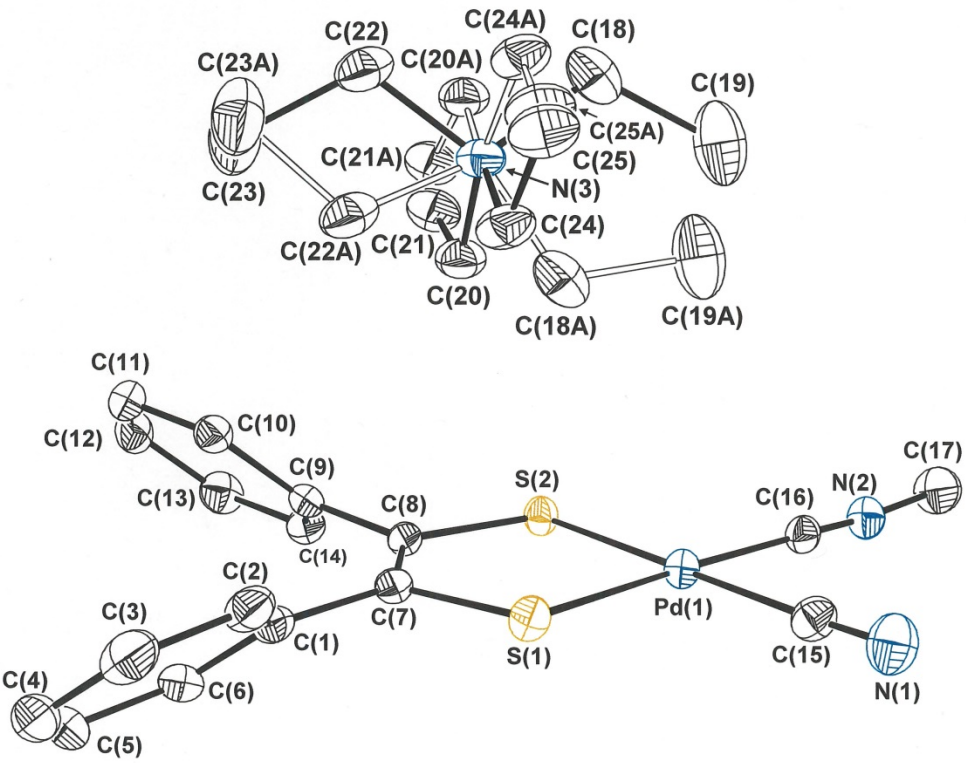

Figure S31. Anisotropic thermal ellipsoid plot at the 50% probability level for $[Et_4N][(Ph_2C_2S_2)Pd(CN)(CNMe)]$. The ethyl groups of the Et_4N^+ cation are disordered and refined as a best fit distribution between two positions. All hydrogen atoms are omitted for clarity.

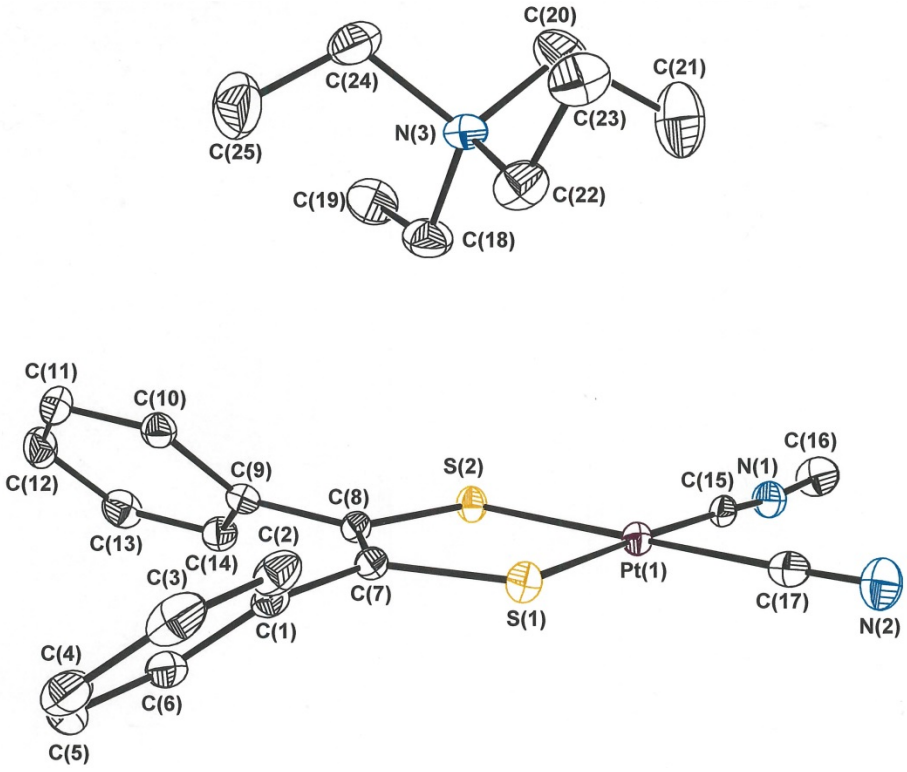

Figure S32. Anisotropic thermal ellipsoid plot at the 50% probability level for $[Et_4N][(Ph_2C_2S_2)Pt(CN)(CNMe)]$. All hydrogen atoms are omitted for clarity. In contrast to $[Et_4N][(Ph_2C_2S_2)Pd(CN)(CNMe)]$ (**Figure S28**), the Et_4N^+ cation is not disordered.

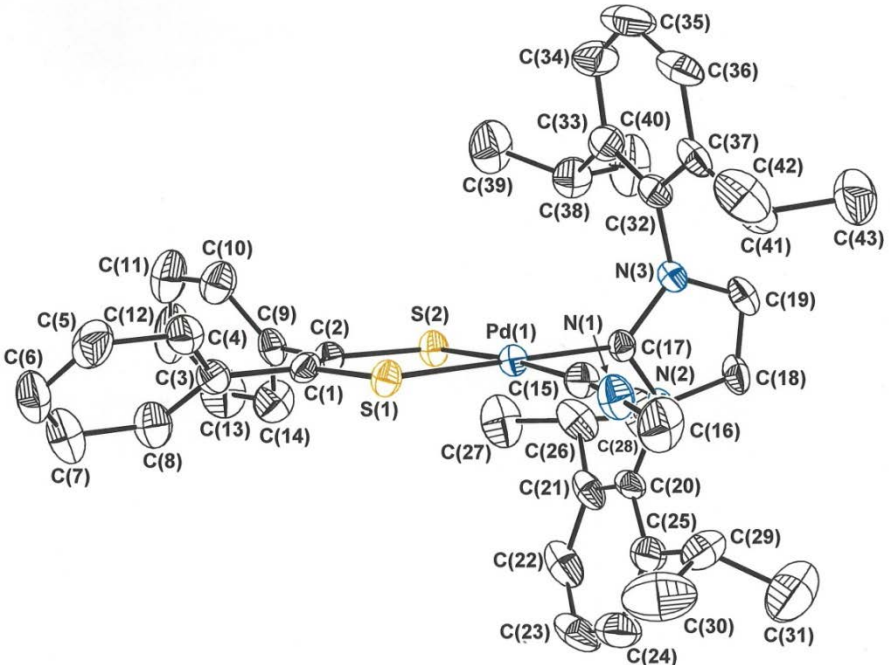

Figure S33. Anisotropic thermal ellipsoid plot at the 50% probability level for [($Ph_2C_2S_2$)Pd(CNMe)(IPr)]. All hydrogen atoms are omitted for clarity.

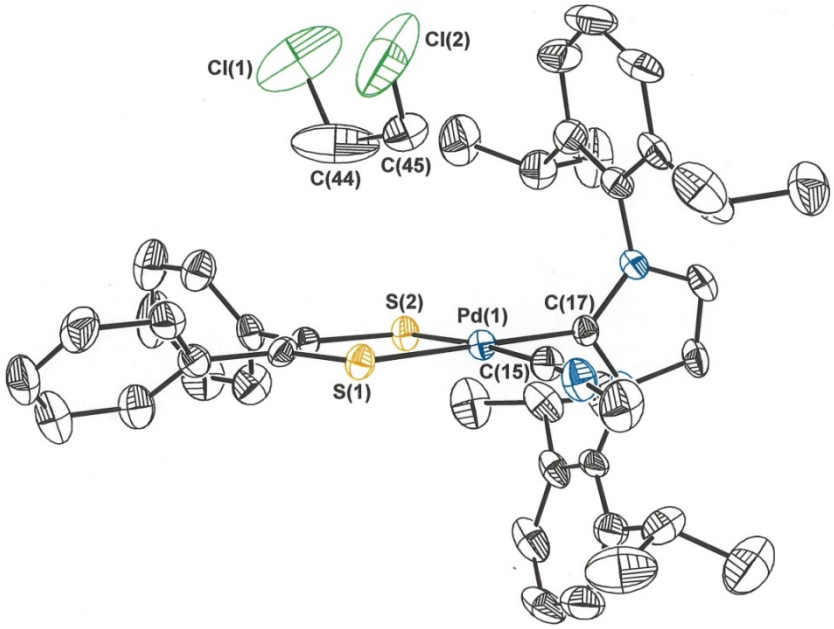

Figure S34. Thermal ellipsoid plot at the 50% probability level for [($Ph_2C_2S_2$)Pd(CNMe)(IPr)] ·$ClCH_2CH_2Cl$ with atom labeling for interstitial $ClCH_2CH_2Cl$ molecule. All hydrogen atoms are omitted for clarity.

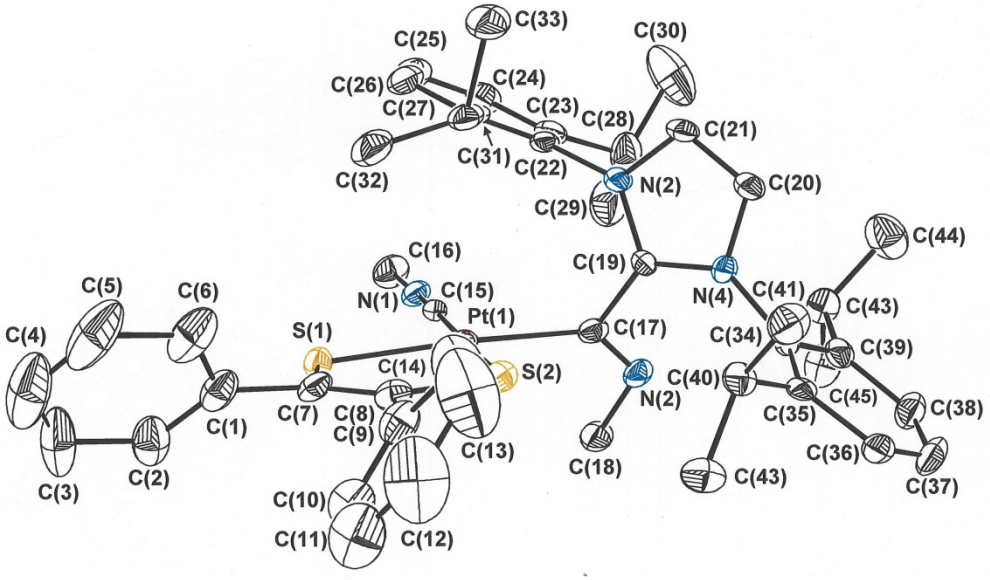

Figure S35. Thermal ellipsoid plot at the 50% probability level for [($Ph_2C_2S_2$)Pt(CNMe)(C(NMe)(IPr))], molecule one of two. All hydrogen atoms are omitted for clarity.

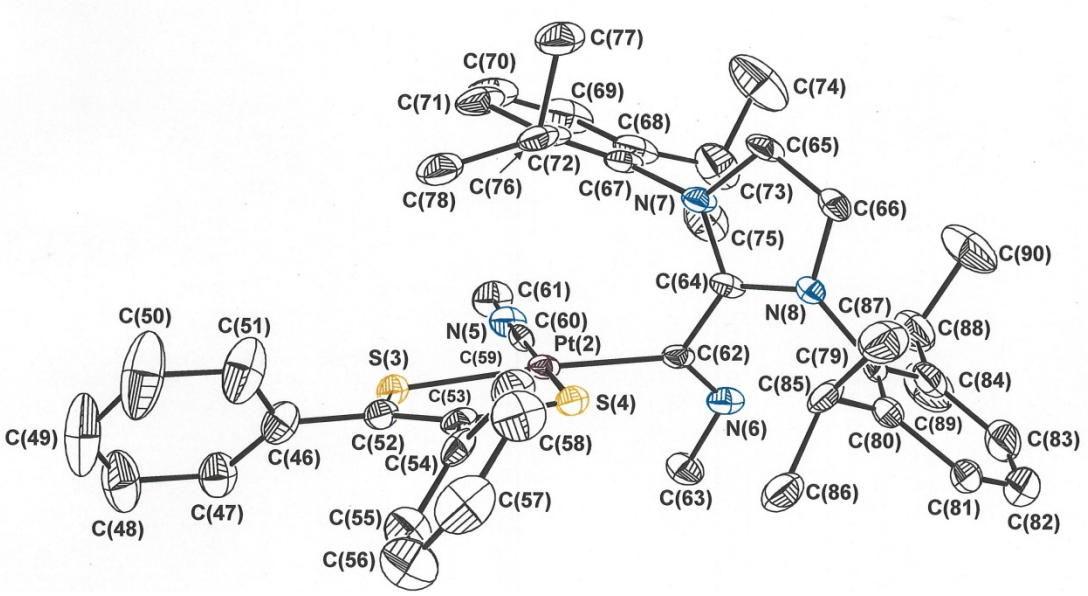

Figure S36. Thermal ellipsoid plot at the 50% probability level for [($Ph_2C_2S_2$)Pt(CNMe)(C(NMe)(IPr))], molecule two of two. All hydrogen atoms are omitted for clarity.

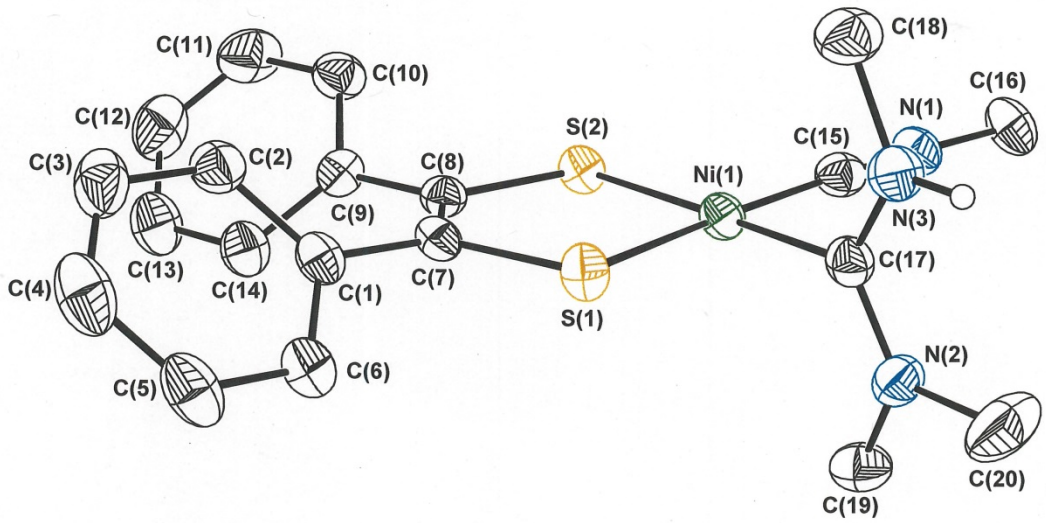

Figure S37. Thermal ellipsoid plot at the 50% probability level for $[(Ph_2C_2S_2)Ni(CNMe)(C(NHMe)(NMe_2)]$. All hydrogen atoms, except that on the NHMe substituent of the $C(NHMe)(NMe_2)$ ligand are omitted for clarity.

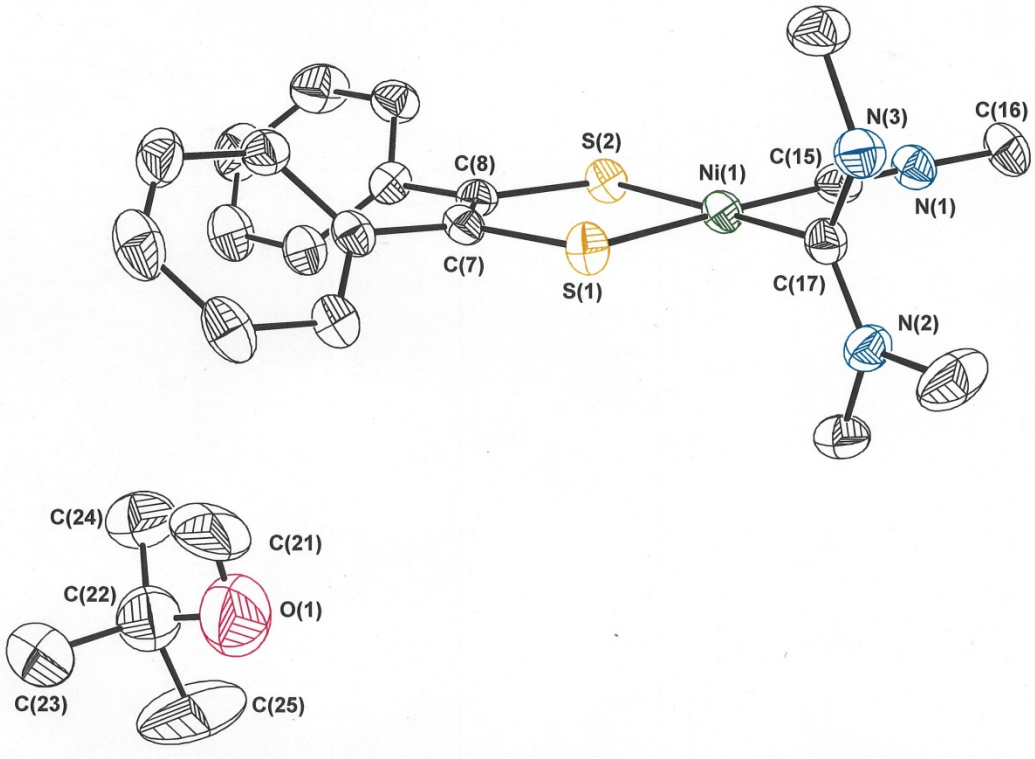

Figure S38. Thermal ellipsoid plot at the 50% probability level for $[(Ph_2C_2S_2)Ni(CNMe)(C(NHMe)(NMe_2)]\cdot{}^{t}BuOMe$ with atom labeling for interstitial $^{t}BuOMe$ molecule. All hydrogen atoms are omitted for clarity.

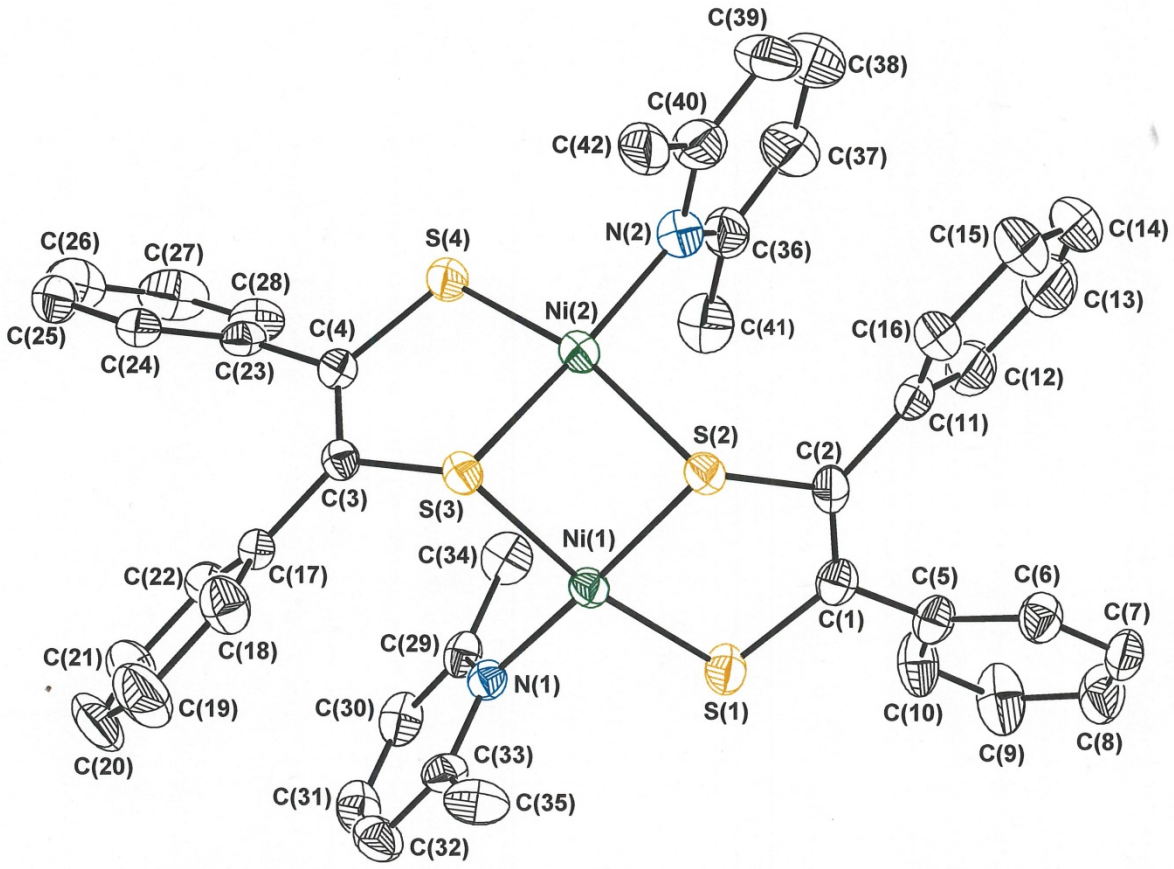

Figure S39. Thermal ellipsoid plot at the 50% probability level for [$Ni_2(\mu\text{-}Ph_2C_2S_2)_2(2,6\text{-}Me_2Py)_2$)] with full atom labeling. All hydrogen atoms are omitted for clarity.

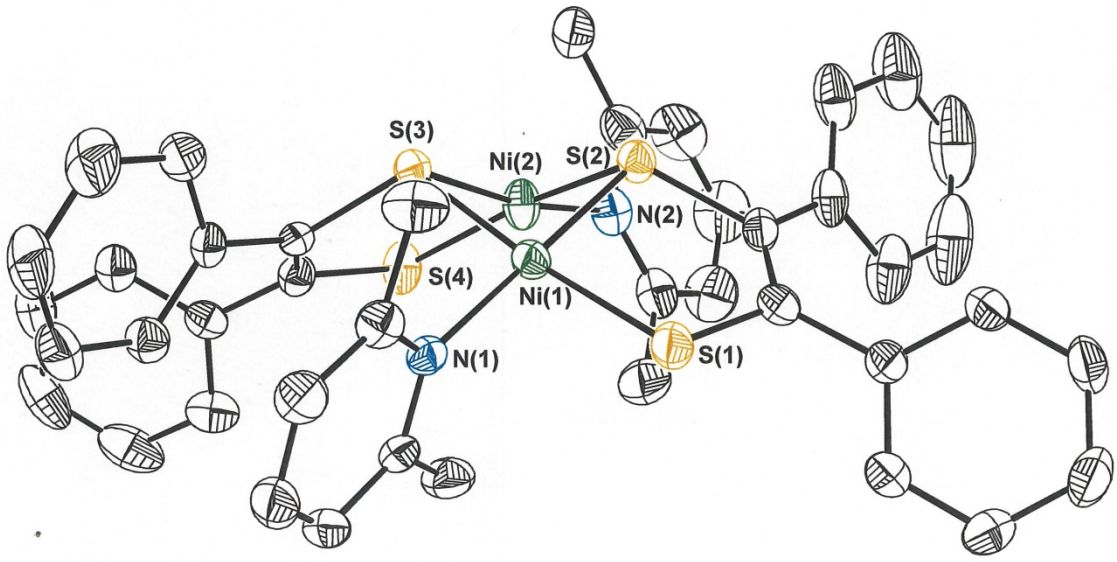

Figure S40. Thermal ellipsoid plot at the 50% probability level for [$Ni_2(\mu\text{-}Ph_2C_2S_2)_2(2,6\text{-}Me_2Py)_2$)], "side-on" view. All hydrogen atoms are omitted for clarity.

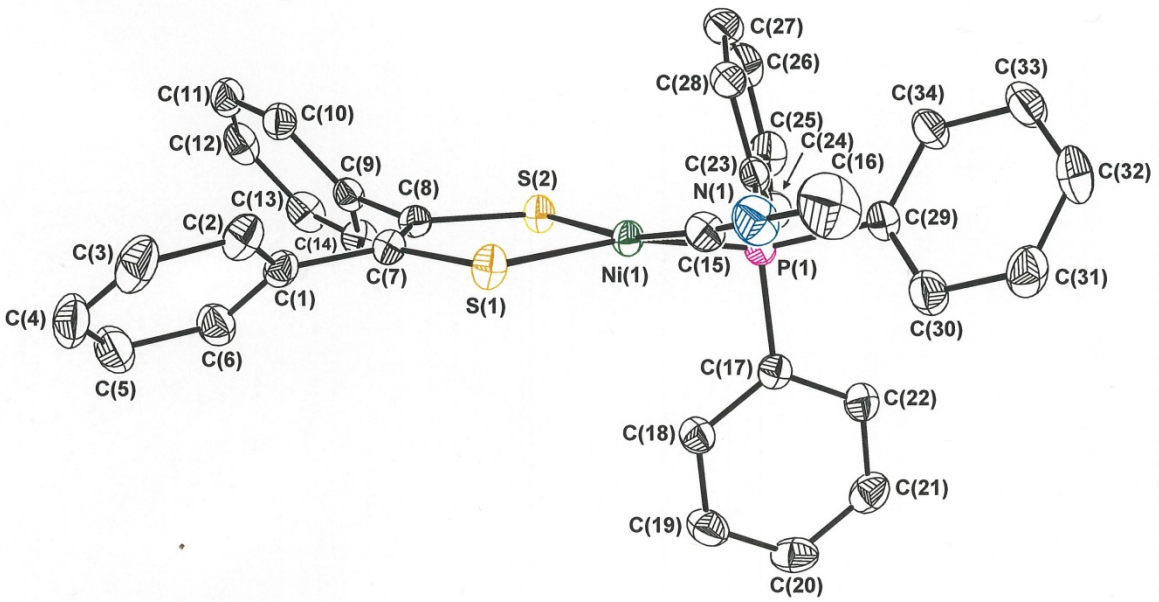

Figure S41. Thermal ellipsoid plot at the 50% probability level for [($Ph_2C_2S_2$)Ni(CNMe)(PPh_3)] with full atom labeling. All hydrogen atoms are omitted for clarity.

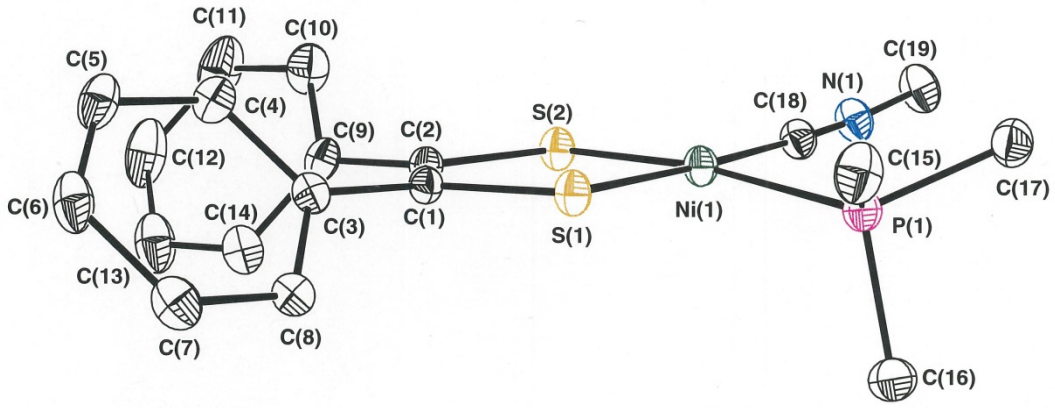

Figure S42. Thermal ellipsoid plot at the 50% probability level for [($Ph_2C_2S_2$)Ni(CNMe)(PMe_3)] with full atom labeling. All hydrogen atoms are omitted for clarity.

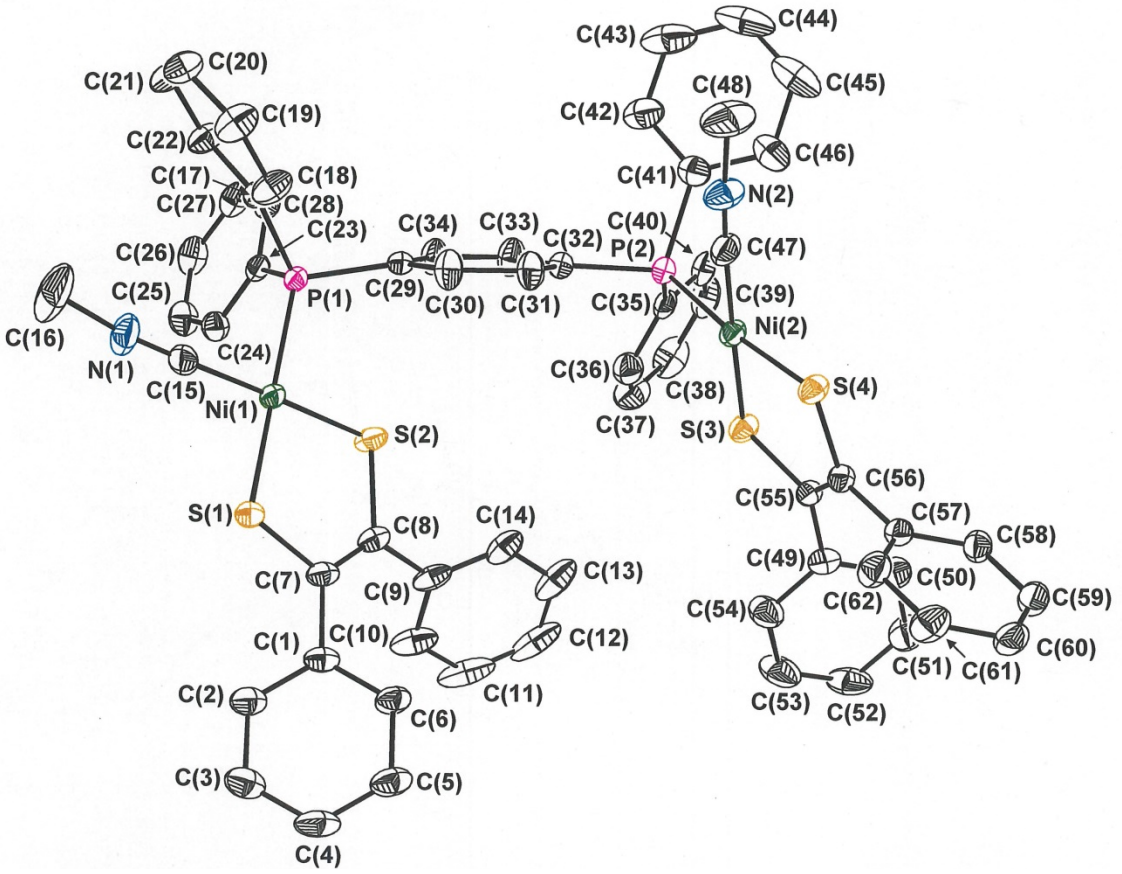

Figure S43. Thermal ellipsoid plot at the 50% probability level for $[(Ph_2C_2S_2)Ni(CNMe)]_2(\mu\text{-}1,4\text{-}(Ph_2P)_2C_6H_4)]$. All hydrogen atoms are omitted for clarity.

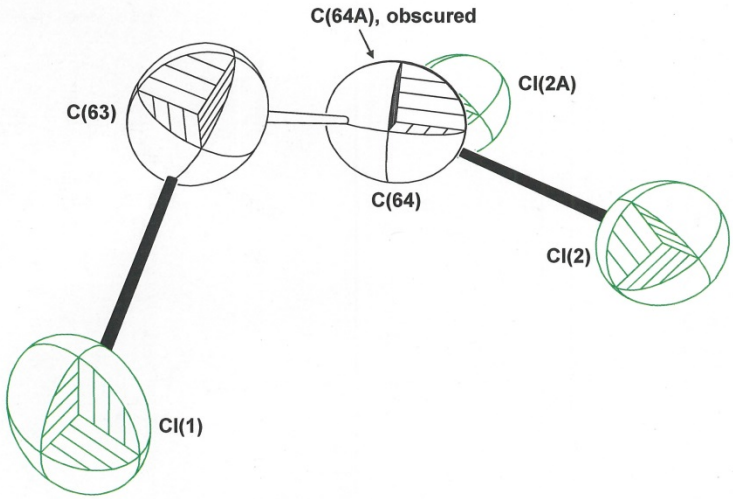

Figure S44. Thermal ellipsoid plot at the 50% probability level for interstitial $ClCH_2CH_2Cl$ molecule in $[(Ph_2C_2S_2)Ni(CNMe)]_2(\mu\text{-}1,4\text{-}(Ph_2P)_2C_6H_4)]\cdot ClCH_2CH_2Cl$. Hydrogen atoms are omitted for clarity.

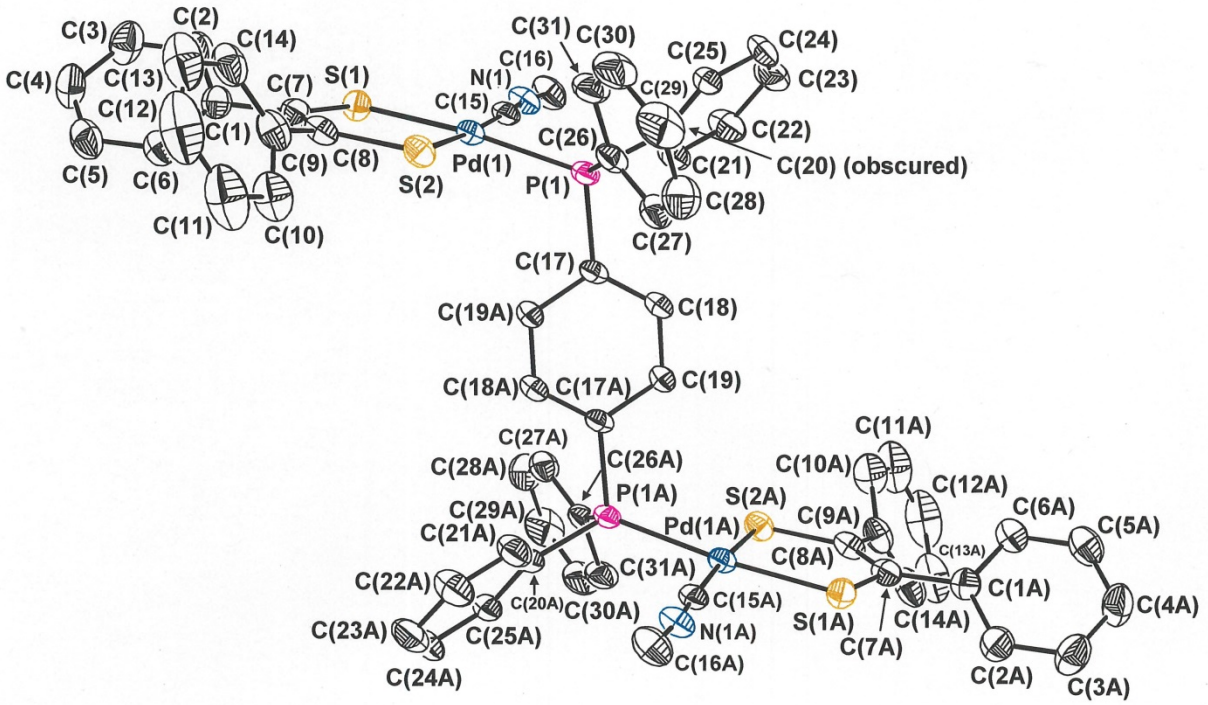

Figure S45. Thermal ellipsoid plot at the 50% probability level for $[(Ph_2C_2S_2)Pd(CNMe)]_2(\mu\text{-}1,4\text{-}(Ph_2P)_2C_6H_4)]$. All hydrogen atoms are omitted for clarity.

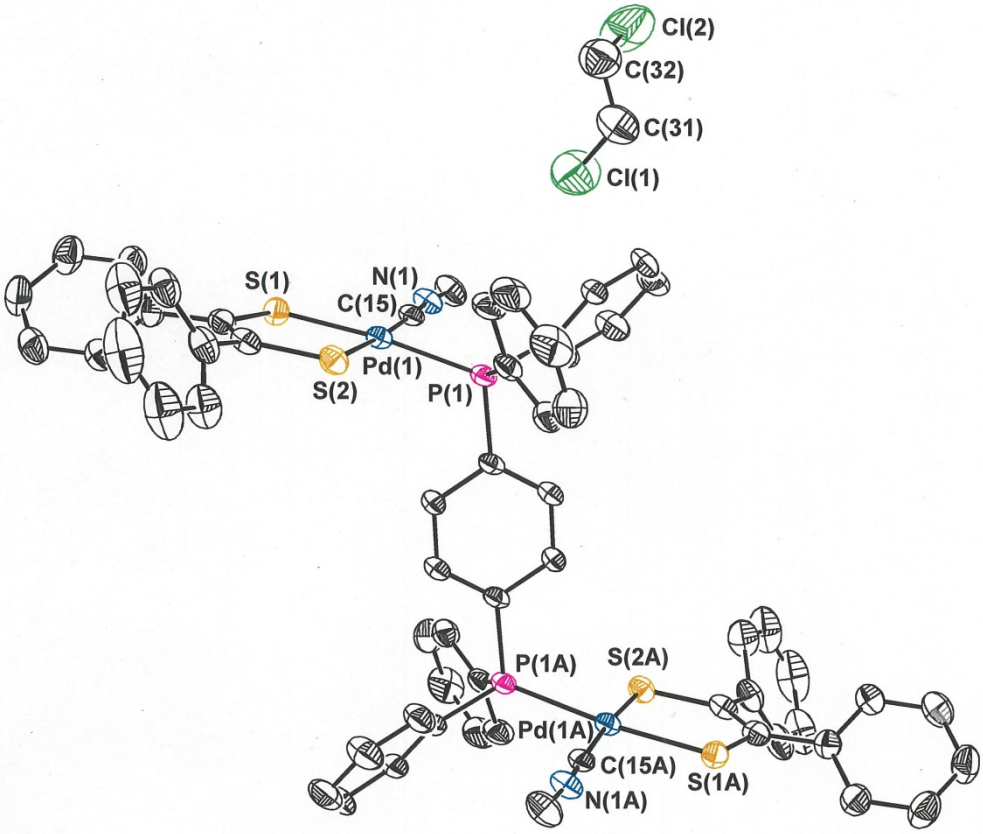

Figure S46. Thermal ellipsoid plot at the 50% probability level for $[(Ph_2C_2S_2)Pd(CNMe)]_2(\mu\text{-}1,4\text{-}(Ph_2P)_2C_6H_4)]\cdot ClCH_2CH_2Cl$ with atom labeling for interstitial $ClCH_2CH_2Cl$ molecule. All hydrogen atoms are omitted for clarity.

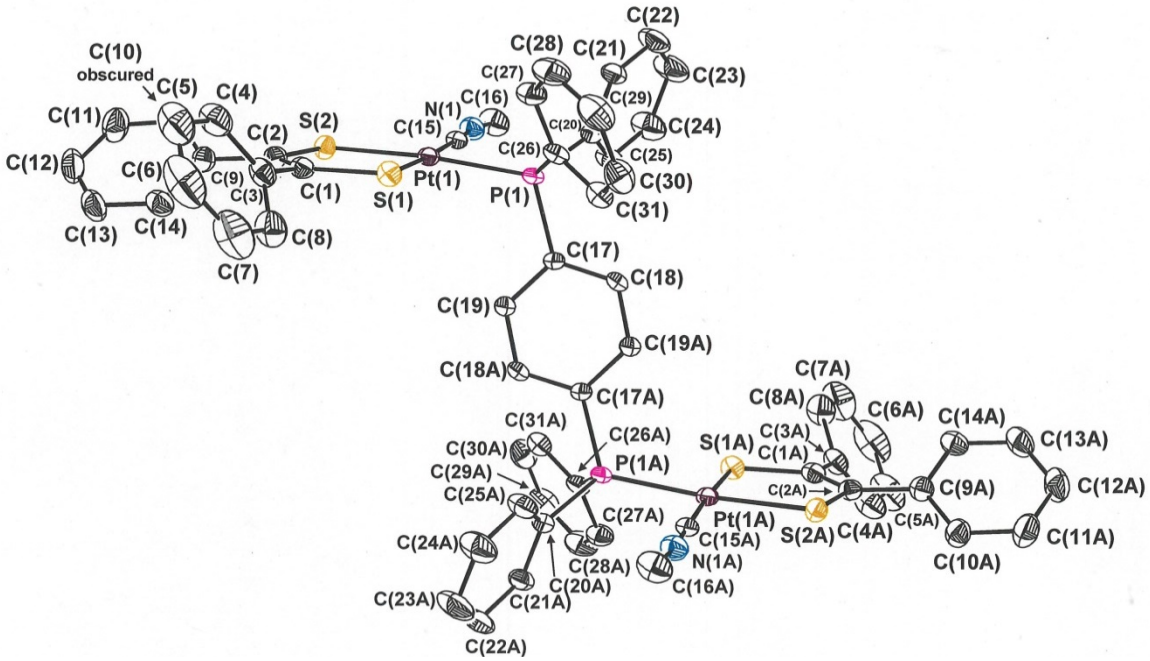

Figure S47. Thermal ellipsoid plot at the 50% probability level for $[(Ph_2C_2S_2)Pt(CNMe)]_2(\mu\text{-}1,4\text{-}(Ph_2P)_2C_6H_4)]$. All hydrogen atoms are omitted for clarity.

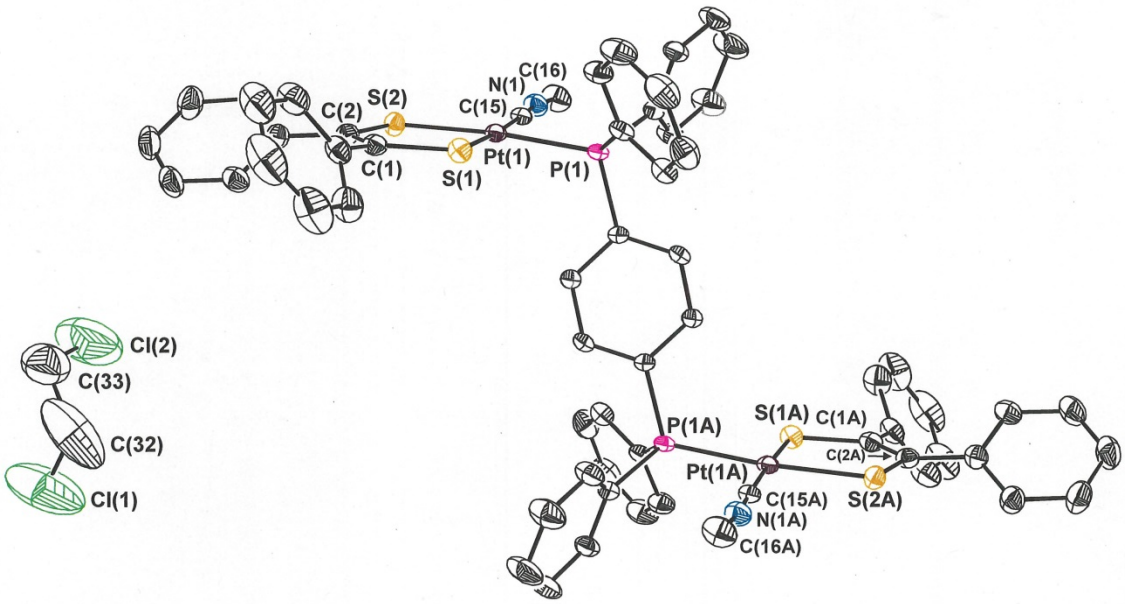

Figure S48. Thermal ellipsoid plot at the 50% probability level for $[(Ph_2C_2S_2)Pt(CNMe)]_2(\mu\text{-}1,4\text{-}(Ph_2P)_2C_6H_4)]\cdot ClCH_2CH_2Cl$ with atom labeling for interstitial $ClCH_2CH_2Cl$ molecule. All hydrogen atoms are omitted for clarity.

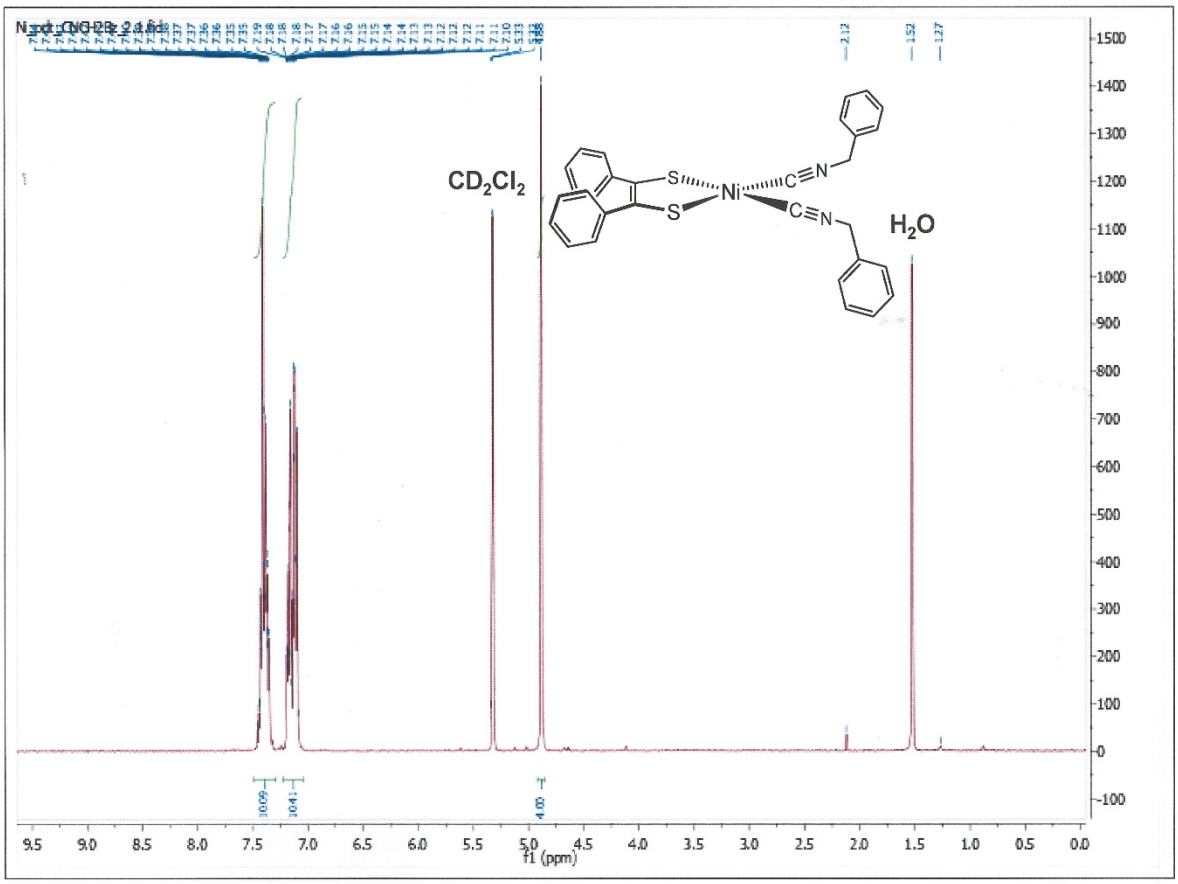

Figure S49. ^{1}H NMR spectrum of $[(Ph_2C_2S_2)Ni(C{\equiv}NCH_2C_6H_5)_2]$ in CD_2Cl_2.

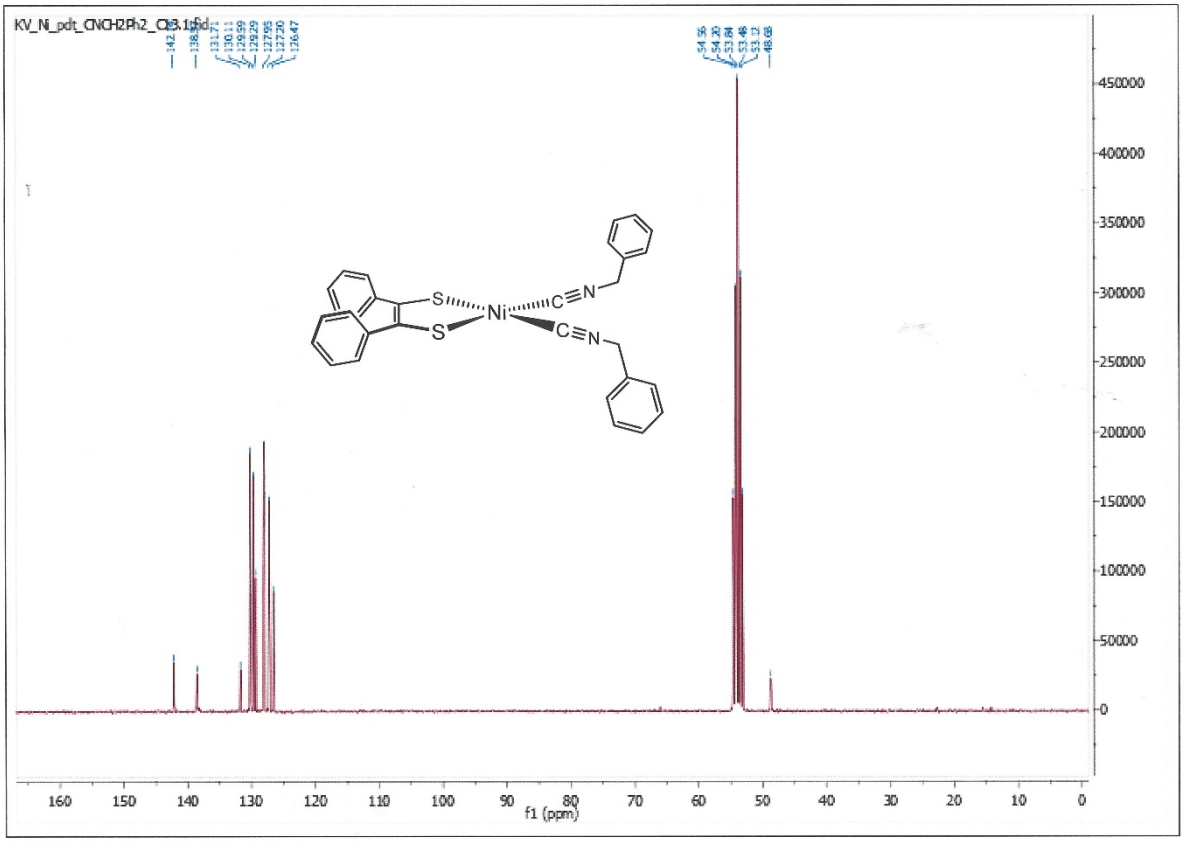

Figure S50. ^{13}C NMR spectrum of $[(Ph_2C_2S_2)Ni(C{\equiv}NCH_2C_6H_5)_2]$ in CD_2Cl_2.

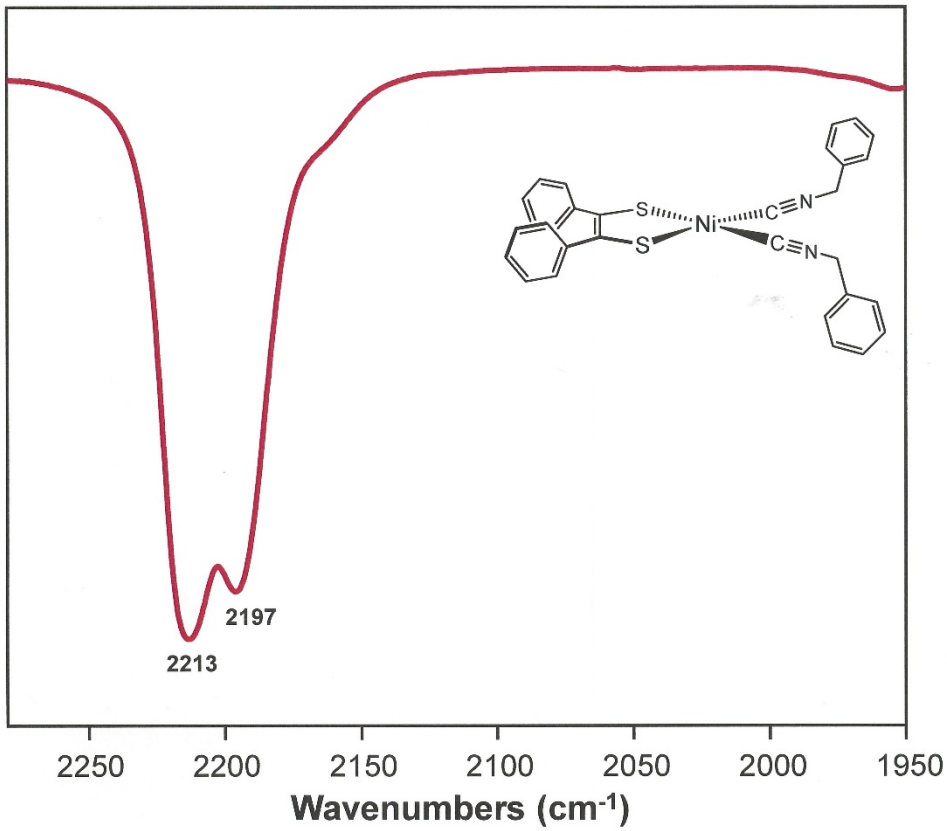

Figure S51. Solution IR spectrum of $[(Ph_2C_2S_2)Ni(C{\equiv}NCH_2C_6H_5)_2]$ in CH_2Cl_2.

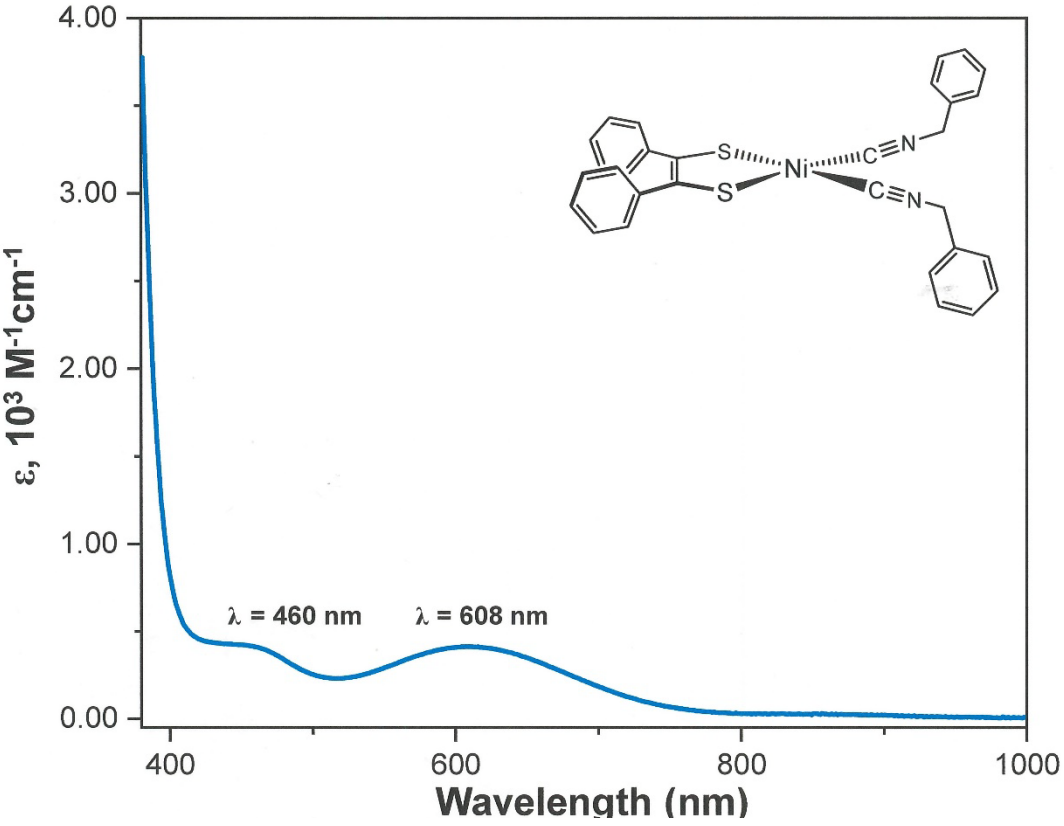

Figure S52. UV-vis spectrum of $[(Ph_2C_2S_2)Ni(C{\equiv}NCH_2C_6H_5)_2]$ in CH_2Cl_2.

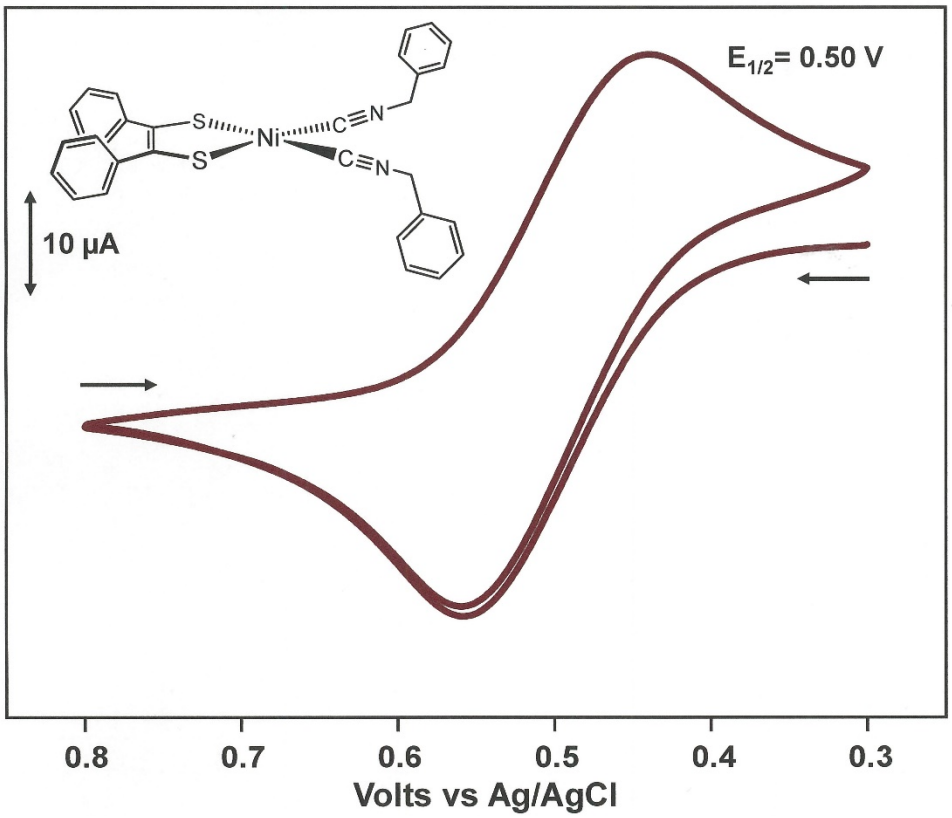

Figure S53. Cyclic voltammogram of $[(Ph_2C_2S_2)Ni(C{\equiv}NCH_2C_6H_5)_2]$ in CH_2Cl_2 with $[^nBu_4N][PF_6]$ supporting electrolyte.

Report Number: 112712 GALBRAITH LABORATORIES, INC Report Date: 2019-02-26

Laboratory Report

Report prepared for:
James P Donahue
Tulane Univ
Dept of Chem
Stern Hall, Room 2015
6400 Freret St
New Orleans, LA 70118
Phone: 504-862-3562
Email: donahue@tulane.edu

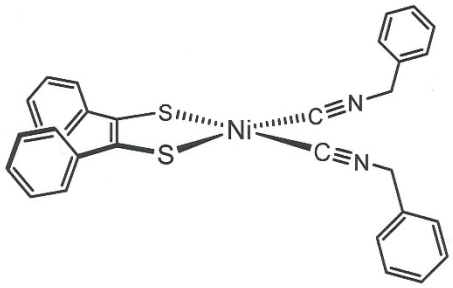

Report prepared by:
Debbie S Robertson

Purchase Order:
Visa,Sanchez,2/14/19

For further assistance, contact:
Debbie S Robertson
Report Production Coordinator
PO Box 51610
Knoxville, TN 37950 -1610
(865) 546-1335
debbierobertson@galbraith.com

Anal. Calcd. for $C_{30}H_{24}N_2NiS_2$: C, 67.31; H, 4.52; N, 5.23.

Sample: JPD172
Lab ID: 2019-I-1984 **Received:** 2019-02-14

Analysis	Method	Result	Basis	Sample Amount Used	Date (Time)
C : Carbon					
	GLI Procedure ME-14	67.18 %	As Received	1.927 mg	2019-02-22
H : Hydrogen					
	GLI Procedure ME-14	4.67 %	As Received	1.927 mg	2019-02-22
N : Nitrogen					
	GLI Procedure ME-14	5.21 %	As Received	1.927 mg	2019-02-22

Signatures:

Created By: Debbie.S.Robertson 2019-02-26T18:07:18.547-05:00
Published By: Debbie.S.Robertson 2019-02-26T18:07:35.8-05:00

- Physical signatures are on file.
- "Published By" signature indicates authorized release of data.

Copyright 2019 Galbraith Laboratories, Inc.
Reported results are only applicable to the item tested.
This report shall not be reproduced, except in full, without the written approval of the laboratory.

Figure S54. Elemental analysis for $[(Ph_2C_2S_2)Ni(C{\equiv}NCH_2C_6H_5)_2]$, Galbraith Laboratories.

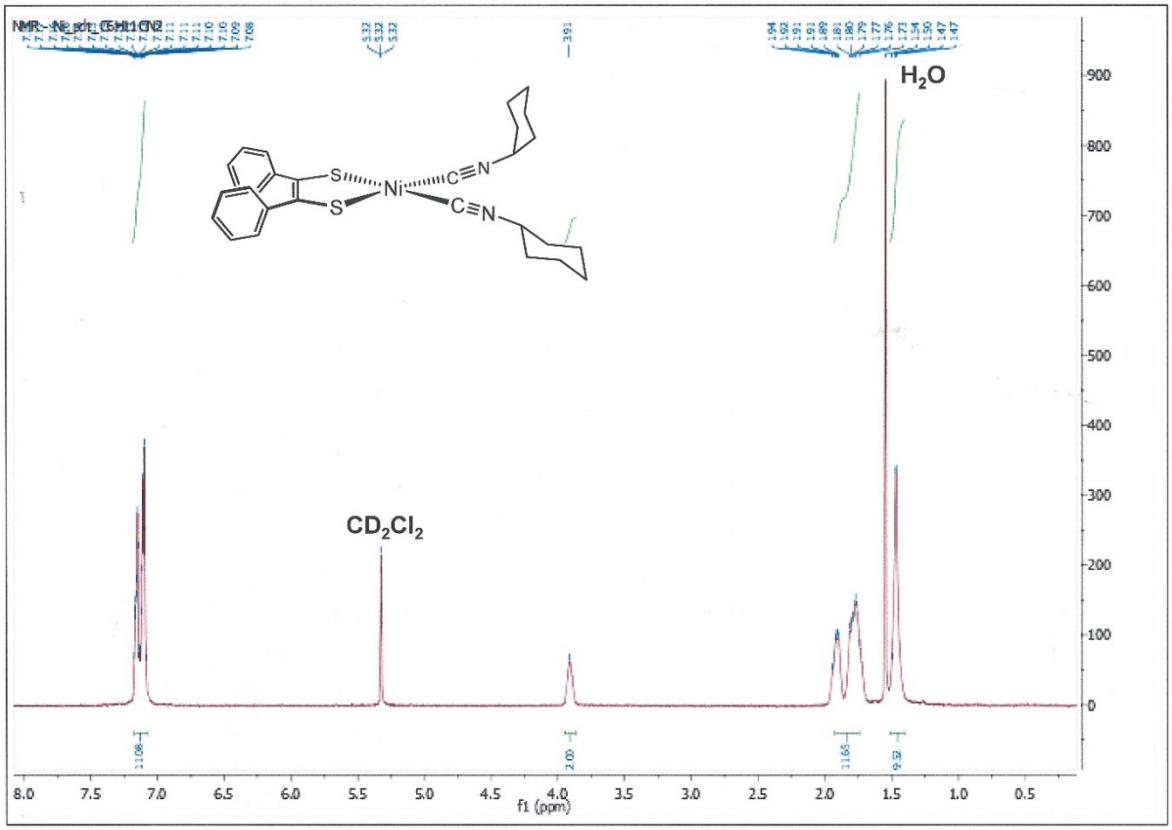

Figure S55. ^{1}H NMR spectrum of [$(Ph_2C_2S_2)Ni(C{\equiv}NCy)_2$] in CD_2Cl_2.

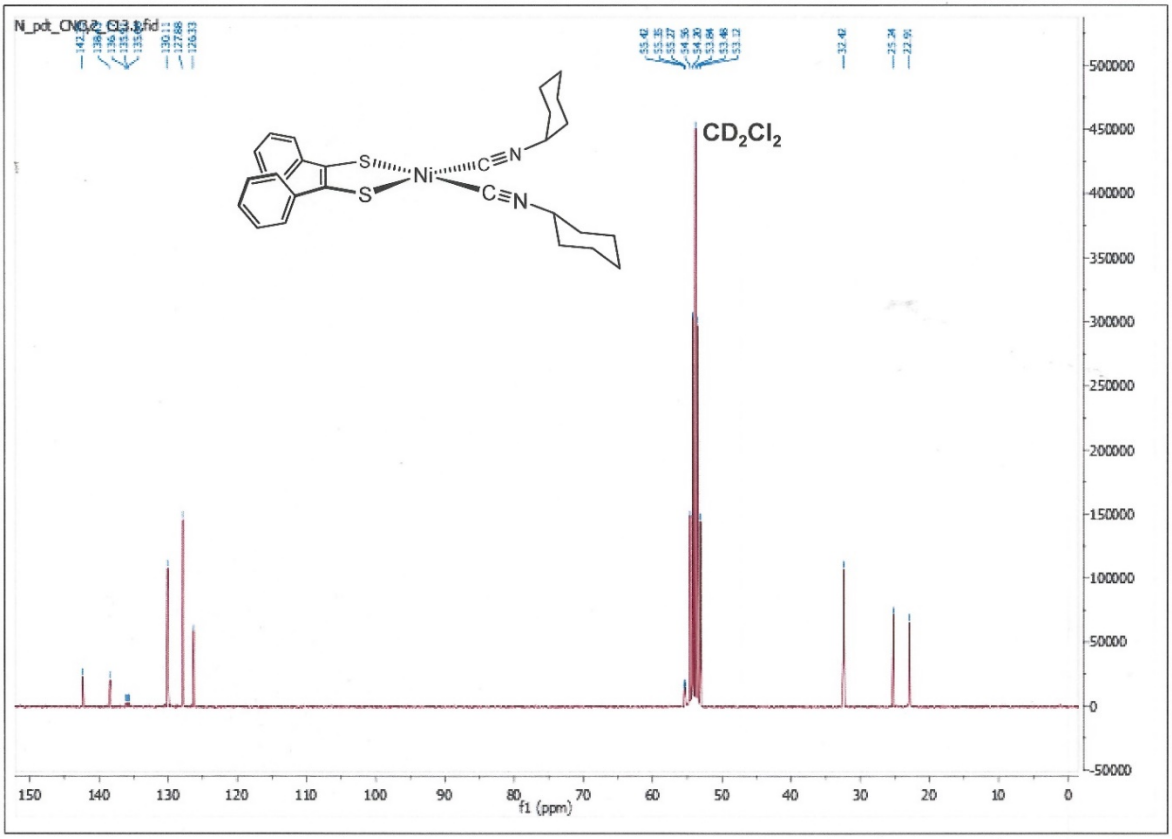

Figure S56. ^{13}C NMR spectrum of [$(Ph_2C_2S_2)Ni(C{\equiv}NCy)_2$] in CD_2Cl_2.

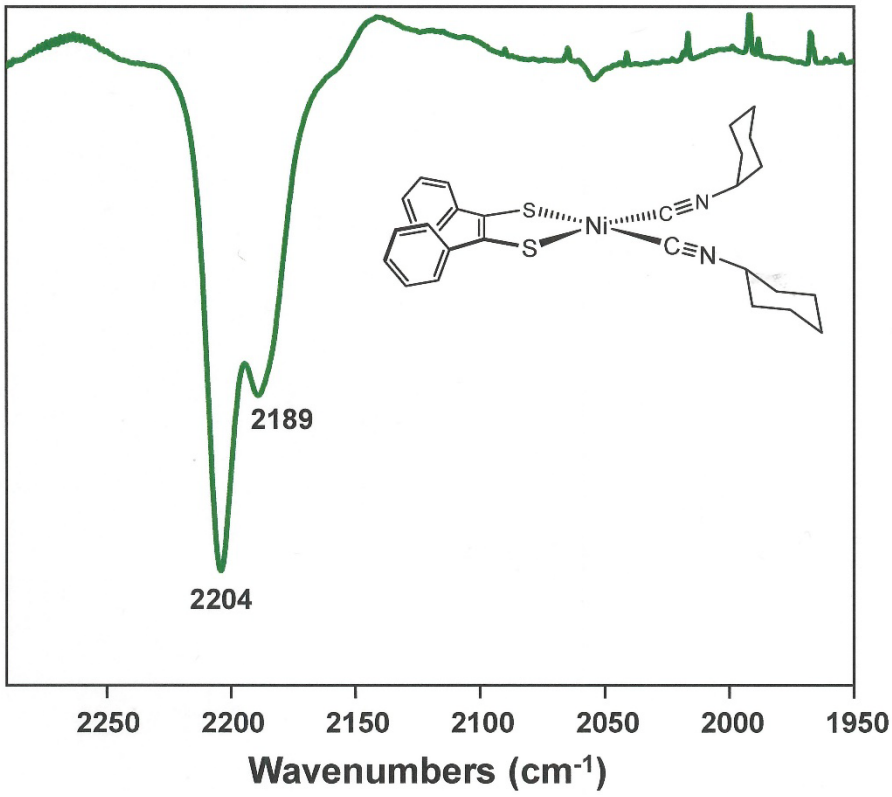

Figure S57. Solution IR spectrum of [($Ph_2C_2S_2$)Ni(C≡NCy)$_2$] in CH_2Cl_2.

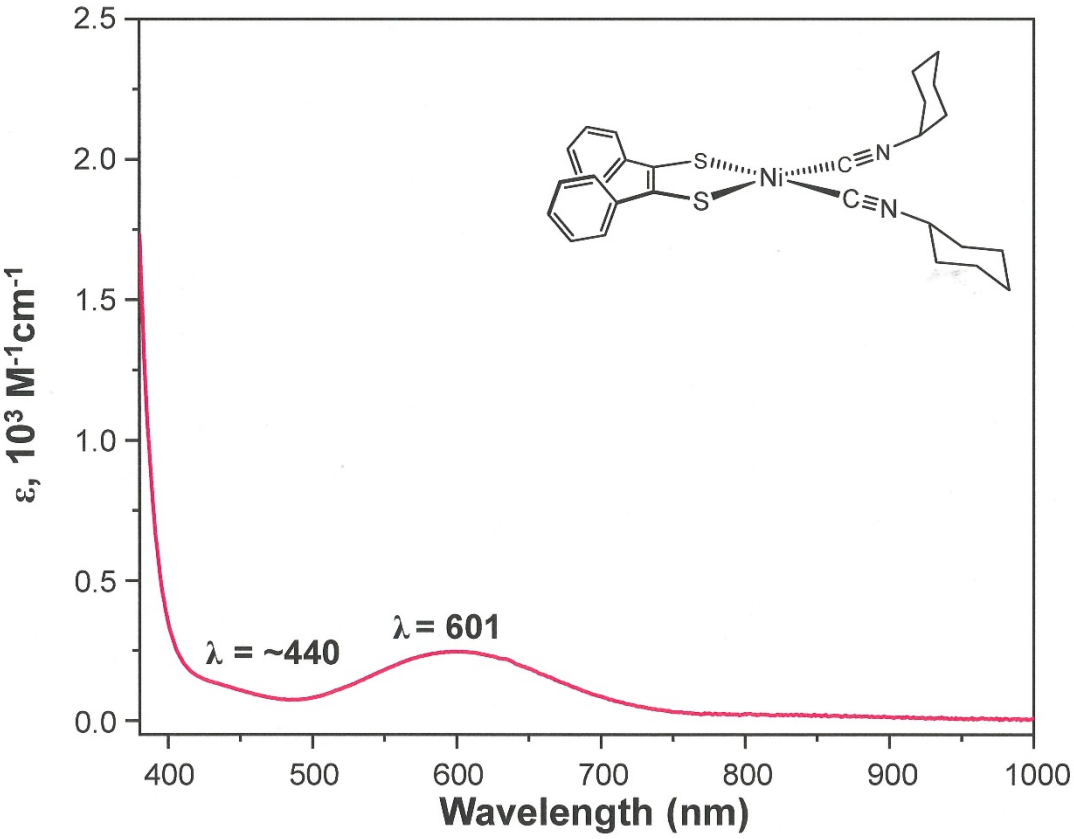

Figure S58. UV-vis spectrum of [($Ph_2C_2S_2$)Ni(C≡NC$_y$)$_2$] in CH_2Cl_2.

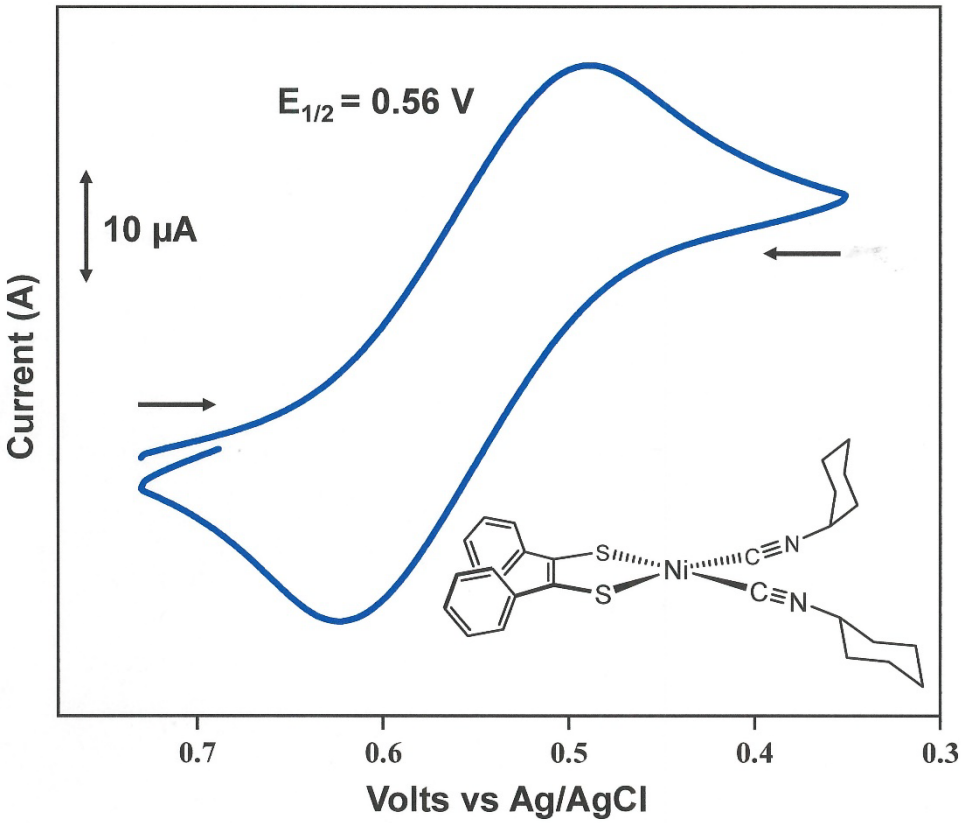

Figure S59. Cyclic voltammogram of $[(Ph_2C_2S_2)Ni(C{\equiv}NCy)_2]$ in CH_2Cl_2 with $[^nBu_4N][PF_6]$ supporting electrolyte.

JPD-123

SAMPLE IDENTIFICATION

James P. Donahue
Dept. of Chemistry, Tulane University
6400 Freret Street
Name New Orleans, LA 70118-5698
City Zip

Date March 31, 2016

Analysis	Theory	% Found	
C	64.74%	64.86	
H	6.22%	5.95	
N	5.39%	5.43	
O	0.00%		
S	12.35%		
Ni	11.30%		

M.P./B.P.

Hygroscopic: Explosive:

Molecular Formula:

To Be Dried: No X
Yes ☐ at °C

ANALYZE for: C, H, N

X Single
☐ Duplicate

m/m Lab Established in 1954
MIDWEST MICROLAB, LLC
7212 N. SHADELAND AVE., SUITE 110 INDIANAPOLIS, IN 46250
PHONE (317) 849-6606 FAX (317) 849-8534

Analysis results may be emailed to donahue@tulane.edu .

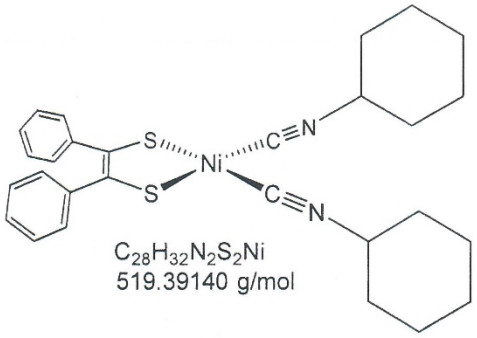

$C_{28}H_{32}N_2S_2Ni$
519.39140 g/mol

Received: APR 12 2016 Completed:

It is suggested that at least 5 mg. of sample be supplied per determination. Liquid samples should be suitably protected by metal foil in the cap if submitted in a screw cap vial. Volatile substances would best be sealed in small ampoules. All samples will be returned for postal charges only.

Figure S60. Elemental analysis for $[(Ph_2C_2S_2)Ni(C{\equiv}NCy)_2]$, Midwest Microlabs.

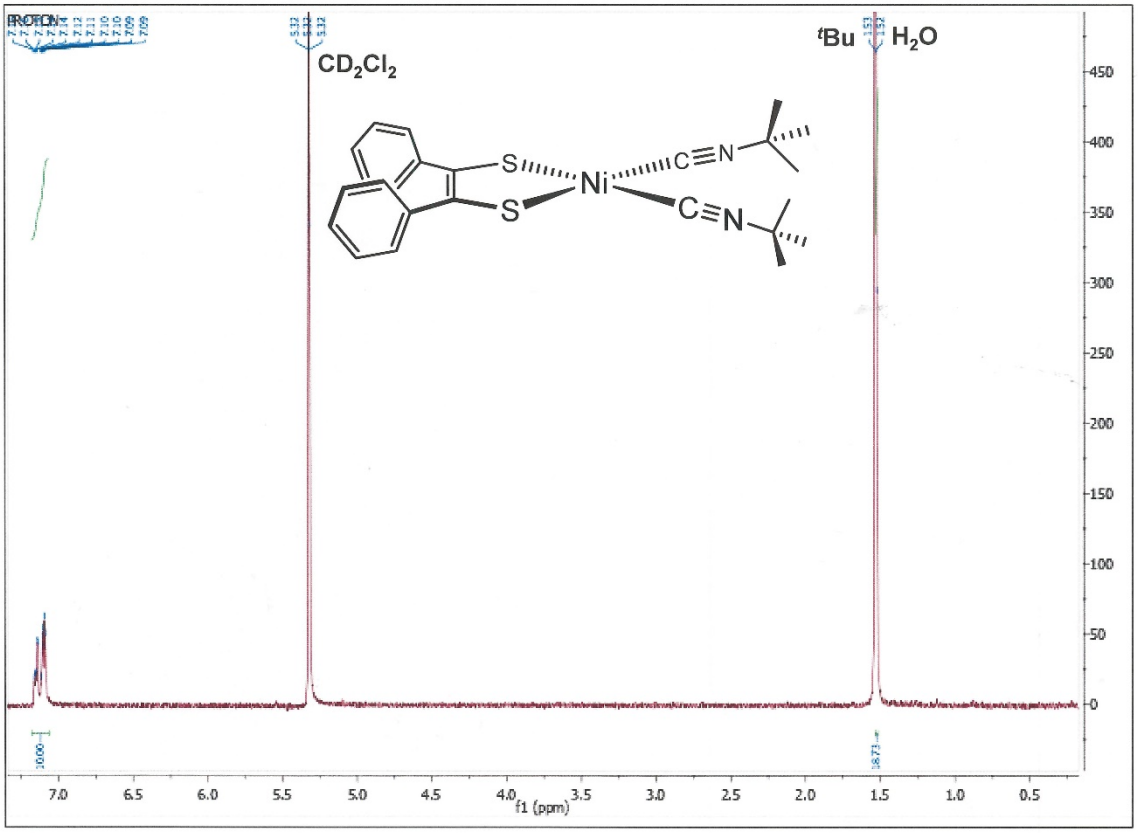

Figure S61. ^{1}H NMR spectrum of [$(Ph_2C_2S_2)Ni(C{\equiv}N^tBu)_2$] in CD_2Cl_2.

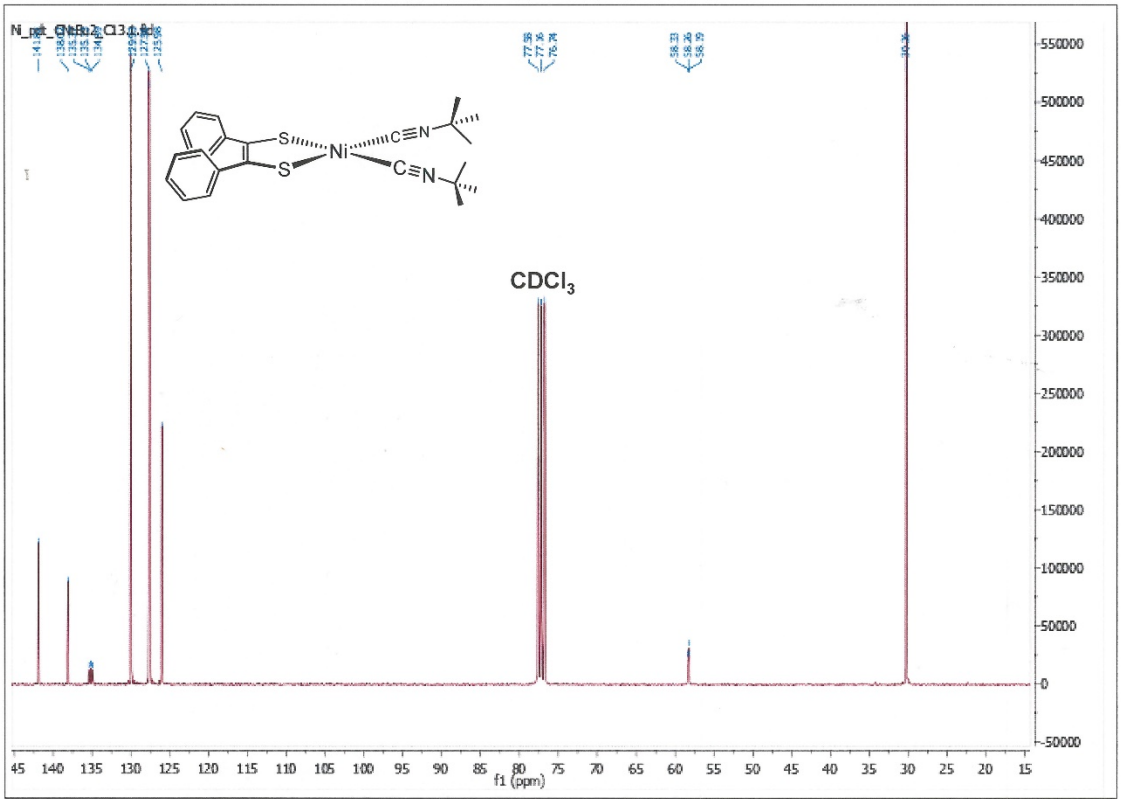

Figure S62. ^{13}C NMR spectrum of [$(Ph_2C_2S_2)Ni(C{\equiv}N^tBu)_2$] in $CDCl_3$.

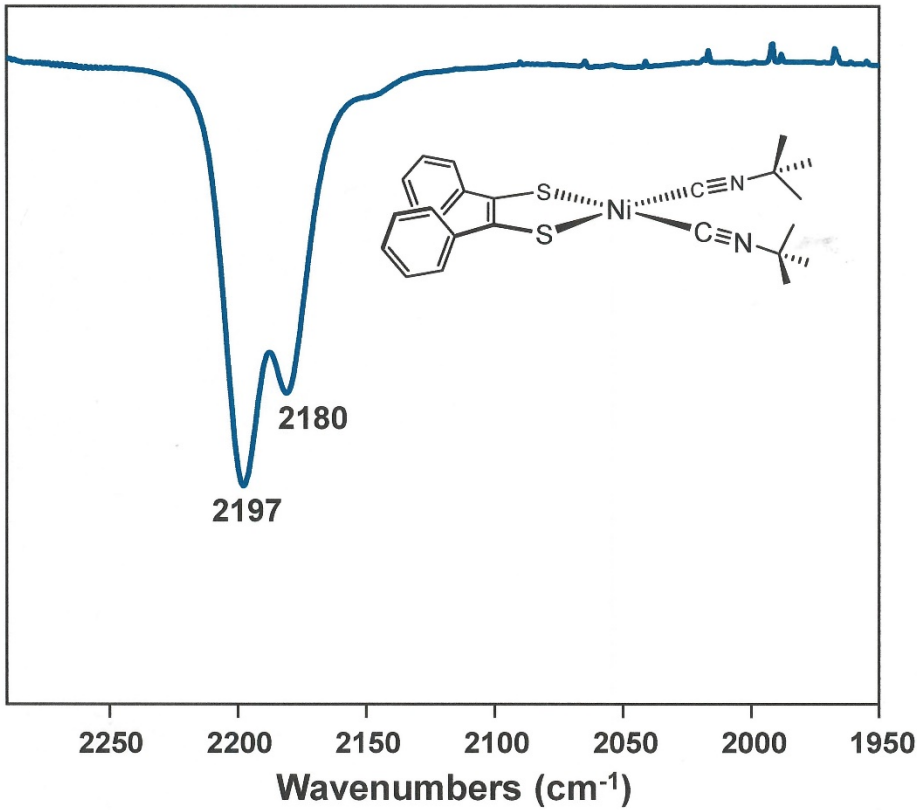

Figure S63. Solution IR spectrum of $[(Ph_2C_2S_2)Ni(C{\equiv}N^tBu)_2]$ in CH_2Cl_2.

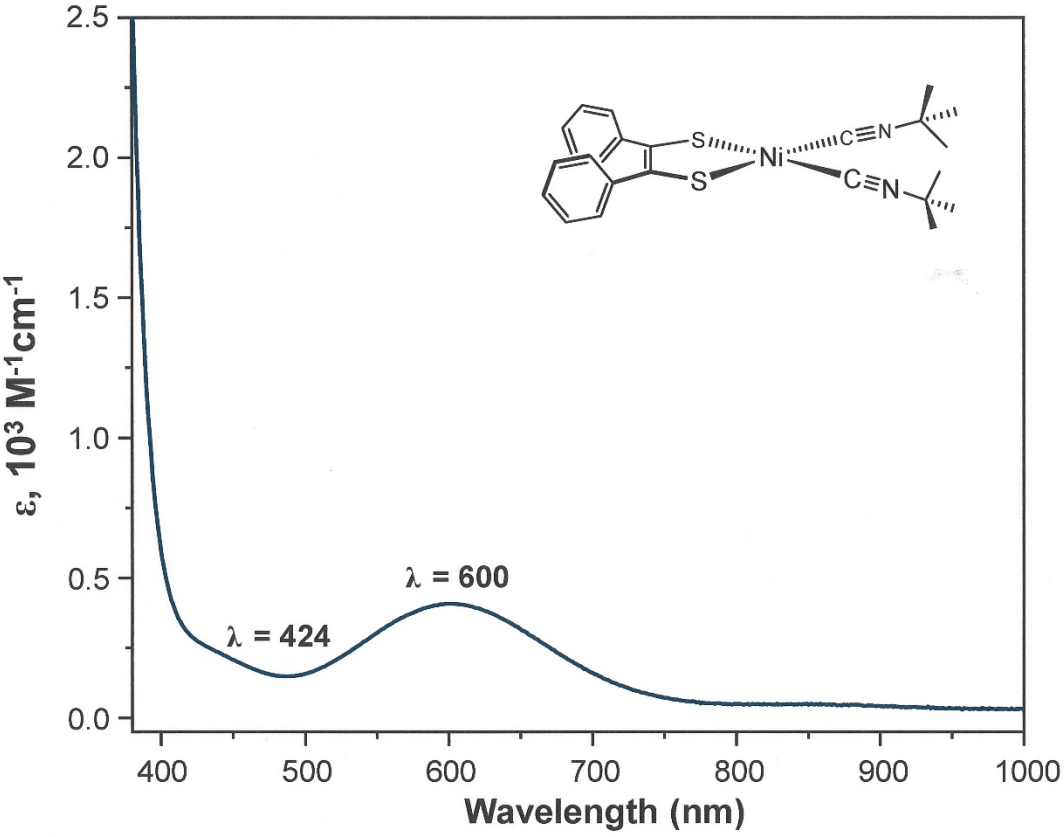

Figure S64. UV-vis spectrum of $[(Ph_2C_2S_2)Ni(C{\equiv}N^tBu)_2]$ in CH_2Cl_2.

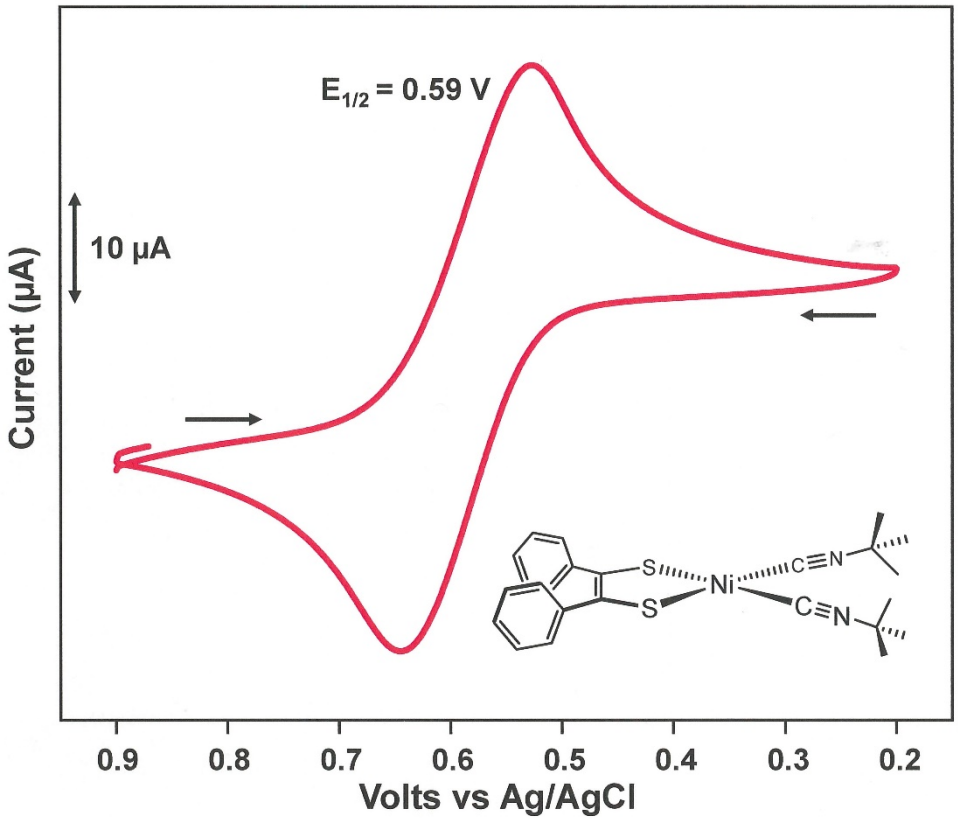

Figure S65. Cyclic voltammogram of $[(Ph_2C_2S_2)Ni(C{\equiv}N^tBu)_2]$ in CH_2Cl_2 with $[^nBu_4N][PF_6]$ supporting electrolyte.

James P. Donahue
Dept. of Chemistry, Tulane University
6400 Freret Street
New Orleans, LA 70118-5698

JPD-112
SAMPLE IDENTIFICATION

Name
City Zip

Date May 27, 2015

Analysis	Theory	% Found	
C	61.68%	61.91	
H	6.04%	6.04	
N	5.99%	6.08	
S	13.72%		
Ni	12.56%		

M.P./B.P.

Hygroscopic: Explosive:

Molecular Formula: $C_{24}H_{28}N_2S_2Ni$

To Be Dried: No ☒
Yes ☐ at °C

ANALYZE for: C, H, N

☒ Single
☐ Duplicate

m/m Lab
Established in 1984

MIDWEST MICROLAB, LLC
7212 N. SHADELAND AVE., SUITE 110 INDIANAPOLIS, IN 46250
PHONE (317) 849-6606 FAX (317) 849-8534

Analysis results may be emailed to donahue@tulane.edu .

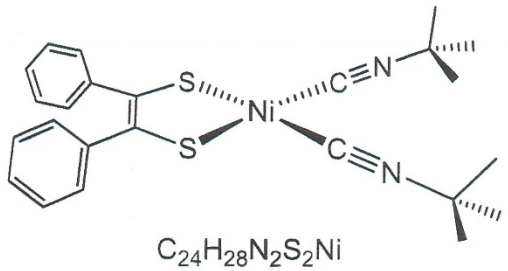

$C_{24}H_{28}N_2S_2Ni$
467.32512 g/mol

Received: JUN - 2 2015 Completed:

It is suggested that at least 5 mg. of sample be supplied per determination. Liquid samples should be suitably protected by metal foil in the cap if submitted in a screw cap vial. Volatile substances would best be sealed in small ampoules. All samples will be returned for postal charges only.

Figure S66. Elemental analysis for $[(Ph_2C_2S_2)Ni(C{\equiv}N^tBu)_2]$, Midwest Microlabs.

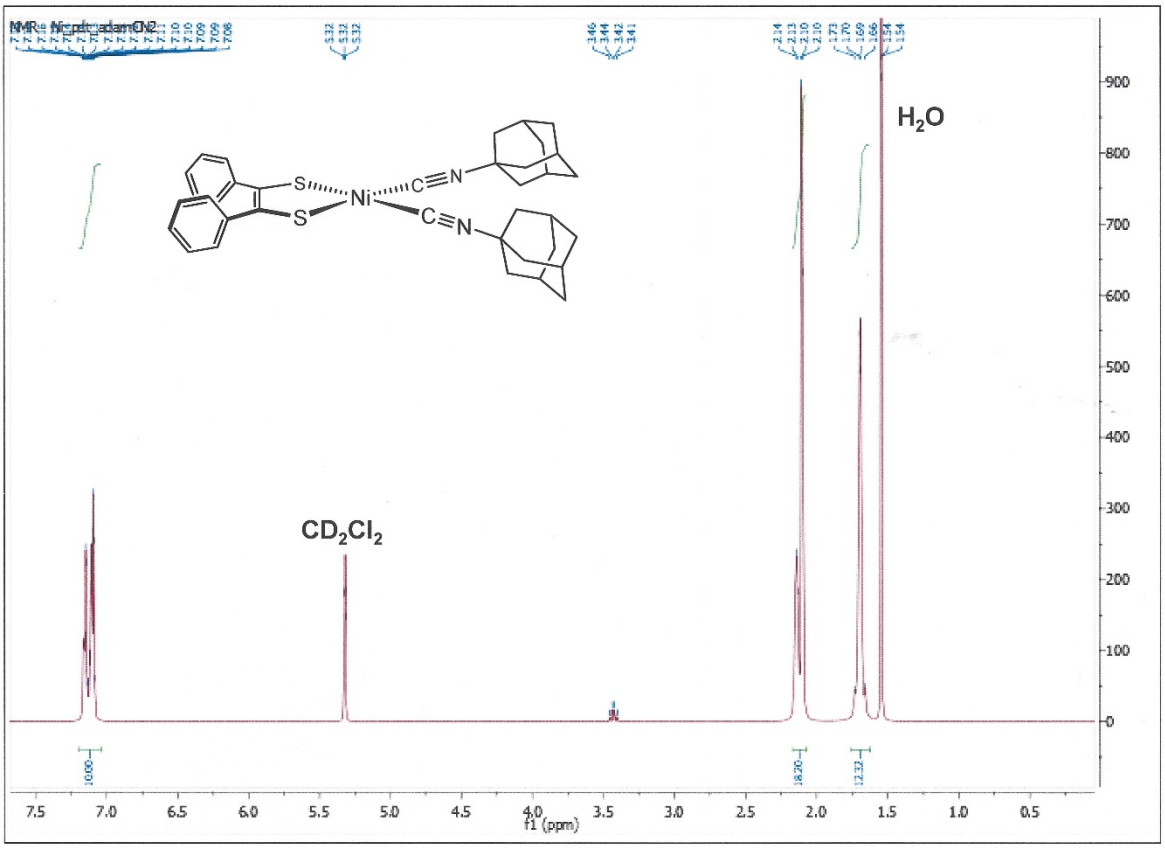

Figure S67. ^{1}H NMR spectrum (CD_2Cl_2) of [($Ph_2C_2S_2$)Ni(C≡N-1-Ad)$_2$].

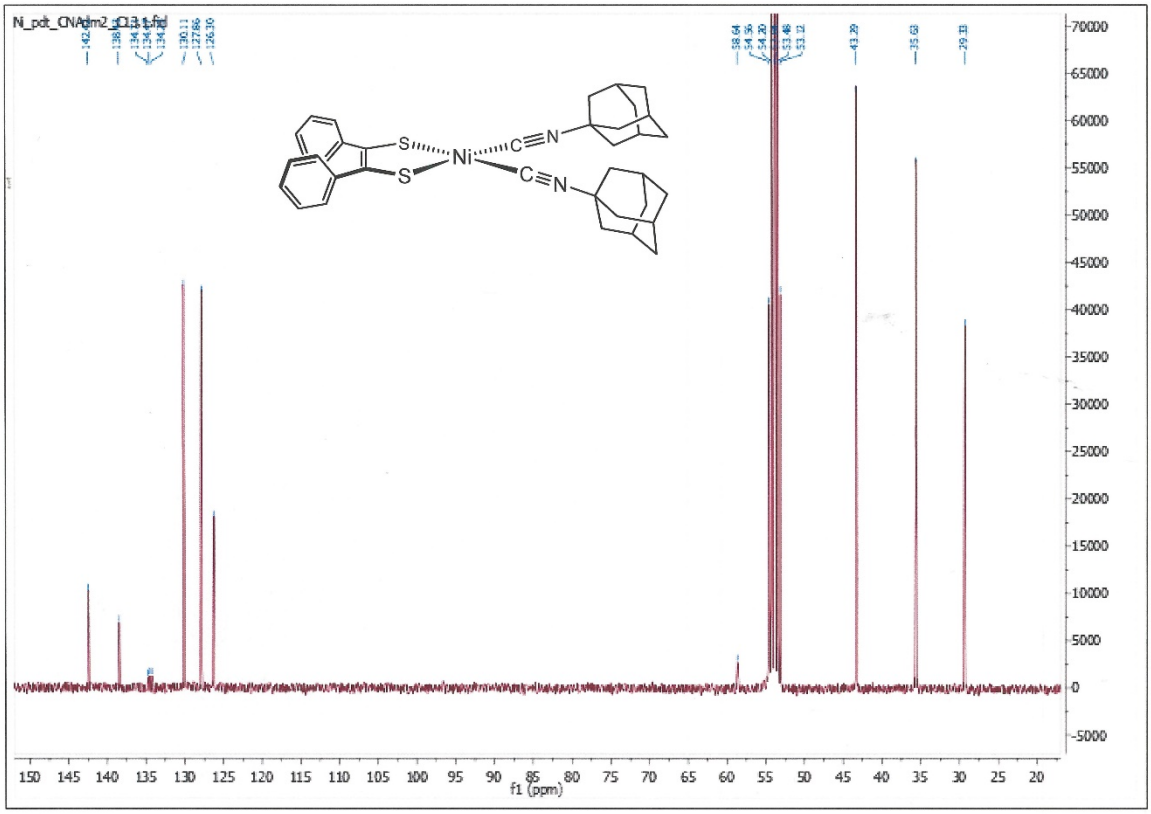

Figure S68. ^{13}C NMR spectrum (CD_2Cl_2) of [($Ph_2C_2S_2$)Ni(C≡N-1-Ad)$_2$].

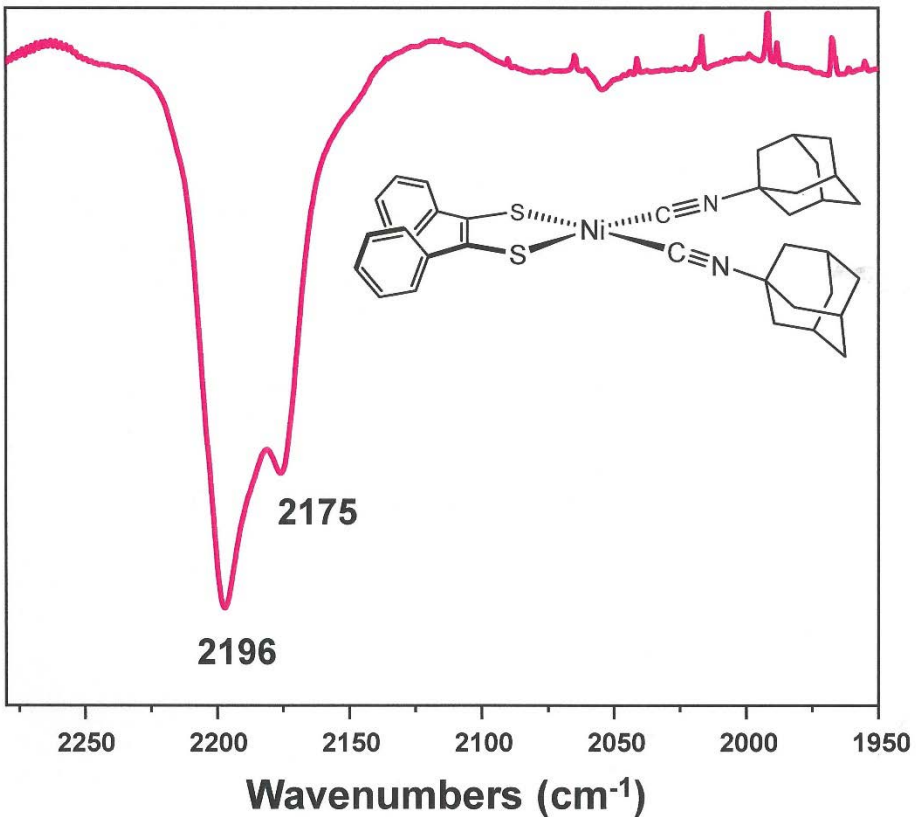

Figure S69. Solution IR spectrum (CH_2Cl_2) of [($Ph_2C_2S_2$)Ni(C≡N-1-Ad)$_2$].

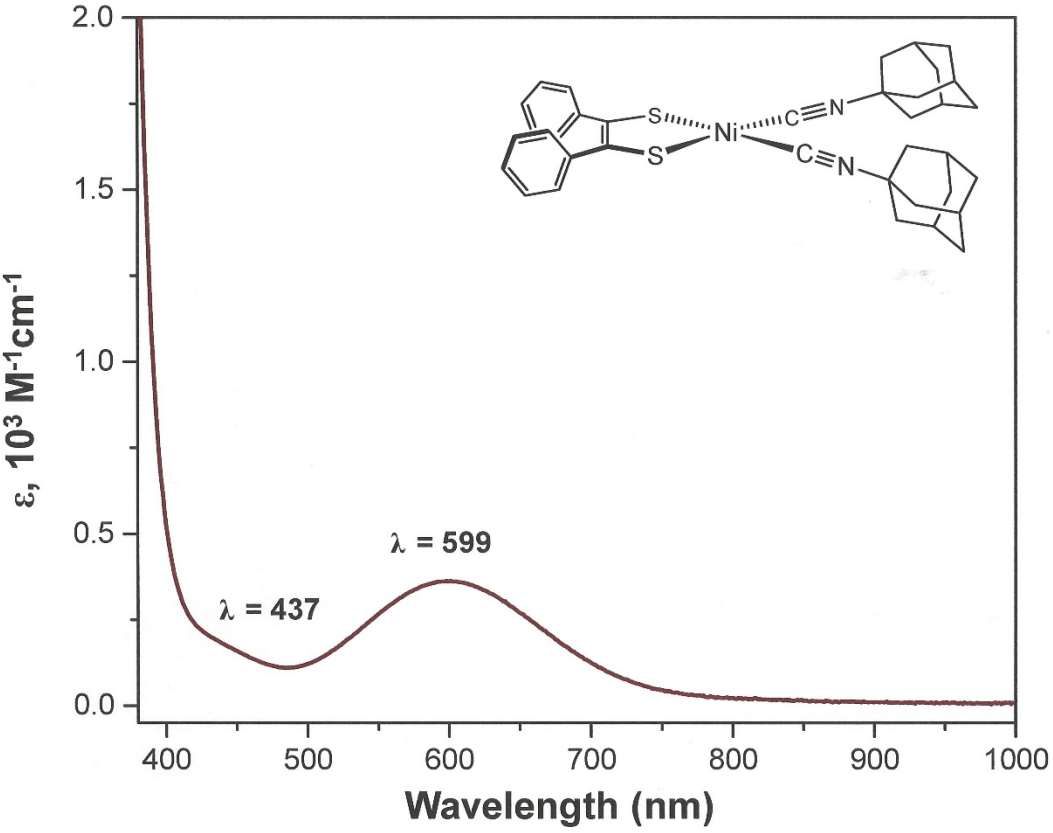

Figure S70. UV-vis spectrum (CH_2Cl_2) of [($Ph_2C_2S_2$)Ni(C≡N-1-Ad)$_2$].

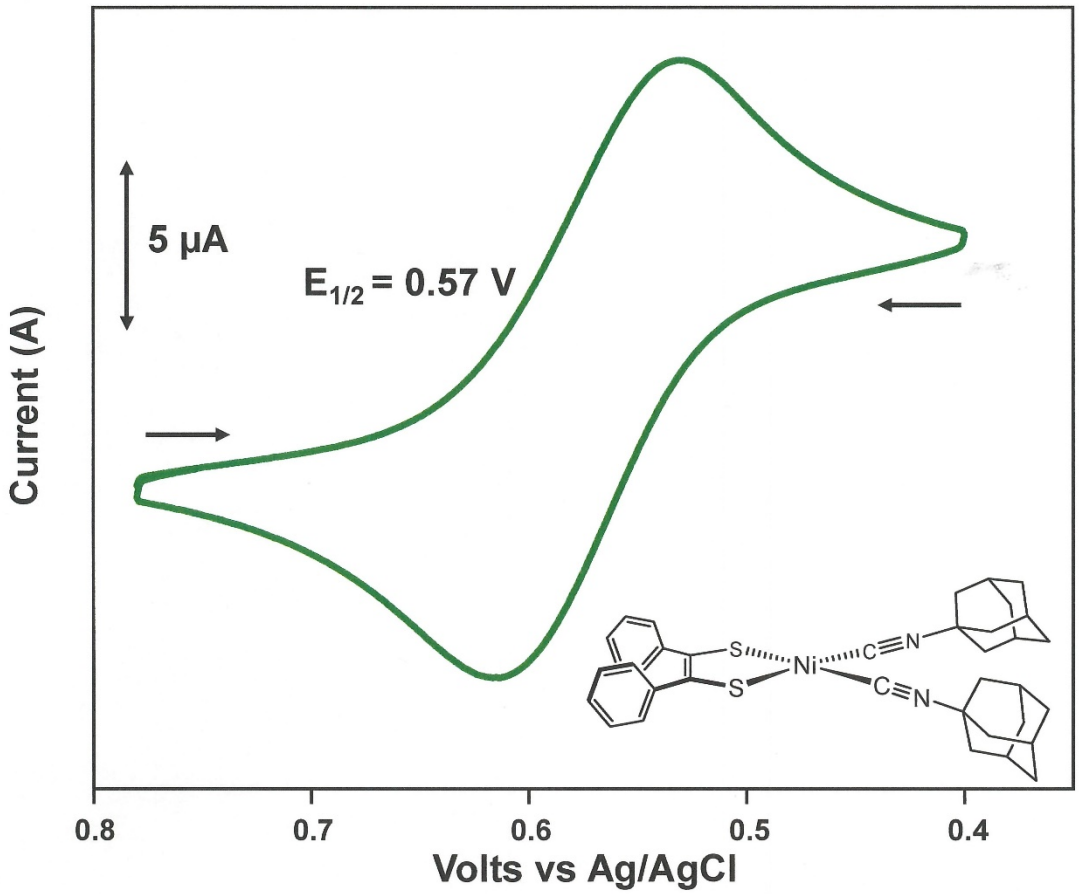

Figure S71. Cyclic voltammogram of (CH_2Cl_2) of [($Ph_2C_2S_2$)Ni(C≡N-1-Ad)$_2$] with [Bu_4N][PF_6] supporting electrolyte.

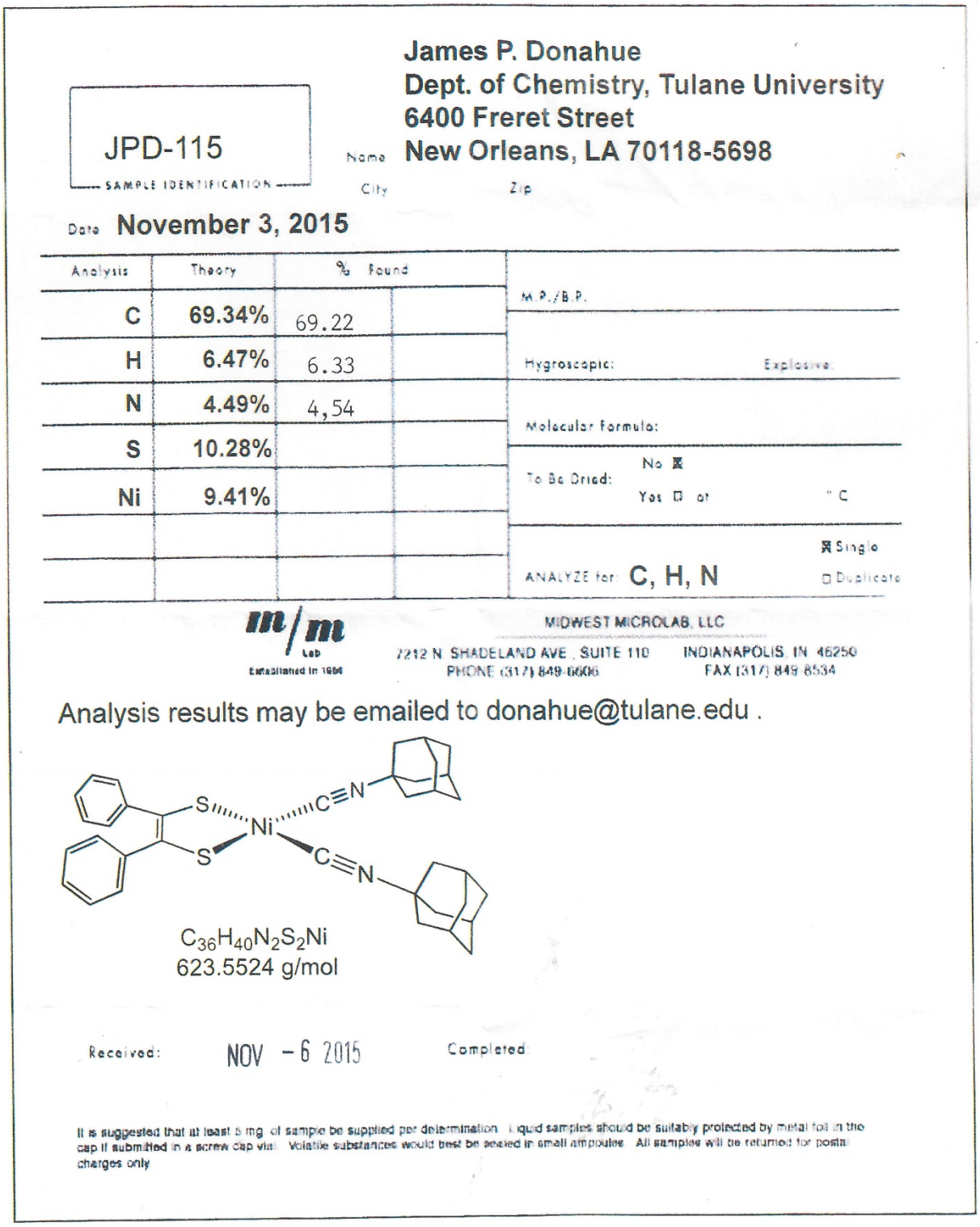

James P. Donahue
Dept. of Chemistry, Tulane University
6400 Freret Street
New Orleans, LA 70118-5698

JPD-115
SAMPLE IDENTIFICATION

Name
City Zip

Date November 3, 2015

Analysis	Theory	% Found	
C	69.34%	69.22	
H	6.47%	6.33	
N	4.49%	4,54	
S	10.28%		
Ni	9.41%		

M.P./B.P.

Hygroscopic: Explosive:

Molecular formula:

To Be Dried: No ☒ Yes ☐ at °C

ANALYZE for: C, H, N ☒ Single ☐ Duplicate

m/m Lab Established in 1994

MIDWEST MICROLAB, LLC
7212 N. SHADELAND AVE., SUITE 110 INDIANAPOLIS, IN 46250
PHONE (317) 849-6606 FAX (317) 849-6534

Analysis results may be emailed to donahue@tulane.edu .

$C_{36}H_{40}N_2S_2Ni$
623.5524 g/mol

Received: NOV – 6 2015 Completed:

It is suggested that at least 5 mg. of sample be supplied per determination. Liquid samples should be suitably protected by metal foil in the cap if submitted in a screw cap vial. Volatile substances would best be sealed in small ampoules. All samples will be returned for postal charges only.

Figure S72. Elemental analysis for [$(Ph_2C_2S_2)Ni(C{\equiv}N\text{-}1\text{-}Adamantyl)_2$], Midwest Microlabs.

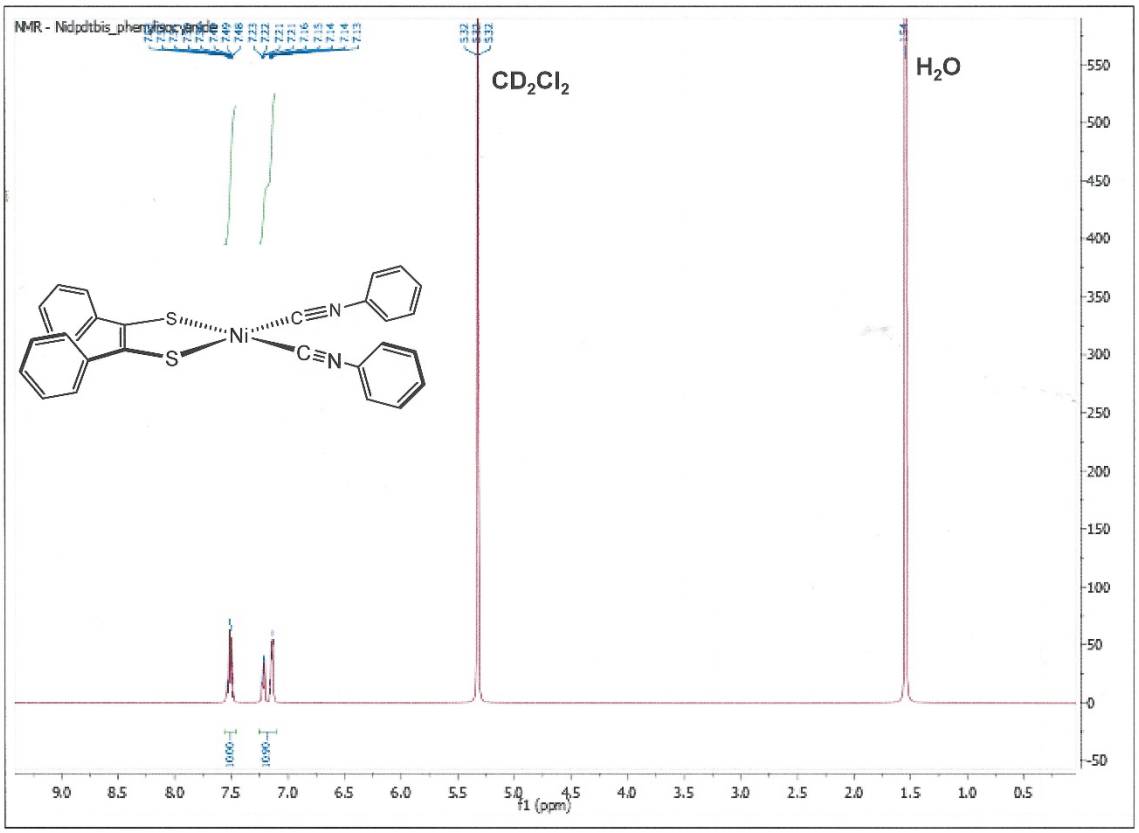

Figure S73. ^{1}H NMR spectrum (CD_2Cl_2) of [($Ph_2C_2S_2$)Ni(C≡NPh)$_2$].

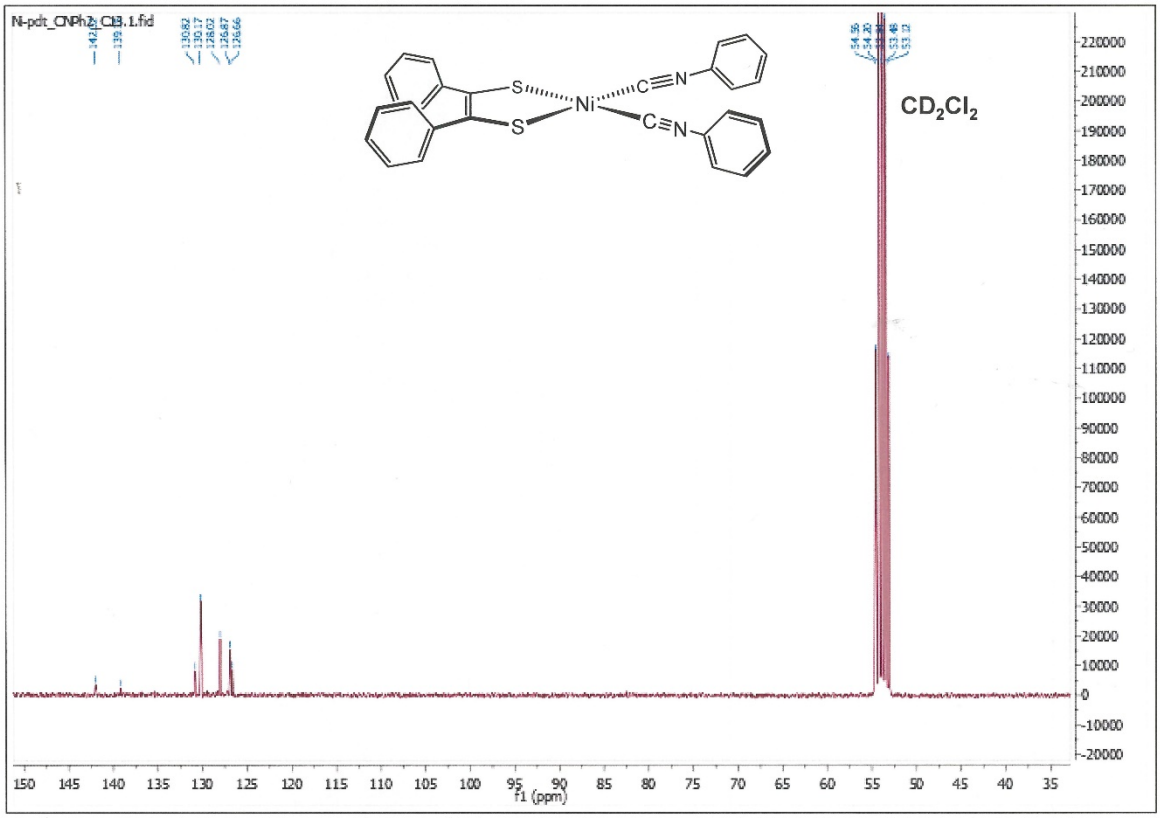

Figure S74. ^{13}C NMR spectrum (CD_2Cl_2) of [($Ph_2C_2S_2$)Ni(C≡NPh)$_2$].

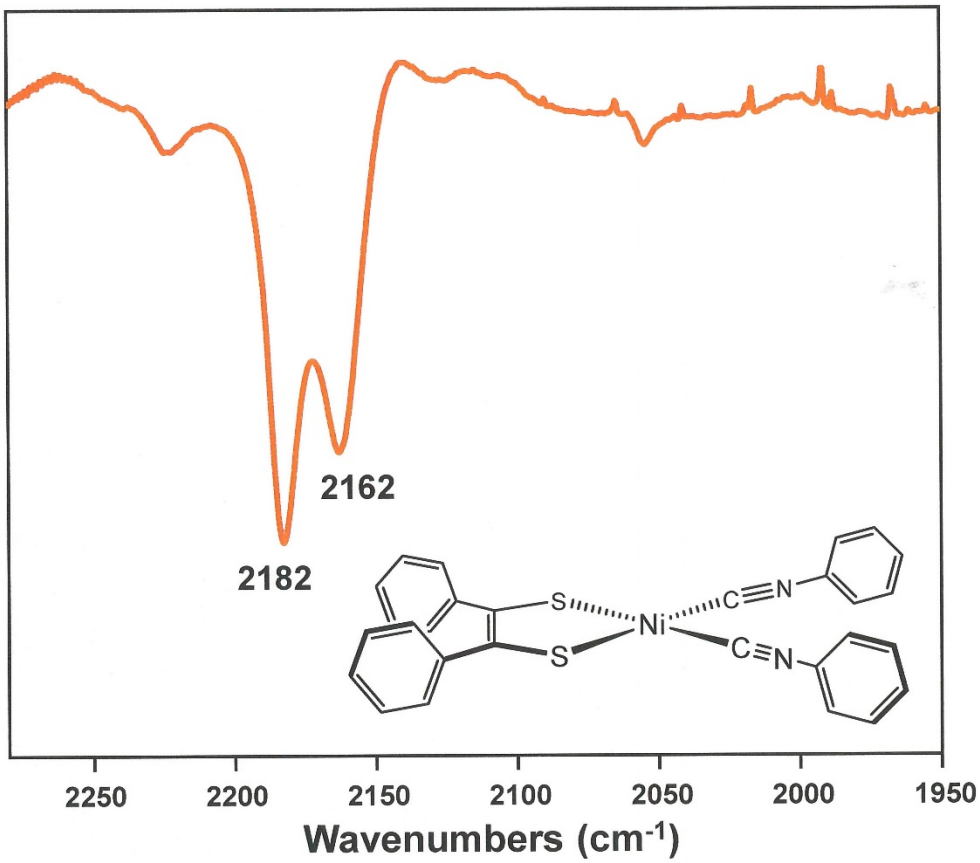

Figure S75. Solution IR spectrum (CH_2Cl_2) of [($Ph_2C_2S_2$)Ni(C≡NPh)$_2$].

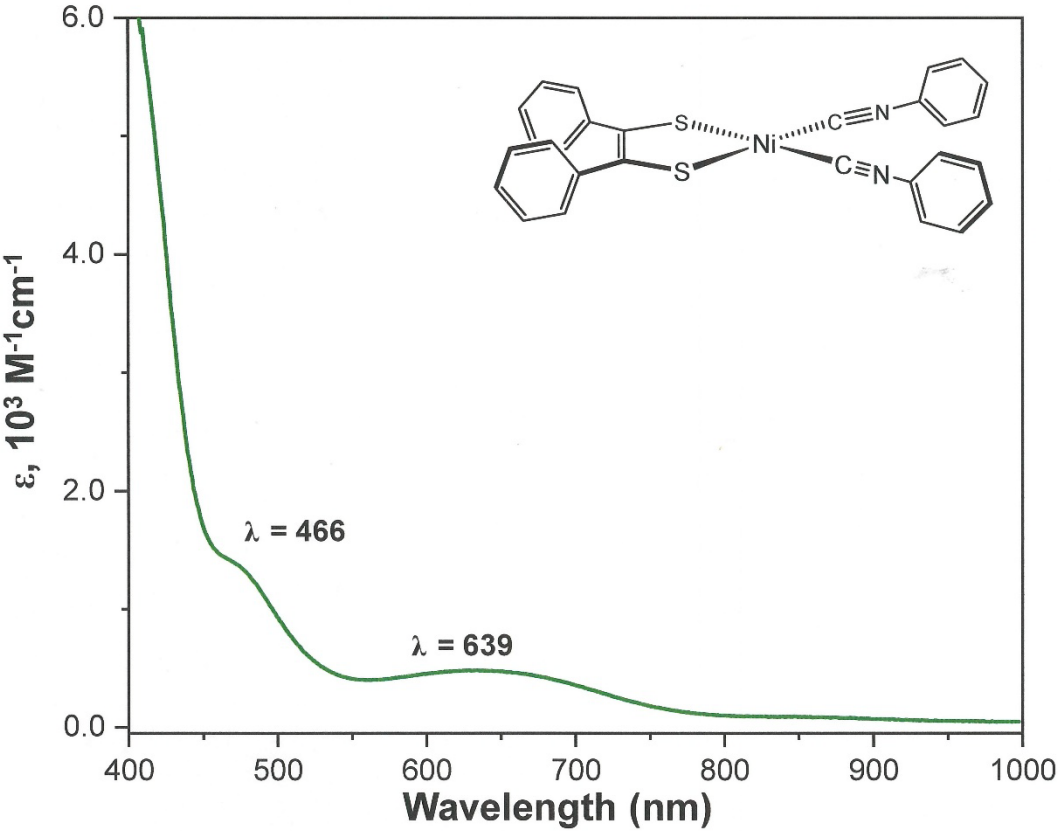

Figure S76. UV-vis spectrum (CH_2Cl_2) of [($Ph_2C_2S_2$)Ni(C≡NPh)$_2$].

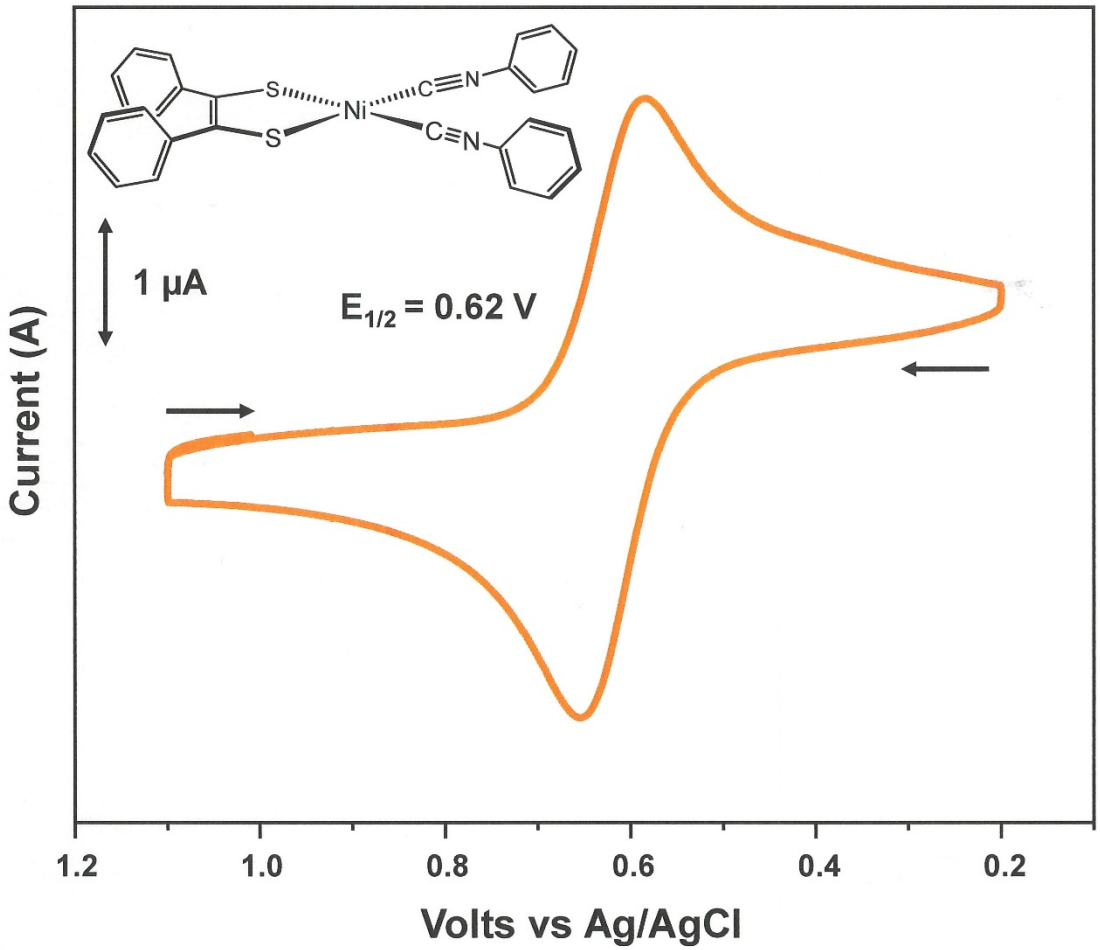

Figure S77. Cyclic voltammogram of (CH_2Cl_2) of [($Ph_2C_2S_2$)Ni(C≡NPh)$_2$] with [Bu_4N][PF_6] supporting electrolyte.

JPD-116

SAMPLE IDENTIFICATION

Name James P. Donahue
Dept. of Chemistry, Tulane University
6400 Freret Street
City New Orleans, LA 70118-5698 Zip

Date November 9, 2015

Analysis	Theory	% Found	
C	66.29%	66.26	
H	3.97%	3.87	
N	5.52%	5.56	
S	12.64%		
Ni	11.57%		

M.P./B.P.

Hygroscopic: Explosive:

Molecular Formula:

To Be Dried: No ☒ Yes ☐ at °C

ANALYZE for: C, H, N

☒ Single ☐ Duplicate

m/m Lab
Established in 1966

MIDWEST MICROLAB, LLC
7212 N. SHADELAND AVE., SUITE 110 INDIANAPOLIS, IN 46250
PHONE (317) 849-6005 FAX (317) 849-8534

Analysis results may be emailed to donahue@tulane.edu .

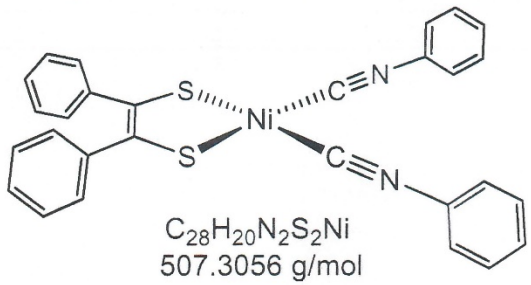

$C_{28}H_{20}N_2S_2Ni$
507.3056 g/mol

Received: NOV 13 2015 Completed:

It is suggested that at least 5 mg. of sample be supplied per determination. Liquid samples should be suitably protected by metal foil in the cap if submitted in a screw cap vial. Volatile substances would best be sealed in small ampoules. All samples will be returned for postal charges only

Figure S78. Elemental analysis for $[(Ph_2C_2S_2)Ni(C{\equiv}NPh)_2]$, Midwest Microlabs.

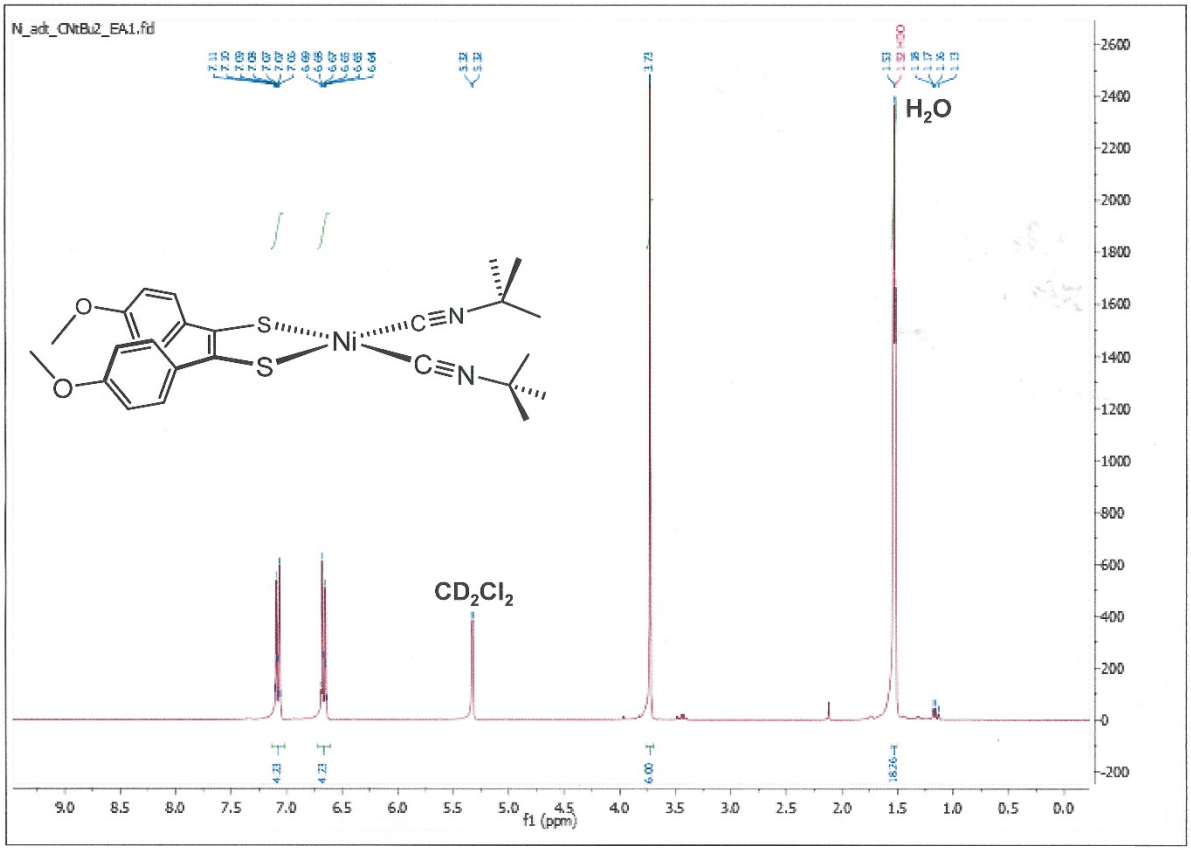

Figure S79. ^{1}H NMR spectrum (CD_2Cl_2) of [((CH$_3$O-*p*-C$_6$H$_4$)$_2$C$_2$S$_2$)Ni(C≡N^{t}Bu)$_2$].

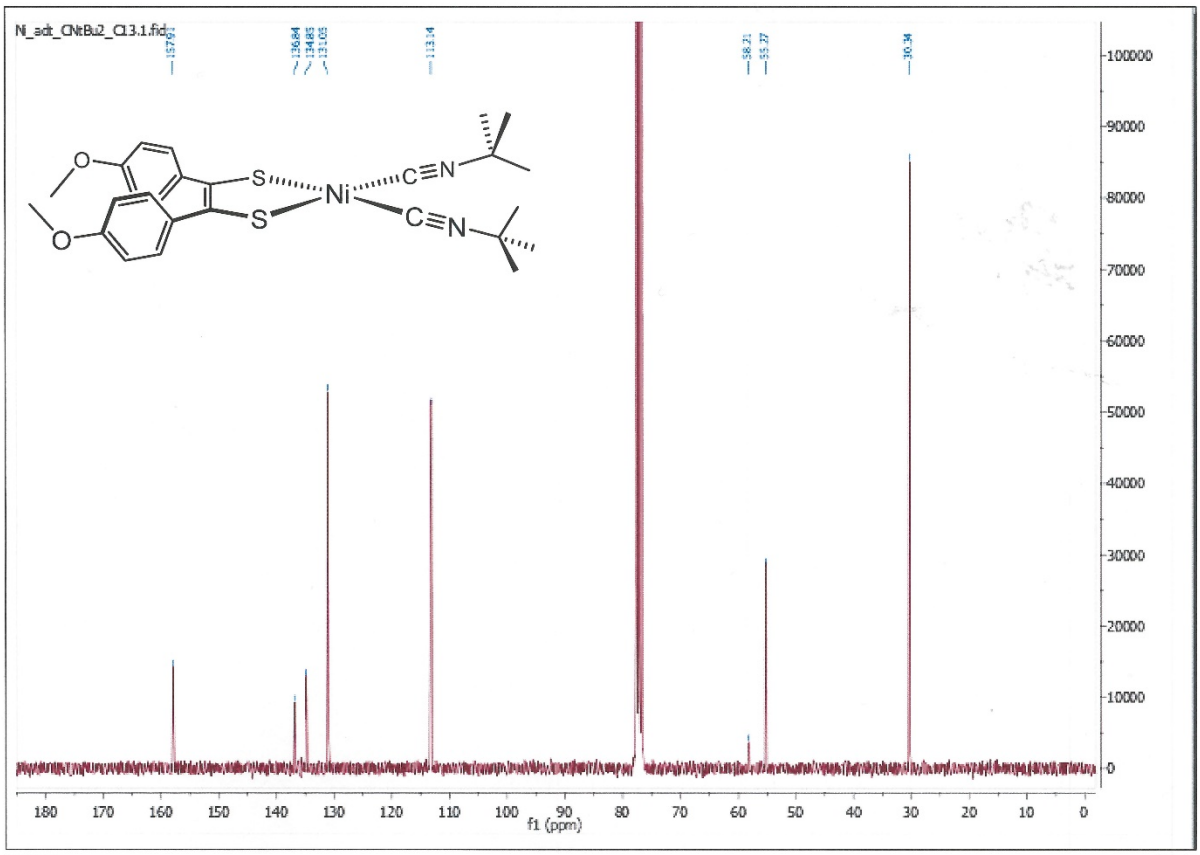

Figure S80. ^{13}C NMR spectrum (CD_2Cl_2) of [((CH$_3$O-*p*-C$_6$H$_4$)$_2$C$_2$S$_2$)Ni(C≡N^{t}Bu)$_2$].

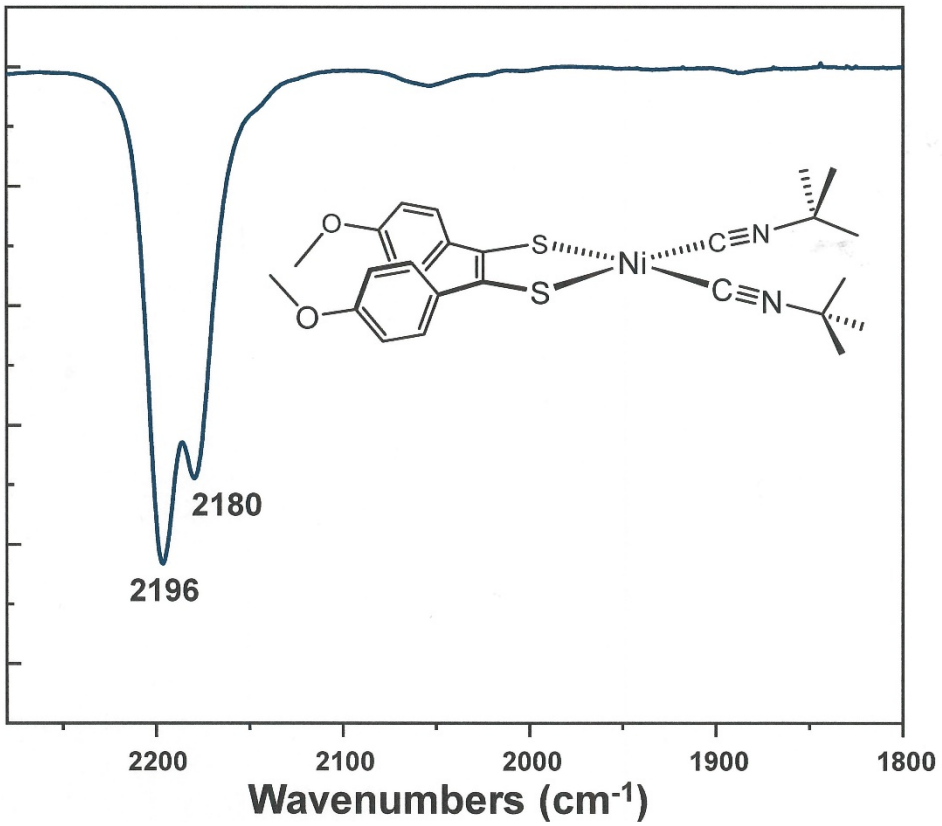

Figure S81. Solution IR spectrum (CH_2Cl_2) of [((CH$_3$O-*p*-C$_6$H$_4$)$_2$C$_2$S$_2$)Ni(C≡N^{t}Bu)$_2$].

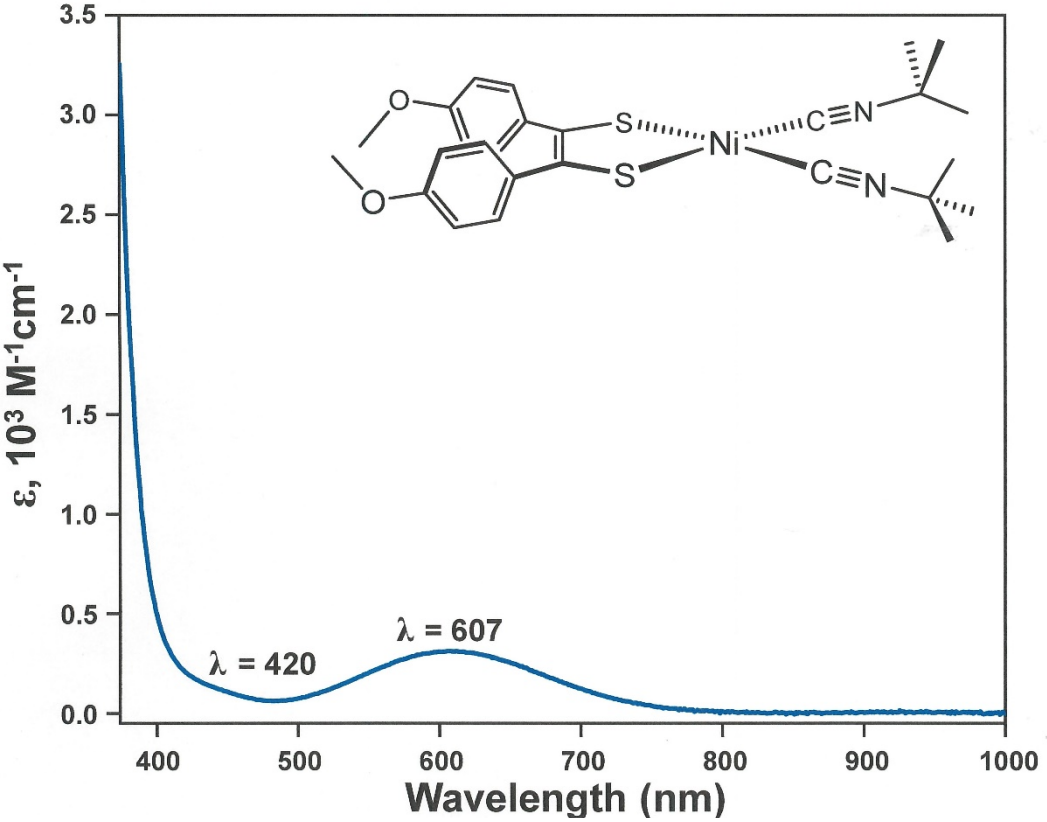

Figure S82. UV-vis spectrum (CH_2Cl_2) of [((CH$_3$O-*p*-C$_6$H$_4$)$_2$C$_2$S$_2$)Ni(C≡N^{t}Bu)$_2$].